TP53-status dependent oncogenic EZH2 Activity in Pancreatic Cancer

DISSERTATION

for the award of the degree

“Doctor rerum naturalium” (Dr. rer. nat.)

of the Georg-August-Universität Göttingen

within the doctoral program *Molecular Medicine*

of the Georg-August University School of Science (GAUSS)

submitted by

Lennart Viktor Versemann

Born in Buxtehude, Germany

Göttingen, May 2022

Thesis Advisory Committee

Prof. Dr. med. Elisabeth Hessmann, Department of Gastroenterology, Gastrointestinal Oncology and Endocrinology, University Medical Center Göttingen

Prof. Dr. med Matthias Dobbelstein, Institute of Molecular Oncology, University Medical Center Göttingen

Prof. Dr. rer. nat. Peter Burfeind, Institute of Human Genetics, University Medical Center Göttingen

Members of the Examination Board

1st Reviewer: Prof. Dr. med. Elisabeth Hessmann, Department of Gastroenterology, Gastrointestinal Oncology and Endocrinology, University Medical Center Göttingen

2nd Reviewer: Prof. Dr. med Matthias Dobbelstein, Institute of Molecular Oncology, University Medical Center Göttingen

Further member of the Examination Board

Prof. Dr. rer. nat. Peter Burfeind, Institute of Human Genetics, University Medical Center Göttingen

Prof. Dr. med. Michael P. Schön, Department of Dermatology, Venerology and Allergology, University Medical Center Göttingen

PD. Dr. rer. nat. Laura Zelarayán-Behrend, Institute of Pharmacology and Toxicology, University Medical Center Göttingen

Dr. rer. nat. Nico Posnien, Department of Developmental Biology, Georg-August-University Göttingen

Date of submission of thesis: 14.05.2022

Date of the oral examination: 14.06.2022

Dedicated To Oskar

Table of Contents

I List of Figures

II List of Tables

III Abbreviations

5-FU	5-Fluoruracil
aa	Amino acids
ADM	Acinar-to-ductal metaplasia
AKT1	RAC(Rho family)-alpha serine/threonine-protein kinase
APC	Allophycocyanin
APS	Ammonium persulfate
ATP	Adenosine triphosphate
BAK	B cell leukemia/ lymphoma 2 homologous antagonist/killer
BAX	B cell leukemia/ lymphoma 2-associated X protein
BCL-2	B cell leukemia/ lymphoma 2
BET	Bromodomain and extra-terminal domain family
bp	Base pair
BSA	Bovine serum albumin
Cas9	Clustered regularly interspaced short palindromic repeats-associated protein9
CC	Coiled-coil domain
CDK	Cyclin-dependent kinase
CDKN1A	Cyclin dependent kinase inhibitor 1A
CDKN2A	Cyclin-dependent kinase inhibitor 2A
cDNA	Complementary DNA
CHIP	C-terminus of HSC70-Interacting Protein
ChIP	Chromatin immunoprecipitation
Co-IP	Co-immunoprecipitation
CRISPR	Clustered regularly interspaced short palindromic repeats
CTD	C-terminal regulatory domain
Ctrl	Control
CXCR4	Hypoxia-inducible factor-driven chemokine receptor 4
DAPI	4′,6-Diamidin-2-phenylindol
DBD	DNA-binding domain
ddH_2O	Double distilled water
DISC	Death-inducing signaling complex
DMEM	Dulbecco’s modified Eagle growth medium
DMSO	Dimethyl sulfoxide
DNA	Deoxyribonucleic acid

DNMT	DNA-methyltransferases
DTT	Dithiothreitol
DZNep	3-Deazaneplanocin A
ECL	Enhanced chemiluminescence
EDTA	Ethylenediaminetetraacetate
EED	Embryonic ectoderm development
EGFR	Epidermal growth factor receptor
EGTA	Ethylene glycol-bis(2-aminoethylether)-*N,N,N′,N′*-tetraacetic acid
EMT	Epithelial-mesenchymal transition
ERα	Estrogen receptor alpha
EZH2	Enhancer of zeste homolog 2
FADD	Fas-associated death domain
FASL	Fas ligand
FCS	Fetal calf serum
FDR *q* value	False Discovery Rate
FOLFIRINOX	Regiment: leucovorin, 5-fluorouracil (5-FU), irinotecan, oxaliplatin
FPKM	Fragments per kilobase of transcript per million fragments mapped
GDP	Guanosine diphosphate
GEMM	Genetically engineered mouse models
GSEA	Gene set enrichment analysis
GO	Gene ontology
GOF	Gain-of-function
GTP	Guanosine triphosphate
H3	Histone 3
H3K27me3	Tri-methylation of histone 3 at lysine 27
HAT	Histone acetyltransferase
HDAC	Histone deacetylase
HE	Haematoxylin and eosin
HEPES	Hydroxyethyl piperazineethanesulfonic acid
HIF	Hypoxia-inducible factor
HNSCC	Head and neck squamous cell carcinoma
HRP	Horse radish peroxidase
IgG	Immunoglobulin G
IHC	Immunohistochemistry
IP	Immunoprecipitation
IPMN	Intraductal pancreatic mucinous neoplasia

KC	$Kras^{G12D}$;Cre
KD	Knockdown
KDM	Lysine demethylases
KEC	*$Kras^{G12D}$;$Ezh2^{fl/fl}$;Cre*
KMT	Lysine methyltransferases
KNPC	$Kras^{G12D}$;NFATc1;$p53^{R172H}$;Cre
$KNP^{null}C$	$Kras^{G12D}$;caNFATc1;$Trp53^{\Delta/\Delta}$;Cre
KO	Knockout
KPC	$Kras^{G12D}$;$p53^{R172H}$;Cre
Kras	Kirsten rat sarcoma viral oncogene homolog
Log2FC	Log 2-fold change
MCN	Mucinous cystic neoplasia
Mdm2	Mouse double minute 2 homolog
MEM	Minimal Essential Medium
mRNA	Messenger ribonucleic acid
MSigDB	Molecular Signatures Database
Mut	Mutant
Nab-paclitaxel	Nanoparticle albumin-bound paclitaxel
NEAA	Non-Essential amino acids
NES	Negative enrichment score
NFATc1	Nuclear factor of activated T cells c1
NF-Y	Nuclear transcription factor-Y
NF-κB	Nuclear factor kappa B
NGS	Normal goat serum
NKC	NFATc1; $Kras^{G12D}$;Cre
ns	Non-significant
NSCLC	Non-Small-Cell-Lung-Cancer
OD	Oligomerization domain
$p14^{ARF}$	Protein 14 alternate reading frame
p16	Protein 16
$p19^{Arf}$	Protein 19 alternate reading frame
p21	Protein 21
p53	Protein 53
p53mut	*TP53* mutant
p53wt	*TP53* wildtype
PAF	PCNA-associated factor

PanIN	Pancreatic intraepithelial neoplasia
PARP	Poly (Adenosine diphosphate-ribose) polymerase
PB	Phosphate buffer
PBS	Phosphate-buffered saline
PBS-T	Phosphate-buffered saline-Tween
PB-T	Phosphate buffer-Tween
PCA	Principal component analysis
PcG	Polycomb
PCR	Polymerase chain reaction
PD-1	Programmed cell death protein 1
PDAC	Pancreatic ductal adenocarcinoma
PFA	Paraformaldehyde
PI	Propidium iodide
PI3K	Phosphoinositide 3-kinase
PLA	Proximity ligation assay
PMSF	Phenylmethylsulfonyl fluoride
PRC2	Polycomb repressive complex 2
PRMT	Arginine methyltransferases
PROTAC	Proteolysis-targeting chimera
PRR	Proline-rich region
PS	Phosphatidylserine
PSC	Pancreatic stellate cell
PUMA	p53 upregulated modulator of apoptosis
qRT-PCR	Quantitative real-time PCR
rcf	Relative centrifugal force
RNA	Ribonucleic acid
RNA-seq	RNA-sequencing
RORα	RAR-related orphan receptor alpha
rpm	Rotations per minute
RPMI	Roswell Park Memorial Institute
RT	Room temperature
SD	Standard deviation
SDS	Sodium dodecyl sulfate
SDS-PAGE	Sodium dodecyl sulfate polyacrylamide gel electrophoresis
shRNA	Small hairpin RNA
siRNA	Small interfering ribonucleic acid

STAT3	Signal transducer and activator of transcription 3
STS	Staurosporine
SUZ12	Suppressor of Zeste 2
SV40	Simian virus 40
SWI/SNF	Switch/sucrose non-fermentable chromatin
TAD	Transactivation domain
TAF	TATA box binding protein-associated factors
T-ALL	T cell acute lymphoblastic leukemia
TBP	TATA box binding protein
TBS-T	Tris buffered saline-Tween
TCGA	The Cancer Genome Atlas
TEMED	N, N, N´,N´- Tetramethyl-ethylendiamin
TFIID	Transcription factor II D
TGFβ	Transforming growth factor β
TNF	Tumor-necrosis factor
TP53	Tumor protein 53 coding gene
TRAIL	Tumor-necrosis factor-related apoptosis-inducing ligand
Tris	Tris(hydroxymethyl)aminomethane
TSS	Transcriptional start site
UMG	University Medical Center Göttingen
UV	Ultra-violet
WCL	Whole cell lysate
Wt	wildtype
αSMA	Alpha smooth muscle actin

IV Abstract

Pancreatic Ductal Adenocarcinoma (PDAC) remains a dismal malignancy with a 5-year survival rate of less than 10%. Predominately, chemoresistance mediated by the dynamic cellular plasticity induced through epigenetic alterations accounts for the high mortality rates of PDAC. The histone methyltransferase enhancer of zeste homolog 2 (EZH2), the catalytic component of the polycomb repressive complex 2 (PRC2), is frequently found overexpressed in PDAC and has crucial functions in the evasion of tumor-suppressive mechanisms. However, recent studies suggest a huge context-dependency of oncogenic EZH2 activity.

The tumor suppressor p53 is well characterized for its anti-tumorigenic capacities. However, in human PDAC, *TP53* mutations occur with a prevalence of 50-80%, potentially resulting in the loss of tumor suppressor function and the gain of oncogenic function suggesting a *TP53*-status-dependent functional behaviour of a cell. However, whether and to what extent mutations of *TP53* indeed functionally or mechanistically influence EZH2-dependent processes in PDAC remains largely elusive. In this study, the impact of a specific genetic background on the activity of epigenetic processes has been investigated. The major aim was to illuminate *TP53*-status-dependent oncogenic EZH2 activity in PDAC progression.

Functionally, we demonstrate that EZH2-dependent target gene regulation is determined by the *TP53*-status and that EZH2 depletion correlates with a better prognosis only in *TP53*wt PDAC. Moreover, we reveal that EZH2 depletion combined with chemotherapy increases apoptosis induction restrictively in *TP53*wt cells. Hence, our study highlights a strong context-dependency of the EZH2 activity specifically regarding the *TP53*-status. Therefore, our data suggest that in PDAC subtypes with *TP53*wt-status, EZH2 depletion together with chemotherapy might represent a beneficial strategy to tackle PDAC, whereas in *TP53*-mutant PDAC, EZH2 depletion is not advantageous.

Furthermore, our findings imply that EZH2 influences p53wt expression on a post-translational level and illustrate that EZH2 targets the *CDKN2A* gene for transcriptional repression, thus abrogating $p14^{ARF}$/$p19^{Arf}$-dependent inhibition of Mdm2-mediated p53 degradation. Moreover, we reveal that PDAC formation is promoted despite *TP53*wt-status and low EZH2 expression, if EZH2-independent *CDKN2A* repression occurs, thus demonstrating the importance of an intact *CDKN2A*-*TP53*wt axis for a beneficial outcome of EZH2 inhibition in PDAC. Moreover, we revealed the existence of a previously unknown EZH2-p53-complex in PDAC, suggesting that also non-canonical functions of EZH2 may contribute to PDAC progression.

Conclusively, our data underline the significance of patient stratification to predict and improve EZH2 inhibition as a potential treatment strategy in PDAC.

1 Introduction

1.1 Pancreatic Ductal Adenocarcinoma

The Pancreas

The pancreas is a 12-18 cm long exo- and endocrine gland that lies behind the stomach in the middle of the abdomen with close contact to the duodenum, the spleen, and the gall bladder (Beger 2018). The exocrine compartment accounts for 99% of the gland and produces digestive enzymes, including trypsin, amylase, and lipases. These enzymes are secreted via a system of pancreatic ducts into the duodenum (Beger 2018). On the contrary, the endocrine part constitutes only 1-2% of the pancreas and is involved in the carbohydrate, lipid, and protein metabolism by producing hormones like insulin, glucagon, somatostatin, and pancreatic polypeptide (Beger 2018).

Pancreatic Ductal Adenocarcinoma

The most common type of pancreatic cancer is pancreatic ductal adenocarcinoma (PDAC) responsible for 90% of all pancreatic tumors arising from the exocrine compartment (Hackeng et al. 2016). PDAC is one of the most aggressive cancer types with a survival rate remaining constantly under 10% which is the lowest survival rate among all solid tumors (Siegel et al. 2018). Hence, despite PDAC being only the tenth most frequent cancer entity in the United States, it is the third most common cause of cancer-related death (Tavakkoli et al. 2020). Given the low survival rate, growing incidence, and no major improvement in the mortality rate, PDAC is predicted to become the second leading cause of cancer-related deaths by 2030 in the United States (Rahib et al. 2014). The major reasons for the poor prognosis of PDAC are the very late diagnosis, rapid tumor growth, early metastasis, resistance to conventional chemotherapy, and mostly unresectable tumors (Hessmann et al. 2020). Consequently, there is great urgency and importance to increase the knowledge on molecular mechanisms underlying PDAC to develop novel therapeutic strategies to improve PDAC patient outcome and survival.

PDAC therapy

Despite extensive progress in targeted cancer treatment in other tumor entities as exemplified by breast cancer and colorectal cancer (Tsuchida et al. 2019, Linnekamp et al. 2015), PDAC therapy mostly still relies on surgical resection and systemic chemotherapy.

However, pancreatic resection still constitutes the only potentially curative treatment possibility for PDAC (Adamska et al. 2017). Given that PDAC is mostly diagnosed at a locally advanced or metastatic stage, only 20% of all cases are operable (Strobel et al. 2019). Additionally, the recurrence rate after resection is about 40% within the first 6-24 months demonstrating that surgical resection is very important but also limited (Hishinuma et al. 2006).

Besides surgical resection, chemotherapy is the main therapeutic treatment choice and the only option for metastatic PDAC. The standard chemotherapy for the past decades is based on gemcitabine monotherapy (Burris et al. 1997). However, gemcitabine resistance, which may be caused by the extensive stroma formation, is often observed in PDAC and limits the use of gemcitabine monotherapy (Kim and Gallick 2008, Neesse et al. 2011, Kamisawa et al. 2016). Therefore, improved therapy response and prolonged survival can be achieved through treatment with the combination of nanoparticle albumin-bound paclitaxel (nab-paclitaxel) plus gemcitabine (Von Hoff et al. 2013). To the present day, the most effective chemotherapeutic regiment for patients in a generally good condition with metastatic PDAC and for adjuvant therapy after PDAC resection is the FOLFIRINOX regiment combining leucovorin, 5-fluorouracil (5-FU), irinotecan, and oxaliplatin (Conroy et al. 2011). Given the development of chemoresistance frequently observed in PDAC and the success in other tumor entities such as breast cancer and colorectal cancer (Tsuchida et al. 2019, Linnekamp et al. 2015), targeted therapy moved to the focus of PDAC therapy, especially for second-line therapy (Moore et al. 2007, Sohal et al. 2018). Unfortunately, to date, no or only marginal improvements were achieved. However, Moore et al. showed that the use of the human epidermal growth factor receptor (HER1/EGFR) inhibitor erlotinib in combination with gemcitabine revealed a prolonged progression-free and overall survival in comparison to gemcitabine monotherapy at least in a subgroup of PDAC patients as the first example of targeted therapy in advanced PDAC (Moore et al. 2007). Another more recent example of targeted therapy in PDAC is the use of poly adenosine diphosphate (ADP)-ribose polymerase (PARP) inhibitors in *BRCA1/2*-deficient PDAC (Golan et al. 2019). PDAC that lack the *BRCA*-mediated DNA damage repair mechanisms strongly rely on the PARP-mediated DNA damage repair pathway to extend survival. Hence, if PARP is inhibited by PARP inhibitors, such as Olaparib, tumor cells undergo apoptosis. Consequently, Olaparib is approved in the United States for the maintenance treatment of advanced PDAC harboring a germline *BRCA*1/2 mutation and that responded to platinum-based chemotherapy (Golan et al. 2019, Chi et al. 2021).

However, despite considerable advances in cancer treatment in general, resistance to therapy remains a big challenge, particularly in PDAC. Therefore, a better understanding of the precise tumor biology in PDAC is necessary to conquer treatment resistance and to identify new susceptible targets in PDAC.

Carcinogenesis of PDAC

Histologically, the pancreas consists of exocrine acinus cells, ductal cells, and endocrine cells (Beger 2018). Although the specific cell of origin of PDAC has been a question of controversial debate for many years, lineage-tracing experiments suggest an acinar origin for PDAC since acinar cells reveal high cellular plasticity (Parsa et al. 1985, Habbe et al. 2008, De La et al. 2008). Given that the pancreas presumably lacks a defined stem cell compartment, this cellular plasticity of acinar cells necessarily mediates pancreatic homeostasis and regeneration (Puri et al. 2015). During this process, acinar cells can trans-differentiate into ductal-like cells in response to different stimuli, including inflammation, stress, and tissue damage (Kopp et al. 2012, Gidekel Friedlander et al. 2009). This process is named acinar-to-ductal metaplasia (ADM), required for normal pancreatic regeneration but also a suitable initial step for the beginning of PDAC carcinogenesis (Figure 1) (Storz 2017).

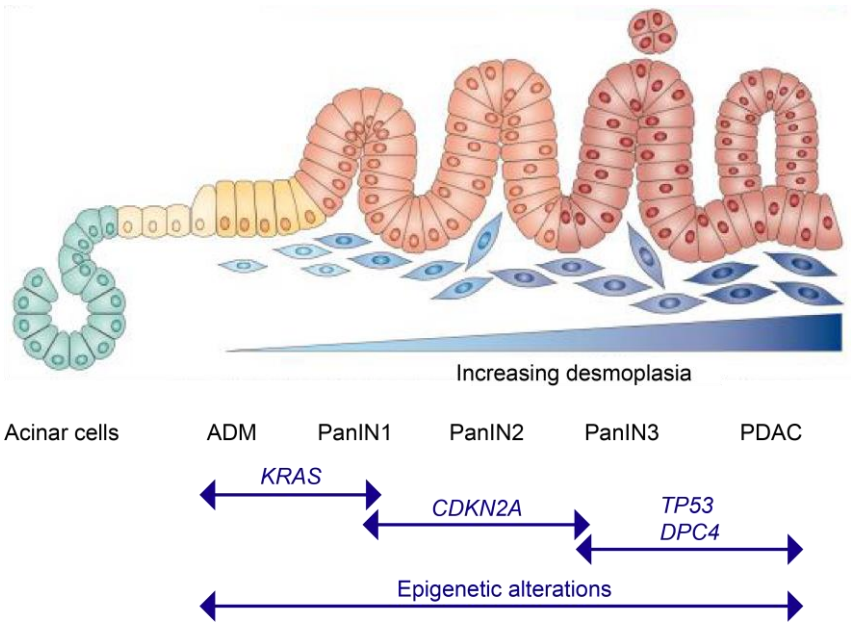

Figure 1: Schematic illustration of the histopathological carcinogenesis of PDAC. Initially, during acinar-to-ductal metaplasia (ADM) acinar cells trans-differentiate into ductal cells. In a stepwise process, pancreatic ductal adenocarcinoma (PDAC) evolves from increasing stages of early pancreatic intraepithelial neoplasia (PanIN1-3) which are graded and characterized by the loss of cellular polarity and nuclear atypia. *(Figure legend continued on next page).*

Common genetic alterations, including constitutive activation of *KRAS* as well as loss of *CDKN2A*, *TP53*, and *DPC4* foster PDAC progression. Additionally, epigenetic alterations highly contribute to PDAC carcinogenesis. Modified from (Hruban et al. 2000, Morris et al. 2010, Orth et al. 2019).

The major reason why ADMs cannot dedifferentiate but rather progress into pancreatic intraepithelial neoplasia (PanIN), is the activating mutation of the oncogene *KRAS* occurring nearly ubiquitously in more than 95% of all PDACs (Bailey et al. 2016, Hruban et al. 2008, Ying et al. 2016). These PanIN lesions are the most common PDAC precursors and can be graded into PanIN1-3 with consideration to their histopathological characteristics, including the loss of cellular polarity and nuclear atypia. The additional accumulation of different mutations of several tumor suppressor genes, namely *CDKN2A*, *TP53,* and *DPC4*, fosters the progression to PDAC (Waddell et al. 2015). Moreover, epigenetic re-programming highly contributes to PDAC formation and plays a significant role in PDAC carcinogenesis (Roe et al. 2017, McDonald et al. 2017, Lomberk et al. 2018) (Figure 1).

Genetic Hallmarks of PDAC

Although PDAC is genetically a very heterogeneous disease with mutations affecting a wide spectrum of different genes, four common driver mutations that characterize PDAC, include the activation of *KRAS* and the inactivation of *CDKN2A*, *TP53,* and *DPC4* (Waddell et al. 2015). As stated earlier, *KRAS* mutations can be found in 95% of all PDAC cases highlighting the central role in PDAC initiation (Bailey et al. 2016, Hruban et al. 2008). The K-Ras protein, encoded by *KRAS*, is a member of the RAS superfamily mediating crucial cellular functions such as differentiation, proliferation, and survival (Campbell et al. 1998, Malumbres and Barbacid 2003). K-Ras is a GTPase meaning that it binds to guanosine triphosphate (GTP) (active) and hydrolyses it into guanosine diphosphate (GDP) (inactive). In the GTP-bound active state, it can activate various downstream signaling pathways, including the MAPK/ERK pathway, the phosphoinositide 3-kinase (PI3K), and the RalGDS pathway (Mihaljevic et al. 2010, Wittinghofer et al. 1997). One very common mutation of *KRAS* in PDAC is the glycine to aspartate point mutation at codon 12 ($KRAS^{G12D}$), leading to a permanent binding of K-Ras to GTP resulting in constitutive activation and stimulation of proliferation, differentiation, and survival without an external stimulus (Malumbres and Barbacid 2003). Studies in mice demonstrate that *KRAS* mutation alone is sufficient to initiate the development of PanIN lesions equal to human lesions, but only rarely leads to full

PDAC demonstrating that additional oncogenic events need to accumulate to progress to full neoplasia (Hingorani et al. 2003).

The second hit found in about 90% of all PDACs is the loss of the tumor suppressor *CDKN2A*, encoding for two different proteins with different promotors: $p16^{INK4a}$ and $p14^{ARF}$ in humans or $p19^{Arf}$ in mice, respectively (Waddell et al. 2015, Serrano 2007). $P16^{INK4a}$ has a crucial role in cell cycle regulation by blockade of the cyclin-dependent kinases 4 and 6 (CDK4, CDK6) resulting in inhibition of the transition from G1 to S-phase (Serrano 2007). $P14^{ARF}$ in humans and $p19^{Arf}$ in mice inhibit Mdm2, thereby preventing the Mdm2-mediated proteasomal degradation of p53 leading to the stabilization of p53 (Kamijo et al. 1998, Pomerantz et al. 1998). Consequently, the loss of the tumor suppressor *CDKN2A* fosters cell cycle progression and destabilization of p53.

The tumor-suppressive function of p53 is not only hindered indirectly through mutations of *CDKN2A* but very frequently also directly through mutations of *TP53*. These mutations are observed in 50-80% of all PDACs, mainly in late-stage PanIN lesions (DiGiuseppe et al. 1995, Waddell et al. 2015) (Figure 1) leading to the loss of tumor suppressor function and even to oncogenic gain-of-function (GOF) (Freed-Pastor and Prives 2012, Brosh and Rotter 2009). The precise role of p53 in PDAC and the consequences of *TP53* mutations are described in more detail in *1.2 The Tumor Suppressor p53* (see p. 6).

Another frequent driver mutation in PDAC associated with late-stage PanIN lesions observed in 50% of all patients is the inactivating mutation of *DPC4*, coding for SMAD4, a central regulator in TGFβ signaling (Hahn et al. 1996, Massagué et al. 2000, Waddell et al. 2015). SMAD4 mediates the translocation of activated receptor SMADs into the nucleus, thereby facilitating gene transcription (Xia et al. 2015). Although TGFβ signaling is highly context-dependent revealing a dual role of tumor-suppressive and tumor-promoting effects, the loss of SMAD4 is rather associated with oncogenic consequences in PDAC (Xia et al. 2015).

Additionally, besides these four driver mutations, a huge number of bystander mutations occur in PDAC affecting a variety of cellular processes, including RNA processing, DNA repair, Wnt signaling, and epigenetic-associated functions. Although the incidences of these bystander mutations decline to less than 10%, they do have prognostic and therapy-predictive relevance (Bailey et al. 2016, Morris et al. 2010).

1.2 The Tumor Suppressor p53

The role of wildtype p53

The protein p53, encoded by the well-studied *TP53* gene, is one of the most important tumor suppressor proteins which acts as a transcriptional activator inducing cell cycle arrest, senescence, or apoptosis (Vousden and Lu 2002). In unstressed cells, p53 is a transient protein with a short half-life undergoing proteasomal degradation mediated through ubiquitination by its negative regulator Mouse double minute 2 homolog (Mdm2). Hence, the protein is frequently not detectable in unstressed conditions although p53 mRNA can be measured (Lakin and Jackson 1999). However, upon internal and external stress signals, including oncogenic and genotoxic stress, p53 induces characteristic tumor protective functions (Vousden and Lu 2002). Hence, p53 is stabilized and activated through plenty of post-translational modifications, including the initial phosphorylation of serine 15 abolishing Mdm2 to bind and destruct p53 (Kruse and Gu 2008, Brooks and Gu 2010). Upon final acetylation of p53, it forms homo-tetramers and induces the transcription of its target genes which are predominantly involved in the regulation of cell cycle progression, senescence, and cell death pathways (Brooks and Gu 2010, Fischer 2017). Therefore, in 1992 p53 was designated as 'the guardian of the genome' demonstrating the significant role of p53 in monitoring the integrity of the genome (Lane 1992).

Structurally, p53 consists of 393 amino acids (aa) and is located in the nucleus. It contains an N-terminal transactivation domain (TAD), followed by a proline-rich region (PRR). The DNA-binding domain consists of 198 aa and is in the center of the protein followed by a flexible linker region, an oligomerization domain (OD), and the C-terminal regulatory domain (CTD) (Joerger and Fersht 2010) (Figure 2).

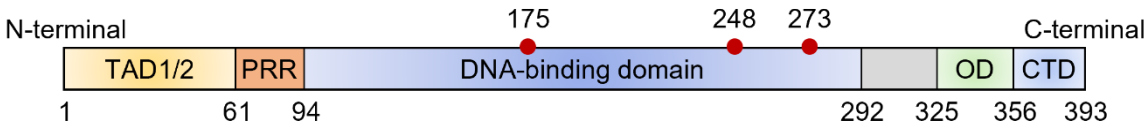

Figure 2: Domain structure of the protein p53. The wildtype protein p53 consists of 393 amino acids (aa). In the N-terminal, p53 contains the transactivation domain (TAD), which can be subdivided into TAD1 and TAD2, and the proline-rich region (PRR), followed by the central DNA-binding domain, a flexible linker region (grey), an oligomerization domain (OD), and the C-terminal regulatory domain (CTD). Red dots indicate the most common mutation sites. Modified after Joerger and Fersht 2010.

Regulation of p53 by Mdm2

As previously mentioned, in normal unstressed cells p53 is quickly degraded by E3-ligases, such as Mdm2, C-terminus of HSC70-Interacting Protein (CHIP), and MdmX. However, the most prominent negative regulator of p53 is Mdm2 (Jones et al. 1995, Montes de Oca Luna et al. 1995). Mdm2 regulates p53 through two mechanisms indicating the importance of the Mdm2-dependent p53 regulation. Mainly, Mdm2 acts as an E3 ligase mediating posttranslational ubiquitination of p53 leading to proteasomal degradation. Additionally, Mdm2 can also bind to the TAD of p53 preventing the transcriptional activation thereby suppressing its function as a transcription factor (Jones et al. 1995, Montes de Oca Luna et al. 1995, Iwakuma and Lozano 2003, Toledo et al. 2006). Interestingly, besides this negative regulatory function, Mdm2 is also a transcriptional p53 target gene. This dual role of Mdm2 as a negative regulator and a transcriptional target of p53 demonstrates the tightly regulated balance of both proteins by the generation of a negative feedback loop.

A functional triangle – p53, Mdm2, and $p14^{ARF}$/$p19^{Arf}$

Mdm2 itself is inhibited by $p14^{ARF}$ in humans or $p19^{Arf}$ in mice, thereby indirectly activating p53 (Lowe and Sherr 2003) (Figure 3). Upon activation by oncogenic stress, as exemplified by the moderate presence of Myc or mTOR, $p14^{ARF}$/$p19^{Arf}$ disrupts the p53-Mdm2 complex by sequestration of Mdm2 into the nucleus, thus abolishing Mdm2-dependent p53 destruction in the cytoplasm (Weber et al. 1999, Sherr 2006). Additionally, $p14^{ARF}$/$p19^{Arf}$ can also directly prevent Mdm2 E3 ligase function leading to p53 stabilization (Honda and Yasuda 1999, Llanos et al. 2001). The tightly regulated complexity of this functional triangle is supported and expanded by the findings that activated p53 decreases $p14^{ARF}$/$p19^{Arf}$ expression through polycomb group (PcG) proteins and histone deacetylases (HDAC) leading to epigenetic silencing $p14^{ARF}$/$p19^{Arf}$ (Zeng et al. 2011, Kung and Weber 2022).

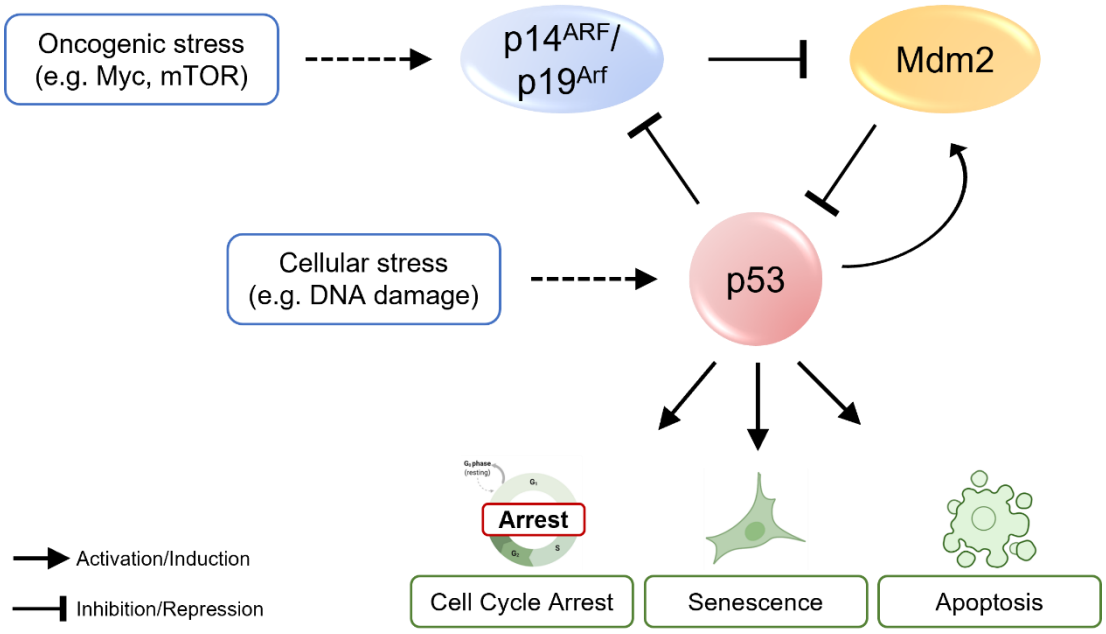

Figure 3: Functional triangle of p53, Mdm2, and p14^{ARF}/p19^{Arf} regulation. Schematic illustration of the complexity of the p53, Mdm2, p14^{ARF}/p19^{Arf} regulation. Upon oncogenic stress, p14^{ARF}/p19^{Arf} is activated and inhibits Mdm2, the negative regulator of p53. P53 itself is activated through cellular stress, induces the transcription of Mdm2, and represses the expression of p14^{ARF}/p19^{Arf}. Upon activation, p53 induces tumor-suppressive functions, such as cell cycle arrest, senescence, and/or apoptosis.

The role of mutant p53

Given the significant role of p53 in inducing tumor-suppressive functions, mutations in the *TP53* gene can be frequently detected in cancer cells resulting in the loss of tumor suppressor function and oncogenic GOF (Freed-Pastor and Prives 2012, Brosh and Rotter 2009). Indeed, more than 50% of all human tumors and 50 – 80% of all PADC patients harbour a mutation in the *TP53* gene rendering *TP53* the most frequently mutated gene in cancer (Vogelstein et al. 2000, Waddell et al. 2015).

Moreover, the significant impact of mutant p53 on tumor formation is highlighted by a rare hereditary disease, called Li-Fraumeni syndrome (Fraumeni and Li 1969). This familial cancer syndrome is an autosomal-dominant disease caused by germline mutations in *TP53*. With a high prevalence, these germline *TP53* mutations result in multiple malignant tumors, including sarcoma and breast cancer (Fraumeni and Li 1969, Malkin et al. 1990). Additionally, studies using a p53$^{-/-}$ mouse model constitutively lacking p53 reveal that 75% of these mice develop tumors, predominantly sarcoma and lymphoma within six months supporting the importance of p53 as a tumor suppressor (Donehower et al. 1992).

In the pancreas, p53 mutations occur in late-stage PanIN lesions, usually not earlier than PanIN3, and force the progression towards invasive PDAC (DiGiuseppe et al. 1995). Given the crucial role of p53 in DNA damage response, it is hypothesized that one reason for the genomic instability in PDAC is the *TP53* mutation frequently observed in PDAC (Mihaljevic et al. 2010). Furthermore, PDACs harbouring *TP53* mutations are characterized by high stromal content, dedifferentiation, and accelerated epithelial-to-mesenchymal-transition (EMT) capacities resulting in a higher aggressiveness and worse prognosis of these PDACs (Brosh and Rotter 2009, Waddell et al. 2015, Bailey et al. 2016).

Mutations of *TP53* predominantly occur within the DNA binding domain of p53 abolishing transcriptional activity of tumor-suppressive-related target genes. The most common *TP53* mutations in all cancer types are missense mutations, such as R175H, R248Q/W, and R273H/C, resulting in single amino-acid substitutions (Petitjean et al. 2007, Bouaoun et al. 2016) (Figure 2). Given that most mutations are monoallelic, meaning that only one allele of p53 is mutated whereas the second allele is still wildtype, mutant p53 displays a dominant-negative activity over wildtype p53. This phenomenon is called loss of heterozygosity (Petitjean et al. 2007).

Alterations in the *TP53* locus lead to an altered gene product which highly accumulates within the cells up to levels that surpass p53 wildtype levels because the strict Mdm2-p53 regulation is abolished in tumors with mutant p53 resulting in tremendous stabilization and accumulation of mutant p53 (Lukashchuk and Vousden 2007). Functionally, these mutations of p53 result not only in the loss of tumor suppressor function such as dysregulation of cell cycle progression and apoptosis but also in oncogenic gain-of-function as exemplified by supporting cell invasion and migration as well as induction of genomic instability demonstrating the significance of the *TP53* status for the cancer cell behaviour (Brosh and Rotter 2009, Freed-Pastor and Prives 2012, Alexandrova et al. 2017, Mantovani et al. 2019). The loss of the tumor-suppressive functions of mutant p53 can be explained by the loss of the ability to bind to p53 wildtype DNA binding elements, thereby losing the activity to induce the transcription of typical p53 wildtype target genes, including *BAX*, *BBC3*, and *CDKN1A* (Brosh and Rotter 2009, Freed-Pastor and Prives 2012). Additionally, the aforementioned accumulation of the mutant p53 protein is a crucial mechanism for mediating oncogenic GOF and correlates with worse survival (Terzian et al. 2008, Brosh and Rotter 2009, Oren and Rotter 2010, Freed-Pastor and Prives 2012). Hence, specifically those mutants with the ability to be highly stabilized can accumulate within the tumor cells resulting in mediating oncogenic GOF. Accumulated mutant p53 can, for instance, bind to other transcription (co-) factors, as exemplified by NF-Y, SREBP, and NRF2, leading to altered transcriptional

activities resulting in tumor progression (Freed-Pastor and Prives 2012, Di Agostino et al. 2006, Dupont et al. 2009, Stambolsky et al. 2010). Moreover, it was shown that accumulated mutant p53 interacts with the SWI/SNF complex in breast cancer, thereby altering the chromatin structure and resulting in altered gene expression (Pfister et al. 2015). Conclusively, the loss of tumor suppressor functions as well as oncogenic GOF of mutant p53 significantly influences the cancer cell behaviour.

1.3 Apoptosis – A mechanism to induce programmed cell death

The ability of cells to kill themselves in a highly programmed, energy-dependent manner is named programmed cell death or apoptosis (Kerr et al. 1972). Importantly, in contrast to necrosis, this process does not induce inflammation, but is a rather physiological mechanism occurring during aging and development to preserve homeostasis in cellular networks in different tissues and organs (Norbury and Hickson 2001). Additionally, apoptosis can be induced due to several apoptotic signals, such as irreversible DNA damage, to avoid harmful, potentially cancer-causing consequences for the organism (Norbury and Hickson 2001). Consequently, biochemical mechanisms, predominantly the activation of different cysteine proteases named ‘caspases’ orchestrate characteristic morphological changes, including disturbance of cellular membranes, breakdown of the cytoplasmic and nuclear skeleton, extrusion of the cytosol, fragmentation of the nucleus, formation of apoptotic bodies, expression of phagocytic ligands, and elimination through phagocytosis (Wyllie et al. 1980).

Generally, there are two different ways to activate the highly coordinated apoptotic processes: the intrinsic mitochondrial pathway and the extrinsic death receptor pathway (Figure 4) (Elmore 2007). The intrinsic pathway is a response to cellular stress situations including DNA damage. Importantly, the p53 pathway plays a crucial role in the activation of pro-apoptotic pathways. Upon DNA damage, p53 gets activated and induces the transcription of pro-apoptotic BH3-only proteins, PUMA, NOXA, and BIM (Aubrey et al. 2018). Normally, pro-survival proteins of the BCL2 family as exemplified by BCL-XL and BCL-2, avoid apoptosis activation. However, the accumulation of pro-apoptotic BH3-only proteins leads to the blockade of the pro-survival BCL2 family members resulting in the assembling of the apoptotic effector proteins BAX and BAK in the outer mitochondrial membrane (Aubrey et al. 2018). The induction of BAX and BAK in turn induces the permeabilization of the outer mitochondrial membrane resulting in an extensive release of cytochrome C (Elmore 2007). Highly augmented cytochrome C levels induce the activation of caspase 9 through several intermediate steps. Caspase 9 is the most essential caspase of the intrinsic apoptosis

pathway and can cleave and activate caspase 3 which has several target proteins that are cleaved for subsequent progression of apoptosis.

The extrinsic pathway gets activated upon extracellular binding of so-called death ligands such as Fas ligand, tumor-necrosis factor (TNF), and TNF-related apoptosis-inducing ligand (TRAIL) to transmembrane receptors of the TNF receptor family (Elmore 2007). Following ligand binding and receptor activation, cytoplasmic adapter proteins including Fas-associated death domain (FADD) are recruited forming a stable multiprotein death-inducing signaling complex (DISC) by binding with caspase 8 (Figure 4). This binding leads to the activation of caspase 8, the central caspase of the extrinsic death receptor pathway (Kischkel et al. 1995). Subsequently, caspase 8 cleaves and activates caspase 3 resulting in the progression of apoptosis (Figure 4) (Elmore 2007).

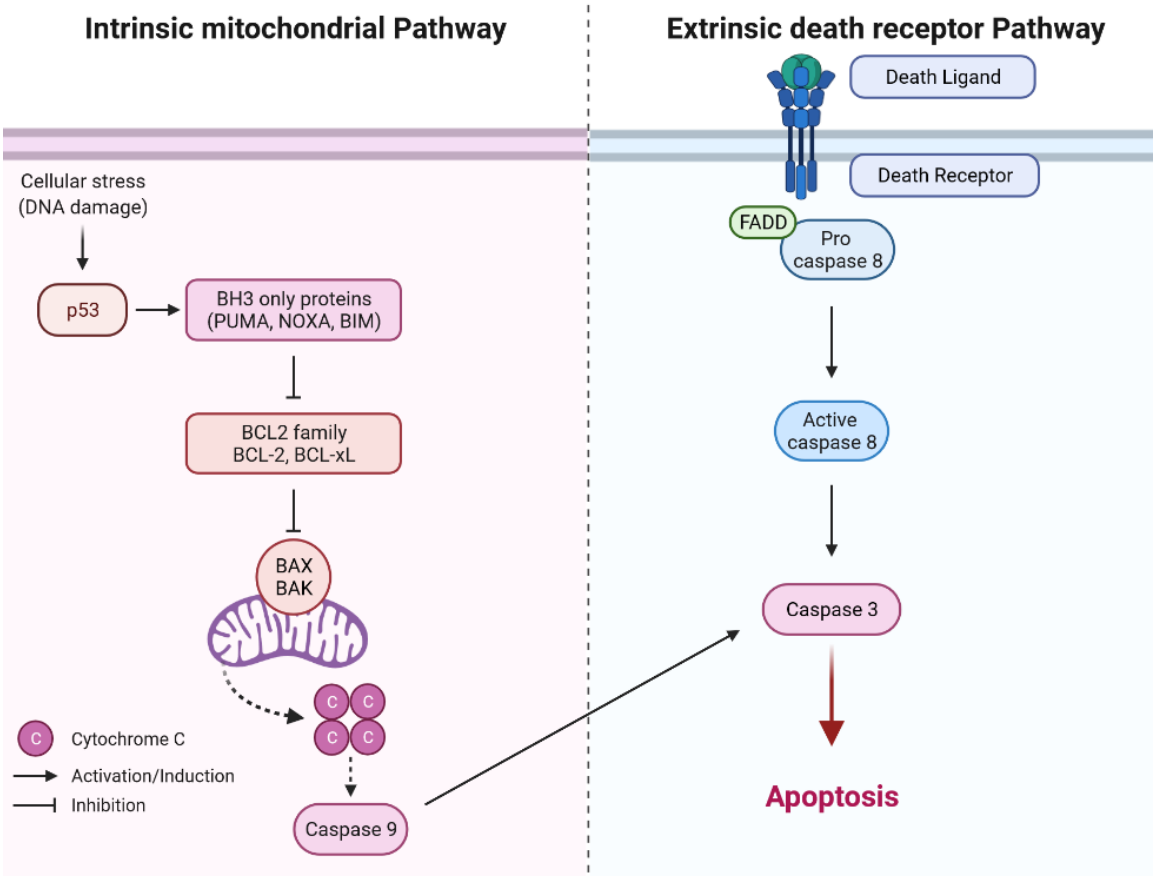

Figure 4: Schematic illustration of the intrinsic and extrinsic apoptosis pathway. Simplified overview of the intrinsic mitochondrial pathway (left) and the extrinsic death receptor pathway (right). Intrinsic mitochondrial pathway: Various pro-apoptotic signals (e.g., DNA damage) induce p53 signaling leading to activation of pro-apoptotic BH3 only proteins and inhibition of pro-survival BCL2 family proteins. *(Figure legend continued on next page).*

Subsequently, BAX and BAK are released and can induce pore formation into the outer mitochondrial membrane resulting in the release of cytochrome C which then activates caspase 9. Caspase 9 induces activation of caspase 3 leading to apoptosis. Extrinsic death receptor pathway: Upon extracellular binding of a death ligand (e.g., FAS ligand), the death receptor gets activated. The adapter protein Fas-associated death domain (FADD) induces caspase 8 activation, followed by caspase 3 activation and subsequent apoptosis progression. The figure was created with BioRender.com.

Given the DNA damage-inducing activity of several chemotherapeutic agents, these drugs can be utilized to force apoptotic processes in cancer cells to eliminate cancerous cells in a programmed and coordinated manner. However, malignant cells harbour of mutations and mechanisms to evade apoptosis. Not surprisingly, almost 100% of all PDAC patients carry mutations associated with apoptosis pathways including mutations in *TP53* demonstrating the significance of pro-apoptotic processes in cancer therapy but also the escape mechanisms of cancer cells to conquer drug-induced apoptotic processes (Jones et al. 2008).

1.4 Molecular Subtyping of PDAC

Given the diverse genetic and epigenetic heterogeneity and the therapy resistance frequently observed in PDAC, molecular subtyping approaches were conducted to identify similarities and differences in the molecular characteristics of different PDAC patients. Various collaborative studies aimed to classify PDAC to elucidate novel therapeutic options and to optimize overall survival upon PDAC therapy. Based on the success of classifying other tumor entities as exemplified by gastric cancer, breast cancer, and lung cancer in the past years (Alexandrov et al. 2015, Bettaieb et al. 2017, Politi and Herbst 2015) whole-genome sequencing studies and transcriptional profiling analyses were performed in PDAC to also identify molecular subgroups of PDAC (Collisson et al. 2011, Biankin et al. 2012, Moffitt et al. 2015, Bailey et al. 2016, Raphael et al. 2017, Puleo et al. 2018, Chan-Seng-Yue et al. 2020). Indeed, mainly based on transcriptomic profiles, and partially on different mutations, PDAC can be generally categorized into two transcriptional subtypes: basal-like and classical subtype. The basal-like subtype includes previously identified subtypes, such as quasi-mesenchymal (Collisson et al. 2011), squamous (Bailey et al. 2016), and pure-basal (Puleo et al. 2018) subtypes and is associated with undifferentiated histology, increased chemoresistance, and worst prognosis (Aung et al. 2018, Moffitt et al. 2015). On the contrary, the classical subtype includes earlier named subtypes like pancreatic

progenitor (Bailey et al. 2016) and pure classical (Puleo et al. 2018) subtype and is associated with better-differentiated histology, improved responsiveness to chemotherapy, and a better overall prognosis (Aung et al. 2018).

Besides the subtype-specific differences in chemosensitivity and prognosis, basal-like and classical subtypes also differ on a molecular level with differences in the expression of gene signatures and epigenetic alterations. The basal-like subtype for instance reveals a more mesenchymal gene expression profile, whereas the classical subtype shows an epithelial gene signatures (Bailey et al. 2016, Collisson et al. 2011, Biankin et al. 2012, Moffitt et al. 2015, Raphael et al. 2017, Puleo et al. 2018, Chan-Seng-Yue et al. 2020, Aung et al. 2018, Lomberk et al. 2018).

Additionally, specifically, the expression of distinct super enhancers and their upstream regulators are unique for each subtype (Lomberk et al. 2018). While the classical subtype is highly dependent on numerous distinct super enhancers (250), the basal-like subtype relies only on some (30) of them. As crucial regulatory elements, super enhancers strongly regulate cell- and state-specific functions through binding with specific transcription factors (Pott and Lieb 2015, Whyte et al. 2013). Consequently, molecular stratification followed by a subtype-specific PDAC treatment provides the opportunity for personalized medicine (Aung et al. 2018)

The most crucial transcription factors controlling classical subtype-specific gene signatures are GATA6, PDX1, BMP1, and HNFs, thereby altering pancreatic morphogenesis (Lomberk et al. 2018, Lomberk et al. 2019). Whereas basal-like subtype-specific super enhancers are predominantly controlled by MET, ΔNp63, and MYC resulting in altering pathways involved in proliferation and epithelial-mesenchymal transition (EMT) (Lomberk et al. 2018, Lomberk et al. 2019, Hamdan and Johnsen 2018, Somerville et al. 2018, Andricovich et al. 2018). Recently, it has been shown that these distinct subtype-specific transcription factors are under strong epigenetic control by either acting as transcriptional co-regulators or influencing their expression (Patil et al. 2020, Andricovich et al. 2018). These findings provide the opportunity to force a switch in the subtype identity by altering these subtype-determining factors by interfering with the epigenetic machinery (Patil et al. 2020, Andricovich et al. 2018). Indeed, the dynamic character of epigenetic mechanisms leads to a high plasticity between the basal-like and the classical subtype. Accordingly, targeting subtype-specific pathways and expression profiles on an epigenetic level offers strategies to identify novel vulnerabilities in PDAC therapy. Especially the reversibility of epigenetic regulations and the availability of epigenetic inhibitors in clinical application render epigenetic therapy a hopeful strategy to sensitize PDAC subtypes to cancer therapy. However, only if the entire

complexity of the diverse plasticity has been fully understood it will be feasible to introduce safe and effective therapeutic approaches aiming at epigenetics.

1.5 The epigenetic regulatory protein EZH2

Epigenetic processes

In addition to the well-characterized genetic mutations including the driver mutations of *KRAS, CDKN2A*, *TP53,* and *DPC4*, epigenetic alterations also highly contribute to pancreatic cancer development and progression (Figure 1: Schematic illustration of the histopathological carcinogenesis of PDAC.Figure 1) as well as to PDAC subtype identity (see *1.4 Molecular Subtyping of PDAC*, p. 12) (Chen et al. 2015, Mazur et al. 2015, Roe et al. 2017, Lomberk et al. 2019). In contrast to genetic alterations, epigenetic alterations do not result in changes in the DNA nucleotide sequence but in heritable but reversible alterations of the gene expression. These alterations in gene expression are achieved through distinct mechanisms, including non-coding RNAs, DNA methylation, and chromatin modifications and remodeling processes (Roy et al. 2014). While non-coding RNAs post-transcriptionally affect gene expression by decreasing mRNA stability, DNA methylation, as well as chromatin modification and remodeling processes result in the activation or repression of gene transcription through influencing the accessibility of the transcription machinery to specific genes by loosening or condensing DNA packaging, respectively (Hessmann et al. 2017).

Given the crucial role of epigenetic mechanisms in gene transcription and their effects on cellular processes, epigenetic and transcriptional dysregulation can be frequently found in PDAC and strongly correlates with accelerated carcinogenesis, tumor progression, and metastasis formation (Mallen-St Clair et al. 2012, Roy et al. 2014, Lomberk and Urrutia 2015, Bailey et al. 2016, McDonald et al. 2017, Roe et al. 2017). Importantly, epigenetic mechanisms are highly dynamic and even reversible, thereby providing a powerful tool to alter gene expression in a context-dependent manner aiming at inducing tumor-suppressive processes and functions in cancer therapies. Indeed, preclinical and clinical studies of pharmacological inhibition of epigenetic processes reveal promising therapeutic strategies for identifying new tumor vulnerabilities or sensitizing cancer cells for chemotherapy (Hessmann et al. 2017, Orth et al. 2019, Hessmann et al. 2020). Currently, several clinical trials are ongoing examining the clinical use of epigenetic inhibitors (Hessmann et al. 2020, Versemann et al. 2022). However, especially in PDAC the effective use is far from being clinical routine.

DNA methylation represents one epigenetic mechanism leading to stable gene silencing, especially when it occurs in the DNA promoter region (Kulis and Esteller 2010). It is mediated by the covalent binding of methyl groups to the DNA caused by DNA-methyltransferases (DNMTs) (Kulis and Esteller 2010). Interestingly, common tumor-suppressor genes, including *CDKN2A*, are hypermethylated in various cancer types, thereby permanently repressing their expression (Iguchi et al. 2016, Arya et al. 2017, Zhou et al. 2017, Serra and Chetty 2018, Lin et al. 2020). To conquer the repression of tumor suppressor genes mediated by DNA methylation in PDAC, DNMTs might be potential targets to inhibit. However, previous findings reveal controversial results of the inhibition of DNA methylation demonstrating the tight context-dependency of epigenetic mechanisms (Shakya et al. 2013, Kohi et al. 2016).

Besides DNA methylation, histone remodeling processes and modifications contribute to the control of chromatin conformation, thereby altering non-covalent interactions of so-called nucleosomes. These nucleosomes are the essential unit of the chromatin consisting of 147 bp DNA twisted around an octameric structure of eight histones (two histones each of H2A, H2B, H3, and H4) (Roy et al. 2014, Hessmann et al. 2017). Nucleosome remodeling alters the whole chromatin architecture by shifting nucleosomes in an ATP-dependent manner achieved by huge multiprotein complexes, such as the switch/sucrose non-fermentable chromatin (SWI/SNF) complex (Hasan and Ahuja 2019). Interestingly, alterations of members of the SWI/SNF complex occurred in 14% of all PDAC patients associated with poor survival and altered susceptibility towards DNA crosslinking agents. These findings demonstrate the significant role of epigenetic alterations in PDAC prognosis and therapy response prediction (Bailey et al. 2016, Yoon et al. 2019, Hasan and Ahuja 2019, Davidson et al. 2018).

Histone modifications including acetylation, methylation, ubiquitination, and phosphorylation are mediated by histone-modifying proteins which generally can be classified into ‘writers’, ‘eraser’, or ‘readers’ which add, eradicate, or detect histone modifications, respectively (Roy et al. 2014, Hessmann et al. 2017). Histone acetylation is a typical histone mark for open chromatin and active gene transcription (Sterner and Berger 2000). The addition of acetyl groups is mediated by histone acetyltransferases (HAT), whereas the removal is regulated by histone deacetylases (HDAC). Bromodomain and extra-terminal domain family (BET) proteins detect acetylated histone residues, thereby belonging to the group of chromatin ‘readers’ (Hessmann et al. 2017). Interestingly, epigenetic processes involved in histone acetylation are frequently found to be altered and imbalanced in PDAC associated with PDAC development and progression (Glozak and Seto 2007, Ouaïssi et al. 2014).

Consequently, interference with factors involved in histone acetylation moved the focus of PDAC therapy. Particularly, BET inhibitors reveal a promising PDAC treatment strategy by significantly impeding tumor growth *in vivo* predominately in combination with HDAC inhibitors (Sahai et al. 2014, Mazur et al. 2015, Garcia et al. 2016). However, despite these promising results, BET inhibitors are still not used as clinical standard therapy in PDAC (Krantz and O'Reilly 2018).

In addition to these histone acetylation-associated proteins, also methylation of histones, particularly at lysine residues, contributes to epigenetic alterations. In contrast to histone acetylation which is generally associated with open chromatin and active gene transcription, histone methylation results either in gene activation or repression depending on the specific localization and the number of methyl groups added (Dambacher et al. 2010). The methylation of histones is installed by lysine methyltransferases (KMTs) and arginine methyltransferases (PRMTs) methylating either lysine or arginine residues, respectively (Di Lorenzo and Bedford 2011). On the contrary, lysine demethylases (KDMs) remove methylation marks (Hessmann et al. 2017).

EZH2 – a methyltransferase

A key player in the methylation of histones is the polycomb (PcG) repressive complex 2 (PRC2). PRC2 is formed out of four subunits: enhancer of zeste homolog 2 (EZH2), suppressor of zeste 12 (Suz12), embryonic ectoderm development (EED), and the histone binding domain RaAp46/48 (Figure 5). EZH2 represents the catalytic active domain of the PRC2 complex. Canonically, EZH2 mediates trimethylation of histone 3 at lysine 27 (H3K27me3) installed by the C-terminal SET domain, conserved in nearly all lysine methyltransferases (Figure 5) (Cao et al. 2002, Viré et al. 2006). Subsequently, polycomb repressive complex 1 (PRC1) recognizes and binds locally accumulated H3K27me3, finally resulting in gene silencing (Margueron et al. 2009, Pasini et al. 2004, Cao and Zhang 2004).

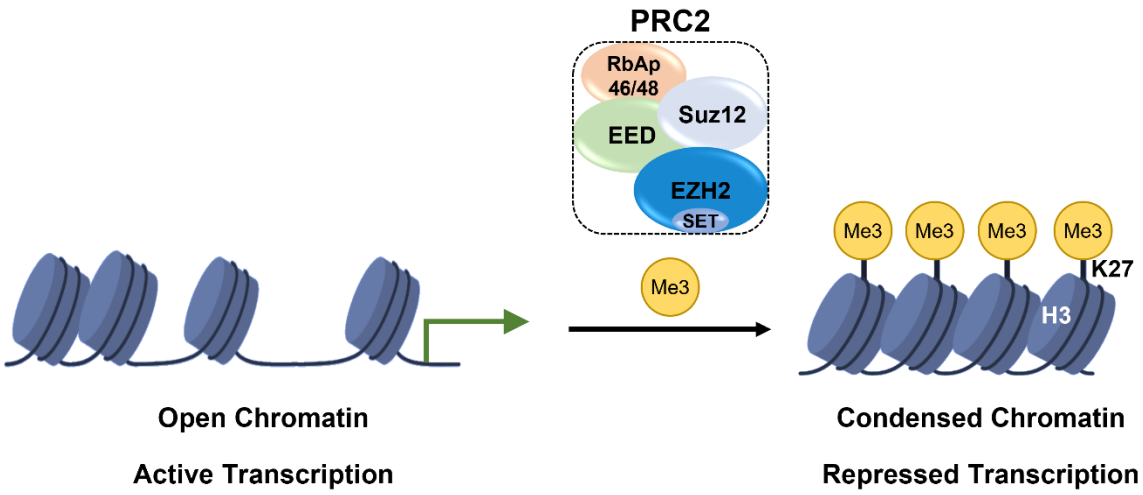

Figure 5: Schematic illustration of EZH2 activity. Enhancer of zeste homolog 2 (EZH2) mediates trimethylation of histone 3 at lysine 27 (H3K27me3) installed by the SET domain, thus leading to condensed chromatin resulting in gene repression. Together with the suppressor of zeste 12 (Suz12), the embryonic ectoderm development (EED) and the histone binding domain RaAp46/48, EZH2 forms the polycomb repressive complex 2 (PRC2). The figure was created with BioRender.com.

However, EZH2 also comprises non-canonical functions. It has been shown that EZH2 post-translationally methylates different transcription factors such as RAR-related orphan receptor alpha (RORα) and GATA4 (He et al. 2012, Lee et al. 2012). Moreover, EZH2 does not only contain repressive but also activating functions, as exemplified through activation of STAT3 in glioblastoma or co-activation of androgen receptors by physical interaction in prostate carcinoma leading to the activation of downstream signaling (Kim et al. 2013b, Xu et al. 2012).

EZH2 in PDAC

As part of the PRC2 complex, EZH2 reveals crucial functions during tissue development in establishing cell identity (Avan et al. 2012). However, EZH2 is frequently overexpressed in various solid cancer entities, including breast, prostate, gastric, and lung cancer (Kleer et al. 2003, Varambally et al. 2002, Matsukawa et al. 2006), mostly associated with poor prognosis, early pathogenic onset, and tumor progression (Wang et al. 2016, Huqun et al. 2012). Accordingly, low EZH2 expression levels are related to metastasis-free survival in breast cancer (Kleer et al. 2003). Importantly, in PDAC as well, EZH2 is found to be highly expressed mediating oncogenic functions associated with high tumor grading and worse

survival (Chen et al. 2017, Ougolkov et al. 2008). Recently, it has been shown that EZH2 fosters pro-tumorigenic processes by controlling proliferation, clonogenicity, cellular plasticity and dedifferentiation *in vitro* as well as mediating PDAC development and progression *in vivo* (Chen et al. 2017, Patil et al. 2020). Furthermore, EZH2 expression and activity correlated with a more aggressive and invasive PDAC phenotype. Mechanistically, EZH2 silences *GATA6* expression thereby counteracting less aggressive classical PDAC subtype identity (Patil et al. 2020).

Consequently, EZH2 inhibitors such as tazemetostat (EPZ-6438) have been developed and are in clinical trials for hematological and solid malignancies, including PDAC (Hessmann et al. 2020, Versemann et al. 2022). However, the strong context-dependency of epigenetic processes and their inhibition suggest that the precise context-determining conditions of EZH2 inhibition should be examined before clinical use and that the inhibition needs to be carefully conducted. In colorectal and ovarian cancer, for instance, beneficial outcome of EZH2 inhibition was predominantly restricted to tumor subtypes bearing an inactivation of the SWI/SNF complex (Kim et al. 2015, Bitler et al. 2015). However, our knowledge about context-determining mechanisms in PDAC is incomplete. Hence, deeper mechanistic and functional insights into context-determining conditions need to be elucidated to safely use EZH2 inhibitors and predict their clinical outcome.

1.6 Aim of this study

Epigenetic processes highly contribute to PDAC carcinogenesis, tumor progression, and metastasis formation (Mazur et al. 2015, Roe et al. 2017). Importantly, these epigenetic alterations constitute dynamic plasticity and reversibility rendering epigenetic processes promising targets for PDAC therapy (Hessmann et al. 2017, Versemann et al. 2022). EZH2 is the catalytic active domain of the PRC2 complex mediating gene repression (Viré et al. 2006). Notably, EZH2 is regularly found to be highly expressed in PDAC generally mediating oncogenic functions (Ougolkov et al. 2008). However, given the strong context-dependency of epigenetic processes in general and EZH2, in particular (Hessmann et al. 2017, Ougolkov et al. 2008, Bremer et al. 2021), precise and in-depth analyses are indispensable in finding context-determining factors influencing EZH2 activity. Specifically, the diverse and heterogeneous genetic alterations occurring in PDAC impacts epigenetic processes in PDAC (Waddell et al. 2015, Bailey et al. 2016). Consequently, a comprehensive mechanistic and functional understanding of crucial genetic events is necessary to elucidate EZH2

activity in PDAC progression and maintenance to predict the consequences of EZH2 inhibition in PDAC.

The tumor suppressor p53 is well characterized for anti-tumorigenic capacities including cell cycle arrest, senescence, and apoptosis (Vousden and Lu 2002). However, *TP53* mutations occur with a prevalence of 50-80% resulting in the loss of tumor suppressor function and oncogenic GOF (Waddell et al. 2015, Bailey et al. 2016, Freed-Pastor and Prives 2012). Hence, the functional behaviour of a cell highly depends on its *TP53*-status. However, whether and to what extent mutations of the *TP53* gene indeed mechanistically or functionally influence epigenetic processes in general and EZH2 activity in particular remains mainly elusive. Therefore, this study aimed at:

I Characterizing the impact of the *TP53*-status on EZH2-dependent target gene regulation.

II Determining the functional consequences and the therapeutic potential of EZH2 inhibition with regard to the *TP53*-status.

III Elucidating the molecular mechanism of a potential EZH2-dependent p53 regulation

IV Examining potential non-canonical functions of EZH2 involved in PDAC progression and maintenance.

Together, our studies will scrutinize the *TP53*-status dependent EZH2 activity in PDAC progression and maintenance to assess whether molecular stratification for the *TP53*-status is required for a successful application of EZH2 inhibition in PDAC treatment.

2 Material and Methods

2.1 Material

2.1.1 Laboratory Equipment, Consumables, Chemicals, and Kits

Table 1: List of Laboratory Equipment

Laboratory Equipment	Company
BD FACSCanto II	BD Bioscience, Heidelberg, Germany
ChemoStar ECL Imager	Intas Science Imaging Instruments, Goettingen, Germany
Double Distilled Water System: Arium pro UV Ultrapure	Sartorius, Goettingen, Germany
Dri-Block Heater DB2A	Techne, Staffordshire, UK
Fluorescence Microscope System for Advanced Imaging Widefield Systems	Leica Biosystems, Wetzlar, Germany
Fridge +4 °C	Liebherr, Bulle, Switzerland
Freezer -20 °C	Liebherr, Bulle, Switzerland
Freezer -80 °C	Sanyo, Moriguchi, Japan
Freezer -150 °C	PHC Corporation of North America, Chicago, USA
FTA-1 Aspirator with trap flask	Grant Instruments, Shepreth, UK
Heracell 240i CO_2 incubator	Thermo Fisher Scientific, Waltham, USA
IKAMAG Magnetic Stirrer RCT	IKA, Staufen, Germany
Light microscope BX43	Olympus, Shinjuku, Japan
Light Microscope CKX53	Olympus, Shinjuku, Japan
Mettler Toledo FE20 FiveEasy Benchtop pH Meter	Thermo Fisher Scientific, Waltham, USA
Microtome RM2265	Leica Biosystems, Wetzlar, Germany
Microwave NN-E209W	Panasonic, Kadoma, Japan
Mini-PROTEAN Tetra Cell	Bio Rad Laboratories, Hercules, USA
MSA Minishaker	IKA, Staufen, Germany
Multifuge X1 Centrifuge Series	Thermo Fisher Scientific, Waltham, USA
Multipette plus	Eppendorf, Hamburg, Germany
NanoPhotometer P-330	Intas Science Imaging Instruments, Goettingen, Germany
Neubauer counting chamber	Assistant, Sondheim/Rhön, Germany
Paraffin embedding station EG 1150H	Leica Biosystems, Wetzlar, Germany
PerfectSpin 24R Refrigerated Microcentrifuge	Peqlab, Erlangen, Germany
PHOmo Microplate Reader	Autobio, Zhengzhou, China

Pipetboy acu 2	INTEGRA Biosciences, Biebertal, Germany
PowerPac Basic Power Supply	Bio Rad Laboratories, Hercules, USA
Precision balance PCB	Kern & Sohn, Balingen, Germany
PSU-20i Orbital Shaking Platform	Grant Instruments, Shepreth, UK
Safe 2020 Class II Biological Safety Cabinets	Thermo Fisher Scientific, Waltham, USA
Scotsman AF80 Ice Flaker	Hubbard Systems, Suffolk, UK
Sequenza slide rack	Ted Pella, Redding, USA
Shandon coverplate	Thermo Scientific, Waltham, USA
Sprout Minicentrifuge	Biozym Scientific, Hessich Oldendorf, Germany
StepOnePlus Real-Time PCR System	Thermo Fisher Scientific, Waltham, USA
Thermomixer 5436	Eppendorf, Hamburg, Germany
Tissue float bath GFL 1052	Gesellschaft für Labortechnik, Burgwedel, Germany
Tissue processor TP1020	Leica Biosystems, Wetzlar, Germany
Trans-Blot Turbo Transfer System	Bio Rad Laboratories, Hercules, USA
TX-400 4 x 400mL Swinging Bucket Rotor	Thermo Fisher Scientific, Waltham, USA
Universal Oven UN55	Memmert, Schwabach, Germany
VacuuHandControl VHC^{pro}	Vacuumbrand, Wertheim, Germany
Vacuum pump: BVC Control	Vacuumbrand, Wertheim, Germany
Water Bath	Memmert, Schwabach, Germany

Table 2: List of Consumables

Material	**Company**
Cell Culture Flask (T25, T75, T175)	Greiner Bio One, Kremsmünster, Austria
Cell Culture multi-well plate (6-, 12-, 96-well)	Greiner Bio One, Kremsmünster, Austria
Cell Scrapers	Sarstedt, Nümbrecht, Germany
Combitips advanced 1.0 ml	Eppendorf, Hamburg, Germany
Cover glasses	Th. Geyer Ingredients, Hoexter, Germany
Cover Slip	Th. Geyer Ingredients, Hoexter, Germany
Falcon Tubes 15 ml, 50 ml	Sarstedt, Nümbrecht, Germany
Liquid blocker Super PAP-Pen	Dako, Jena, Germany
MicroAmp Fast Optical 96-Well Reaction Plate	Thermo Fisher Scientific, Waltham, USA
MicroAmp Optical Adhesive films	Thermo Fisher Scientific, Waltham, USA
Nitrocellulose Membrane	Bio Rad Laboratories, Hercules, USA

Paraffin wax	Sasol Wax, Hamburg, Germany
PCR reaction tubes	Sarstedt, Nümbrecht, Germany
Pipette tips (10 µl, 200 µl, 1000 µl)	StarLab, Hamburg, Germany
Pipette filter tips (10 µl, 200 µl, 1000 µl)	StarLab, Hamburg, Germany
Polystyrene FACS tubes	Thermo Fisher Scientific, Waltham, USA
Polystyrene Tube with Screw Cap	Greiner Bio One, Kremsmünster, Austria
Reaction Cups 0.5 ml, 1.5 ml, 2 ml	Sarstedt, Nümbrecht, Germany
Serological Pipettes 2 ml, 5 ml, 10 ml, 25 ml, 50 ml	Sarstedt, Nümbrecht, Germany
Superfrost Plus slides	Thermo Fisher Scientific, Waltham, USA

Table 3: List of Chemicals and Reagents

Chemicals/Reagents	**Company**
4',6-diamidino-2-phenylindole (DAPI)	Sigma-Aldrich, St. Louis, USA
Agarose A Beads	Merck Millipore, Billerica, USA
Agarose G Beads	Merck Millipore, Billerica, USA
Ammonium persulfate (APS)	Sigma-Aldrich, St. Louis, USA
Ampuwa	Fresenius Kabi, Bad Homburg, Germany
Annexin-V-Binding Buffer	BioLegend, San Diego, USA
Bovine Serum Albumin (BSA)	Sigma-Aldrich, St. Louis, USA
Bromophenol blue	Sigma-Aldrich, St. Louis, USA
Chloroform	Carl Roth, Karlsruhe, Germany
Citric acid monohydrate	Carl Roth, Karlsruhe, Germany
Complete Protease Inhibitor Cocktail	Roche, Basel, Switzerland
Dimethyl sulfoxide (DMSO)	Sigma-Aldrich, St. Louis, USA
Dithiothreitol (DTT)	Sigma-Aldrich, St. Louis, USA
Eosin	Sigma-Aldrich, St. Louis, USA
Ethanol	Sigma-Aldrich, St. Louis, USA
Ethylene glycol-bis(2-aminoethylether)-*N,N,N′,N′*-tetraacetic acid (EGTA)	Sigma-Aldrich, St. Louis, USA
Ethylenediaminetetraacetate (EDTA)	Thermo Fisher Scientific, Waltham, USA
Fluorescence Mounting Medium	Thermo Fisher Scientific, Waltham, USA
Glycerine	Carl Roth, Karlsruhe, Germany
Glycine	Carl Roth, Karlsruhe, Germany
Haematoxylin	Merck, Darmstadt, Germany
Hydrogen peroxide 30 % (H_2O_2)	Carl Roth, Karlsruhe, Germany
Hydroxyethyl piperazineethanesulfonic acid (HEPES)	Sigma-Aldrich, St. Louis, USA

Isopropanol	Sigma-Aldrich, St. Louis, USA
Leupeptin	Sigma-Aldrich, St. Louis, USA
Lipofectamine 2000	Thermo Fisher Scientific, Waltham, USA
Normal Goat Serum (NGS)	Abcam, Cambridge, UK
Normal mouse IgG	Santa Cruz Biotechnology, Santa Cruz, USA
Normal rabbit IgG	Santa Cruz Biotechnology, Santa Cruz, USA
PageRuler Prestained Protein Ladder	Thermo Fisher Scientific, Waltham, USA
Phenylmethylsulfonyl fluoride (PMSF)	Sigma-Aldrich, St. Louis, USA
Phosphate Buffered Saline (PBS)	Merck Millipore, Billerica, USA
Ponceau S Solution	Sigma-Aldrich, St. Louis, USA
Powdered milk	Carl Roth, Karlsruhe, Germany
Propidium Iodide (PI)	Thermo Fisher Scientific, Waltham, USA
Protein Assay Dye Reagent Concentrate	Bio Rad Laboratories, Hercules, USA
RNase A	Sigma-Aldrich, St. Louis, USA
Rotiphorese Gel 30 (37,5:1)	Carl Roth, Karlsruhe, Germany
silentFect Lipid	Bio Rad Laboratories, Hercules, USA
Sodium chloride (NaCl)	Sigma-Aldrich, St. Louis, USA
Sodium dodecyl sulfate (SDS)	Carl Roth, Karlsruhe, Germany
Sodium fluoride (NaF)	Sigma-Aldrich, St. Louis, USA
Sodium orthovanadate (NaO)	Carl Roth, Karlsruhe, Germany
Sodium phosphate (dibasic)	Sigma-Aldrich, St. Louis, USA
Sodium phosphate (monobasic)	Sigma-Aldrich, St. Louis, USA
Tetramethylethylenediamine (TEMED)	Bio Rad Laboratories, Hercules, USA
Tetrasodium Pyrophosphate Decahydrate ($Na_7P_2O_7$ * 10 H_2O)	Sigma-Aldrich, St. Louis, USA
Tris Base	Carl Roth, Karlsruhe, Germany
Tris-hydrochloric acid	Sigma-Aldrich, St. Louis, USA
Triton X-100	Carl Roth, Karlsruhe, Germany
TRIzol Reagent	Thermo Fisher Scientific, Waltham, USA
Tween20	Sigma-Aldrich, St. Louis, USA
Western Lightning Plus Enhanced Chemi-luminescence (ECL)	PerkinElmer, Waltham, USA
Western Lightning *Ultra*	PerkinElmer, Waltham, USA
Xylene	AppliChem, Darmstadt, Germany
β-mercaptoethanol	Merck Millipore, Billerica, USA

Table 4: List of utilized Kits

Kit name	Company
Bioanalyzer High Sensitivity DNA Analysis	Agilent, Santa Clara, USA
DAB ImmPACT	Vector Laboratories, Burlingame, USA
Duolink Proximity Ligation Assay	Sigma-Aldrich, St. Louis, USA
iScript cDNA Synthesis Kit	Bio Rad Laboratories, Hercules, USA
iTag Universal SYBR Green Supermix	Bio Rad Laboratories, Hercules, USA
M.O.M. (Mouse on Mouse) Immunodetection Kit	Vector Laboratories, Burlingame, USA
Masson's Trichrome Stain Kit	Polysciences, Warrington, USA
MycoAlert Mycoplasma Detection Kit	Lonza Group, Basel, Switzerland
Peroxidase Mouse IgG Vectastain ABC Kit	Vector Laboratories, Burlingame, USA
Peroxidase Rabbit IgG Vectastain ABC Kit	Vector Laboratories, Burlingame, USA
Qubit dsDNA HS Assaykit	Thermo Fisher Scientific, Waltham, USA
SureSelect^{QXT} Reagent Kit	Agilent, Santa Clara, USA
SureSelect$^{XT\ HS}$ Reagent Kit	Agilent, Santa Clara, USA
Trans-Blot Turbo RTA Midi Nitrocellulose Transfer Kit	Bio Rad Laboratories, Hercules, USA
TruSeq RNA Library Prep Kit v2 Set A, B	Illumina, San Diego, USA

2.1.2 Buffers and Solutions

Table 5: Buffers and Solutions

Buffer/Solution	Composition
Blocking Solution	5 g milk powder in 100 ml TBS-T (5 %)
Citrate buffer (pH 6.0)	10 mM citric acid monohydrate in H_2O
Laemmli sample buffer (5x)	225 mM Tris/HCl, pH 6.8 50 % Glycerine 5 % SDS 100 mM DTT 0.02 % bromophenol blue 5 % β-Mercaptothanol (added fresh) in H_2O

Lysis buffer (WCL)	50 mM HEPES, pH 7.5 – 7.9 150 mM NaCl 1 mM EGTA 10 % Glycerine 1 % TritonX-100 100 mM NaF 10 mM $Na_7P_2O_7$ * 10 H_2O in H_2O
Lysis buffer (WCL) plus components	Lysis buffer (WCL) 1x Complete Protease Inhibitor Cocktail 1 µM sodium orthovanadate (NaO) 1 µM NaF
PB (pH 7.4)	20 mM NaH_2PO_4 80 mM Na_2HPO_4 in H_2O
PB-T	PB 0.4 % Triton-X100
PBS	137 mM NaCl 2,7 mM KCl 8 mM Na_2HPO_4 1.5 mM KH_2PO_4 in H_2O
PBS-T	PBS 0.1 % Tween 20
Running Buffer, 10x	250 mM Tris base 50 % Glycine 1 % SDS in H_2O
Separation gel buffer (10 %) (“ready-to-use”)	25 ml Separation gel buffer (stock solution) 33.3 ml Acrylamide/ Bisacrylamide (30 %/0.8 %) 5 ml Glycerine 36.7 ml ddH_2O
Separation gel buffer (15 %) (“ready-to-use”)	25 ml Separation gel buffer (stock solution) 50 ml Acrylamide/ Bisacrylamide (30 %/0.8 %) 5 ml Glycerine 20 ml ddH_2O
Separation gel buffer (stock solution) (pH 8.8)	1.5 M Tris base 0,4 % SDS in H_2O
Stacking gel buffer (“ready-to-use”)	25 ml Stacking gel buffer (stock solution) 16 ml Acrylamide/ Bisacrylamide (30 %/0.8 %) 59 ml ddH_2O

Stacking gel buffer (stock solution) (pH 6.8)	0.5 M Tris base 0,4 % SDS in H_2O
TBS-T	20 mM Tris base, pH 7.6 137 mM NaCl 0.1 % Tween 20 in H_2O
Triton-200 buffer	50 mM Tris base, pH 8.5 200 mM NaCl 0.1 % Tween 20 in H_2O
Triton-200 buffer plus components	Triton-200 buffer 1x Complete Protease Inhibitor Cocktail 1 µM sodium orthovanadate (NaO) 1 µM NaF
Turbo-Blot Buffer	200 ml 5x TransferBuffer 200 ml Ethanol 600 ml ddH_2O

2.1.3 Cell Culture Reagents

Table 6: List of utilized cell lines

Cell line	Genotype (if relevant)	Species	p53 status
GöCDX5		Human	p53mut (R248W)
GöCDX13		Human	p53wt
Panc-1		Human	p53mut (R273H)
KC	*Kras^{G12D}*	Mouse	p53wt
KNPC	*Kras^{G12D};caNFATc1;Trp53$^{R172H/+}$*	Mouse	p53mut (R172H)
KNP^{null}C	*Kras^{G12D};caNFATc1;Trp53$^{\Delta/\Delta}$*	Mouse	p53 null
KPC	*Kras^{G12D};Trp53$^{R172H/+}$*	Mouse	p53mut (R172H)
NKC	*caNFATc1;Kras^{G12D}*	Mouse	p53wt

Table 7: Cell Culture Media and Reagents

Product	Company
Bovine pituitary extract	Thermo Fisher Scientific, Waltham, USA
Dulbecco's Modified Eagle Medium (DMEM)	Thermo Fisher Scientific, Waltham, USA
Epidermal growth factor	Sigma-Aldrich, St. Louis, USA
Fetal Calf Serum (FCS)	Sigma-Aldrich, St. Louis, USA
Keratinocyte-SFM	Thermo Fisher Scientific, Waltham, USA
Modified Eagle Medium (MEM) Non-Essential Amino Acids Solution (100X) (NEAA)	Thermo Fisher Scientific, Waltham, USA
Opti-Minimal Essential Medium (MEM)	Thermo Fisher Scientific, Waltham, USA
Penicillin-Streptomycin	Sigma-Aldrich, St. Louis, USA
Roswell Park Memorial Institute (RPMI) 1640 Medium	Thermo Fisher Scientific, Waltham, USA
Trypsin-EDTA (0.5 %)	Thermo Fisher Scientific, Waltham, USA

Table 8: Growth Media

Medium	Supplements	Used for
DMEM	10 % FCS 1 % NEAA	KC, KNPC, KNP^{null}C, KPC, NKC
DMEM	10 % FCS	Panc-1
Keratinocyte-SFM: RPMI (in 3:1 ratio)	2 % FCS 1 % Penicillin-Streptomycin Bovine pituitary extract Epidermal growth factor	GöCDX5, GöCDX13

Table 9: List of small interfering RNA (siRNA)

Target	Company	ID
Eed	Ambion	159465
EZH2	Ambion	61436
Mdm2	Ambion	68152
Negative Control	Ambion	4635
Suz12	Ambion	186542
p19^{Arf}	Ambion	262856

Table 10: List of utilized DNA vectors

Plasmids	Back-bone	Origin
pCEP4	pCEP4	Pietenpol et al. 1994, kindly gifted by Prof. Matthias Dobbelstein, University Medical Center, Goettingen
VP1680-p53	pCEP4	Pietenpol et al. 1994, kindly gifted by Prof. Matthias Dobbelstein, University Medical Center, Goettingen
p53-343CC	pCEP4	Pietenpol et al. 1994, kindly gifted by Prof. Matthias Dobbelstein, University Medical Center, Goettingen
VP1680-p53-343CC	pCEP4	Pietenpol et al. 1994, kindly gifted by Prof. Matthias Dobbelstein, University Medical Center, Goettingen
pCMV	pCMV	Kindly gifted by Prof. Matthias Dobbelstein, University Medical Center, Goettingen
p53wt	pCMV	Kindly gifted by Prof. Matthias Dobbelstein, University Medical Center, Goettingen
p53mut	pCMV	Kindly gifted by Prof. Matthias Dobbelstein, University Medical Center, Goettingen

Table 11: List of pharmacological Inhibitors

Inhibitor	Usage	Concentration	Time	Control	Company
5-fluorouracil (5-FU)	Apoptosis induction	10 µM	24 h	DMSO	Sigma-Aldrich, St. Louis, USA
Cyclo-heximide	Protein trans-lation inhibitor	20 mg/ml	7-18 min	H_2O	Cell Signaling Technology, Cambridge, UK
MG132	Proteasome inhibitor	10 µM	1 h	DMSO	Merck Millipore, Billerica, USA
Staurosporine (STS)	Apoptosis induction	500 nM	24 h	DMSO	Cell Signaling Technology, Cambridge, UK
Tazemetostat (EPZ-6438)	EZH2 inhibitor	750 nM	72 h	DMSO	ChemieTek, In-dianapolis, USA

2.1.4 Oligonucleotides

Table 12: List of Primers for qRT-PCR

Target	Direction	Sequence
Cdkn2a	forward	CGCAGGTTCTTGGTCACTGT
Cdkn2a	reverse	TGTTCACGAAAGCCAGAGCG
Ezh2	forward	CAACCCGAAAGGGCAACAAA
Ezh2	reverse	ACC AGT CTG GAT AGC CCT CT
Itgb5	forward	GAAGTGCCACCTCGTGTGAA
Itgb5	reverse	GGACCGTGGATTGCCAAAGT
Ltbp1	forward	GGTCGCATCAAGGTGGTCTTT
Ltbp1	reverse	GTGGTGGTATTCCCCTTCTGG
Rnf130	forward	CTGCCCATCCACGGAGTTG
Rnf130	reverse	CAAGGCGATCCACTGTTTGA
Rplp0	forward	TGGGCAAGAACACCATGATG
Rplp0	reverse	AGTTTCTCCAGAGCTGGGTTGT
Trp53	forward	AGGTGTGCGTAGCACC
Trp53	reverse	CCCCACAACACCAGTG
Wnt7b	forward	CTTCACCTATGCCATCACGG
Wnt7b	reverse	TGGTTGTAGTAGCCTTGCTTCT

Table 13: List of Primers for qRT-PCR following ChIP experiments

Target	Direction	Sequence
Cdkn2a TSS	forward	GACCGTGAAGTTCAGC
Cdkn2a TSS	reverse	GGGGTCGCTTCTTCGG

2.1.5 Antibodies

Table 14: List of Antibodies used for Western Blotting

Antibody	Dilution	Species	Company	Number
Primary Antibody				
Actin-HRP	1:40000	Mouse	Sigma-Aldrich, St. Louis, USA	A3854
Cleaved caspase 3	1:500	Rabbit	Cell Signaling Technology, Cambridge, UK	9661
Eed	1:1000	Rabbit	Merck Millipore, Billerica, USA	09-774
ERK1/2	1:1000	Rabbit	Cell Signaling Technology, Cambridge, UK	9102

EZH2	1:1000	Rabbit	Cell Signaling Technology, Cambridge, UK	5246
H3	1:1000	Rabbit	Abcam, Cambridge, UK	1791
H3K27me3	1:500	Rabbit	Cell Signaling Technology, Cambridge, UK	9733
Mdm2	1:250	Mouse	Santa Cruz Biotechnology, Santa Cruz, USA	965
$p19^{Arf}$	1:250	Rat	Santa Cruz Biotechnology, Santa Cruz, USA	32748
p21	1:200	Mouse	Santa Cruz Biotechnology, Santa Cruz, USA	6246
p53	1:1000	Mouse	Cell Signaling Technology, Cambridge, UK	2524
p53-HRP	1:1000	Mouse	Novus Biologicals, Littleton, USA	NB200-103H
PARP	1:1000	Rabbit	Cell Signaling Technology, Cambridge, UK	9542
Suz12	1:1000	Rabbit	Cell Signaling Technology, Cambridge, UK	3737
Secondary Antibody				
Anti-mouse (IgG) HRP	1:6500	Horse	Cell Signaling Technology, Cambridge, UK	7076
Anti-rabbit (IgG) HRP	1:6500	Goat	Cell Signaling Technology, Cambridge, UK	7074
Anti-rat (IgG) HRP	1:5000	Goat	Santa Cruz Biotechnology, Santa Cruz, USA	2006

Table 15: List of Antibodies utilized for Chromatin immunoprecipitation (ChIP)

Antibody	Amount	Species	Company	Number
EZH2	2 µg	Rabbit	Diagenode, Denville, USA	C15410039-classic
H3K4me3	2 µg	Rabbit	Cell Signaling Technology, Cambridge, UK	9751
Rabbit IgG	2 µg	Rabbit	Diagenode, Denville, USA	C15410206

Table 16: List of Antibodies utilized for Immunoprecipitation (IP)

Antibody	Amount	Species	Company	Number
EZH2	6 µl	Rabbit	Cell Signaling Technology, Cambridge, UK	5246
p53	6 µl	Mouse	Cell Signaling Technology, Cambridge, UK	2524
p53	6 µl	Mouse	Novus Biologicals, Littleton, USA	NB200-103
Mouse IgG	3 µl	Mouse	Santa Cruz Biotechnology, Santa Cruz, USA	2025
Rabbit IgG	2 µl	Rabbit	Merck Millipore, Billerica, USA	12-370

Table 17: List of Antibodies utilized for Immunohistochemistry (IHC)

Antibody	Dilution	Species	Company	Number
EZH2 (mouse)	1:100	Rabbit	Cell Signaling Technology, Cambridge, UK	5246
EZH2 (human)	1:50	Mouse	Leica Biosystems, Wetzlar, Germany	NCL-L-EZH2
Ki-67	1:600	rabbit	Thermo Fisher Scientific, Waltham, USA	RM9106
αSMA	1:100	Mouse	Agilent, Santa Clara, USA	M0851
$p14^{ARF}$	1:400	Mouse	Cell Signaling Technology, Cambridge, UK	2407

Table 18: List of Antibodies utilized for Immunofluorescence (IF)

Antibody	Dilution	Species	Company	Number
Primary Antibody				
$p19^{Arf}$	1:100	Rat	Santa Cruz Biotechnology, Santa Cruz, USA	32748
Secondary Antibody				
Anti-mouse (IgG) HRP	1:500	Donkey	Invitrogen, Carlsbad, USA	A21208

Table 19: List of Antibodies utilized for Proximity Ligation Assay (PLA)

Antibody	Dilution	Species	Company	Number
EZH2	1:100	Mouse	Cell Signaling Technology, Cambridge, U K	3147
p53 (FL393)	1:500	Rabbit	Santa Cruz Biotechnology, Santa Cruz, USA	6243

2.1.6 Software and Databases

Table 20: List of utilized Software and Databases

Software	Company/Reference
Adobe Illustrator	Adobe, San José, USA
Adobe Photoshop	Adobe, San José, USA
AUTOsoft 2.6	Autobio, Zhengzhou, China
BD FACSDIVA Software	BD Bioscience, Heidelberg, Germany
Bioinformatics & Evolutionary Genomics (Venn Diagram)	http://bioinformat-ics.psb.ugent.be/webtools/Venn/
cellSense Software	Olympus, Shinjuku, Japan
Chemostar Software	Intas Science Imaging Instruments, Goettingen, Germany
Cuffdiff, 2.2.1	(Trapnell et al. 2012)
Cuffnorm 2.2.1.1	(Ghosh and Chan 2016)
DESeq2, 1.22.1	(Anders and Huber 2010, Love et al. 2014)
Enrichr	maayanlab.cloud/Enrichr/ (Xie et al. 2021, Kuleshov et al. 2016, Chen et al. 2013)
Fiji	(Schindelin et al. 2012)
FlowJo	FlowJo LLC, USA
Gene Set Enrichment Analysis (GSEA), 4.0.3	(Subramanian et al. 2005, Mootha et al. 2003)
ggplot2, 3.3.5	(Wickham 2016)
GraphPad PRISM 8	GraphPad Software, La Jolla, USA
HTSeq, 0.9.1	(Anders et al. 2015)
ImageJ 1.50i	Wayne Rasband, National Institute of Health, USA
Leica Application Suite (LAS) X Software	Leica Camera, Wetzlar, Germany
NanoPhotometer P-Class PVC Software	Intas Science Imaging Instruments, Goettingen, Germany
Pheatmap, 1.0.12	(Kolde 2019)
R Project, 4.0.0	(RCoreTeam 2021)
R Studio, 1.2.5042	R Studio Team, Bosten USA (RStudioTeam 2020)
Sequence Pilot Software	JSI Medical Systems GmbH
StepOne Software	Thermo Fisher Scientific, Waltham, USA
TopHat, 2.1.0	(Kim et al. 2013a)
usegalaxy.org	(Afgan et al. 2016)

2.2 Cell Culture Methods

2.2.1 Cell Cultivation

For our *in vitro* analysis, we utilized various PDAC human and murine cancer cell lines (Table 6). The well-established murine *Trp53* wildtype KC and *Trp53* mutant KPC cells were derived from tumor-bearing *Kras*^{G12D} (*KC*) and *Kras*^{G12D}*;Trp53*$^{R172H/+}$ (*KPC*) mice, respectively (Hingorani et al. 2003, Hingorani et al. 2005). They were kindly provided by Prof. Dr. Dr. med. Albrecht Neesse, Department of Gastroenterology, Gastrointestinal Oncology and Endocrinology, UMG. KPC cells harbour a clean *C57BL/6J* background rendering these cells suitable for orthotopic transplantation. CRISPR/Cas9-mediated *Ezh2* knockout (KO) clones of KPC cells have been established and described earlier (Patil et al. 2020). *Trp53* wildtype NFATc1-driven murine NKC PDAC cells were derived from *caNFATc1;Kras*^{G12D} mice (Baumgart et al. 2014). Stable EZH2 knockout clones of NKC cells using shRNA were already established and available in the Hessmann group (Patil et al. 2020). *Trp53* mutant KNPC and *Trp53* deficient KNP^{null}C cells originated from *Kras*^{G12D}*;caNFATc1;Trp53*$^{R172H/+}$ and *Kras*^{G12D}*;caNFATc1;Trp53*$^{\Delta/\Delta}$ mice, respectively (Singh et al. 2015).

The well-established human PDAC cell line Panc-1 originated from a 56-year-old male with adenocarcinoma in the head of the pancreas which invaded the duodenal wall. It has an activating *KRAS* and a *TP53*^{R273H} GOF mutation (Deer et al. 2010). The establishment of stable Panc-1 EZH2 knockout cell clones by CRISPR/Cas9-technique has been previously described (Chen et al. 2017). GöCDX5 and GöCDX13 are primary patient-derived xenograft (PDX) cell lines established in the context of the Clinical Research Unit 5002 at the Department of Gastroenterology, Gastrointestinal Oncology and Endocrinology, UMG (Patil et al. 2020). Molecular characterization of PDX tissue and CDX cells was conducted in the Institute of Human Genetics (UMG) using gene panel sequencing. Briefly, 200 ng genomic DNA isolated from tumor biopsies was used to perform targeted multigene panel sequencing. SureSelect$^{XT\ HS}$ and SureSelect^{QXT} target enrichment Kit with enzymatic fragmentation was used following manufacturer's protocol for library preparation. Libraries were sequenced on an Illumina NextSeq 550 with 2.5 High output chemistry and 150 bp read length. To align sequences to a human reference sequence (hg19) and for variant calling Sequence Pilot Software was used. Samples were screened for variants in *TP53* (ENST00000269305) and *CDKN2A* (ENST00000304494). Variants were assessed according to the American College of Medical Genetics (ACMG) guidelines (Richards et al. 2015) to identify likely pathogenic or pathogenic variants. The generation of translational PDAC models and their molecular

characterization have been approved by the ethical review board of the UMG (8/1/17). GöCDX5 harbour a *TP53*^{R248W} mutation and GöCDX13 are *TP53* wildtype.

For the following studies, the murine cells were cultured in DMEM containing 4.5 g/L D-Glucose, L-Glutamine supplemented with 10 % FCS and 1 % NEAA. Panc-1 cells were cultivated in DMEM containing 4.5 g/L D-Glucose, L-Glutamine supplemented with 10 % FCS and the PDX cell lines were cultured in Keratinocyte-SFM:RPMI (in 3:1 ratio) media supplemented with 2 % FCS, 1 % Penicillin-Streptomycin, bovine pituitary extract, and epidermal growth factor (Table 8). Generally, cells were maintained at 37 °C in a humidified atmosphere with 5 % CO_2. At confluency of 85 to 95 %, they were passaged by removing the medium, washing the cells with pre-warmed PBS, and incubating the cells in trypsin-EDTA at 37 °C for 5-10 min. After trypsinization resulted in the detachment of more than 95 % of the cells, enzyme reaction was stopped by adding a suitable volume of growth medium. Cells were separated gently, diluted appropriately, and passaged. Mycoplasma contamination was excluded regularly using MycoAlert Mycoplasma Detection Kit. For the following analysis, cells were counted in a Neubauer chamber, and the respective cell number was seeded in an appropriate cell culture dish format suitable for subsequent analysis steps.

For long-term storage, cells were kept at -150 °C. Therefore, cells were centrifuged for 3 min at 1200 rpm and RT. Subsequently, cells were resuspended in the respective growth medium (Table 8) supplemented with 10 % DMSO and aliquoted in 1 ml into cryotubes. After a slow and constant cool-down to -80 °C, cells were transferred to -150 °C the next day. For the revival of cell stocks, 1 ml cryo-preserved cells were thawed in a water bath at 37 °C and mixed with 9 ml pre-warmed growth medium. Cells were centrifuged for 3 min at 1200 rpm and RT and resuspended in growth medium prior to seeding into a cell culture flask. The next day, medium was changed.

2.2.2 Transfection

For transient knockdown of genes, cells were transfected using small interfering RNA (siRNA). Double-stranded siRNA targets a specific complementary mRNA leading to its degradation resulting in silencing of the target gene (Huppi et al. 2005). After seeding the cells into one well of a six-well plate, cells were allowed to attach for 24 h. The next day, specific siRNA was introduced into cells using siLentFect Lipid. Negative control RNA was used as control. Therefore, 200 µl Opti-MEM, 6 µl siLentFect Lipid, and 6 µl siRNA (20 nmol) (Table 9) were mixed in a polystyrene low-binding tube and incubated at RT for 20 min. Subsequently, the old medium was removed, and 1.3 ml fresh growth medium was

added carefully onto the cells alongside with 200 µl of the siLentFect Lipid-siRNA mixture. 6-8 hours after addition, medium was changed. In case of further 24 h treatments with drugs, medium was additionally changed 24 h after transfection, and cells were incubated for additional 24 h with a new drug-containing growth medium. Cells were harvested 48 h after transfection.

Transient overexpression of specific genes in eukaryotic cells can be achieved by introducing foreign DNA vectors into cells (Prelich 2012). 24 h prior to transfection, cells were seeded in one well of a 6-well plate or in a 10 cm dish, respectively. The different DNA vectors used for overexpression are listed in Table 10. For the six-well format, 200 µl Opti-MEM, 2 µg DNA construct and 5 µl Lipofectamine 2000 were mixed in a low-binding polystyrene tube and incubated at RT for 10 min. For the 10 cm dish format, 800 µl µl Opti-MEM, 8 µg construct DNA and 20 µl Lipofectamine 2000 were mixed incubated. Next, the medium was removed, and 1.3 ml fresh growth medium together with 200 µl of the Lipofectamine-DNA mixture were added onto the cells in one 6-well. For the 10 cm dish, 5 ml fresh growth medium together with 800 µl of the Lipofectamine-DNA mixture were added onto the cells. Transfection with the respective empty vector served as negative control. Cells were incubated at 37 °C and harvested 24 h after transfection. If an additional drug treatment of cells was necessary, treatment started 8 hours after transfection for the respective period and extended transfection time accordingly. Transfection success was confirmed by western blotting analysis.

2.2.3 Treatment

For drug treatment, cells were allowed to attach by seeding 24 h before treatment started. All pharmacological inhibitors and drugs and their treatment condition are listed in Table 11. Drugs were dissolved in the respective solvent and mixed with pre-warmed growth medium to reach the respective target concentration and added to the cells. Addition of the solvent reagent alone served as treatment control.

2.3 Nucleic Acid Techniques

2.3.1 RNA Isolation and Concentration Determination

Cells were cultures in a 6-well plate and total RNA was isolated from cells using TRIzol (Rio et al. 2010). After removing the medium and washing the cell with cold PBS, 800 µl TRIzol was added to each well, incubated for 3 min at RT, and scrape harvested. Following addition of 200 µl chloroform, the suspension was mixed properly and incubated for 5 min at RT. After centrifugation for 15 min at 17,200 rcf and 4 °C, the upper RNA comprising clear phase was transferred into a new tube containing 500 µl isopropanol. The samples were mixed properly, incubated for 10 min at RT, and centrifuged for 30 min at 17,200 rcf and 4 °C. The resulting RNA pellet was washed twice with 75 % ethanol and centrifuged for 5 min at 17,200 rcf and 4°C. Finally, the remaining RNA pellet was air-dried for 30 min at RT and dissolved in 30 µl RNA-free ddH_2O. Concentration and purity were determined by measuring the absorbance at 230 nm, 260 nm, and 280 nm with NanoPhotometer P-330. RNA was stored at -80 °C.

2.3.2 cDNA Synthesis

Upon isolation, RNA was transcribed into complementary DNA (cDNA) using the iScript cDNA Synthesis Kit according to the manufacturer´s manual. Briefly, 4 µl of 5x iScript Reaction Mix and 1 µL iScript reverse transcriptase were added to 1 µg total RNA and filled with nuclease-free ddH_2O to a final volume of 20 µl. The reaction mixture was incubated for priming (5 min at RT), for reverse transcription (20 min at 46 °C), and for stopping the reaction (1 min at 95 °C). Samples were diluted in nuclease-free ddH_2O (1:5) and stored until further use at 20°C.

2.3.3 Quantitative Real-Time PCR

Quantitative real-time PCR (qRT-PCR) enables quantitative measurement of the amplification of cDNA with a specific sequence during PCR in real-time (Higuchi et al. 1993). QRT-PCR analysis was performed using SYBR Green. 1 µl transcribed cDNA was mixed with 5 µl SYBR Green, 0.05 µl forward primer (10 µM), 0.05 µl reverse primer (10 µM), and 3.9 µl ddH_2O in one well of a MicroAmp Fast Optical 96-Well Reaction Plate. The utilized primer sequences for the specific target genes are listed in Table 12. The qRT-PCR reaction was performed in a StepOnePlus Real-Time PCR System with standard settings according to

the manufacturer´s manual. Gene expression levels were determined in triplicates and normalized to the housekeeping mRNA encoding *RPLP0*. The analysis was conducted utilizing ΔΔCt method (Livak and Schmittgen 2001).

Chromatin immunoprecipitation (ChIP) analysis was conducted by Dr. Shilpa Patil, Department of Gastroenterology, Gastrointestinal Oncology and Endocrinology, UMG (Patil et al. 2020). All antibodies used for ChIP are depicted in Table 15. Following precipitation and DNA isolation, qRT-PCR was performed with the input and ChIP samples in duplicates. The expression of ChIP samples was normalized to the expression of the input samples. The primers utilized for qRT-PCR following ChIP are listed in Table 13.

2.3.4 RNA Sequencing

KC, KPC, and KNPC cells were seeded in triplicates in a six-well plate and EZH2 knockdown was conducted using siRNA. RNA was isolated and its integrity and purity were validated by separation on a 1 % agarose gel. Library preparation of 500 ng of total RNA was performed using the True seq RNA library preparation kit according to the manufacturer´s manual following cDNA library concentration determination using Qubit and fragment size control using Bioanalyzer High Sensitivity DNA Analysis kit. Sequencing was performed by the NGS Integrative Genomics Core Unit (NIG) of the UMG. Furthermore, publicly available shRNA-mediated EZH2 knockdown RNA-seq data in NKC cells was utilized (GSE153537) (Patil et al. 2020), but analysed with the same pipeline used for KC, KPC, and KNPC cells. The analysis of FastQ files was performed using the open-source platform Galaxy (https://usegalaxy.org/). Reads were aligned to murine transcriptome mm9 using TopHat2 (version 2.1.0). Fragment Per Kilobase Million (FPKM) values were measured using Cuffnorm (version 2.2.1.1) and Cuffdiff (version 2.2.1). Genes with FPKM values < 0.01 were excluded from the analysis to reduce background signals, implying approximately 70% of the mouse genome. Genes were considered as significantly differentially regulated with a log2fold change of <-0.5 and >0.5, and a *q* value of <0.05. Principal component analysis (PCA) and sample-to-sample distances analysis were performed in R (version 4.0.0) using read counts generated with HTSeq (version 0.9.1) to evaluate similarities of replicates. Gene set enrichment analysis (GSEA) (version 4.0.3) of our data in the indicated publicly available gene sets was conducted using Signal2Noise metric for gene ranking. EnrichR analysis tool (https://maayanlab.cloud/Enrichr/) enabled Gene Ontology (GO) analysis. Pathways with a *q* value of <0.05 were considered significantly regulated pathways. Heatmaps were illustrated with log10 values of FPKM data using pheatmap function in R.

Venn diagrams were generated with Bioinformatics Evolutionary Genomics (http://bioinformatics.psb.ugent.be/ webtools/Venn/) to overlay gene lists. All software and databases and their references are summarized in Table 20.

2.4 Protein Methods

2.4.1 Protein Isolation and Concentration Determination

For whole-cell lysis and protein extraction from attached cells, cells were washed with 4 °C cold PBS and scrape-harvested with 30 - 40 µl of cold Lysis buffer (WCL) plus components (Table 5). For protein extraction from murine PDAC tissue, a small piece of tissue (0.1-0.4 cm^3) was transferred into 200-300 µl Lysis buffer (WCL) plus components (Table 5) and homogenized. Following incubation on ice for 30 min, the suspension was centrifuged for 20 min at 17,200 rcf and 4 °C and the supernatant was transferred into a fresh tube. Protein concentration was determined using Bradford Reagent. (Bradford 1976). Therefore, BSA standards with known concentrations ranging from 1.0 µg/ml to 6.0 µg/ml were used to generate a standard curve by adding the appropriate volume (1-6 µl) of BSA (1 µg/ml dissolved in lysis buffer) to 200 µl Bradford Reagent in a 96 well microplate. For concentration determination of the samples, 1 µl of the respective lysate was mixed with 200 µl Bradford Reagent. The protein concentration was determined by measuring the absorbance with PHOmo Microplate Reader at 595 nm using AUTOsoft 2.6 software and compared to the BSA standard. Remaining protein sample was stored at -20 °C for short-term storage and at -80 °C for long-term storage.

2.4.2 SDS-PAGE and Western blotting

To separate proteins according to their molecular weight, sodium dodecyl sulfate polyacrylamide gel electrophoresis (SDS-PAGE) was performed. Given the similar charge density of proteins after denaturing by and interaction with the negatively charged SDS, proteins separate in an electric field linearly to their molecular weight. Smaller proteins which are decorated with fewer SDS migrate faster than bigger proteins decorated with more SDS (Laemmli 1970). The SDS-polyacrylamide gels comprise a stacking gel to form a narrow protein band and a separation gel to separate the proteins according to their size. A thin stopping gel at the bottom of the separation gel can be performed to prevent leakage during pouring the gel. To separate larger proteins (40-150 kDa), 10 % polyacrylamide gels were used and to separate smaller proteins (15-50 kDa), 15 % polyacrylamide gels were utilized.

To allow gel polymerization, APS and TEMED were added to the “ready-to-use” stacking and separation gel buffers (Table 5). Generally, 15-20 µg of protein lysate were diluted with lysis buffer up to an equal sample volume and mixed with 5x Laemmli sample buffer with β-mercaptoethanol (Table 5). After boiling the samples at 95 °C for 5 min, protein lysates were separated by SDS-PAGE. 5 µl of PageRuler Prestained Protein Ladder was utilized to monitor and compare protein size. The electrophoresis chamber was assembled and filled with 1x running buffer (Table 5). Initially, samples were separated at 120 V until the protein marker has been separated, subsequently, voltage was increased up to 160 V until the running front reached the end of the gel.

Following separation, proteins were transferred onto a nitrocellulose membrane using the semi-dry Trans-Blot Turbo-Transfer System according to the manufacturer’s instruction. Briefly, 10 % polyacrylamide gels were blotted at 1.0 A and 25 V for 22 min and 15 % gels for 15 min. A sandwich of filter paper, nitrocellulose membrane, and polyacrylamide gel were equilibrated with Turbo-Blot buffer (Table 5) and the transfer equipment was assembled. Successful protein transfer was confirmed by Ponceau S staining. After the transfer, the membrane was blocked for 1 h at RT in 5 % powdered milk in TBS-T (Table 5) and primary antibody binding was enabled overnight at 4 °C in 5 % powdered milk in TBS-T. All antibodies and their dilution used in this study are depicted in Table 14. Following three washing steps with TBS-T (Table 5) for 5-10 min, HRP-labelled secondary anti-mouse or anti-rabbit antibodies, respectively, were incubated in 5 % powdered milk in TBS-T for 1 h at RT. Three washing steps with TBS-T for 5-10 min each were followed to remove unspecific antibody binding. Enhanced chemiluminescence solutions were added equally covering the whole membrane. Chemiluminescence signals were detected and recorded using ChemoStar ECL Imager.

2.4.3 Immunoprecipitation

Co-Immunoprecipitation (co-IP) was performed to analyse protein-protein interactions. Cells were cultured and harvested in Triton-200 buffer plus components (Table 5). Initially, protein G beads were washed three times in PBS and centrifuged for 2 min at 850 rcf and 4 °C. Subsequently, beads were resuspended in half of the initial volume to reach 50 % slurry beads suspension. To avoid unspecific protein-binding, pre-clear was performed by adding 20 µl washed beads to 500 µg protein lysate in a final volume of 1 ml. The mixture was rotated overhead for 30 min at 10 rpm and 4 °C prior to centrifugation for 2 min at 850 rcf and 4 °C. The remaining supernatant was transferred into a new tube and 6 µl of the

respective antibody was added. As a control, 2 µl normal mouse or rabbit IgG, respectively, were added to the respective tube. All antibodies used for immunoprecipitation are listed in Table 16. For pull-down of endogenous p53, p53 antibody from Cell Signaling (2524) was utilized and for precipitation of re-expressed p53 and its variants, p53 antibody from Novus Biologicals (NB200-103) was utilized. All samples were rotated overhead at 10 rpm and 4 °C overnight. The next day, 25 µl of washed protein G beads were added per sample and rotation was performed for 2 h at 10 rpm and 4 °C. Subsequently, samples were centrifuged for 2 min at 850 rcf and 4 °C. Pellets were washed two times in 500 µl Triton-200 buffer and, additionally, two times in 500 µl PBS. Following the last centrifugation step for 2 min at 850 rcf and 4 °C, beads were mixed with 65 µl 2x Laemmli sample buffer with β-mercaptoethanol, incubated for 15 min on ice, and boiled at 95 °C for 5 min. 20 µl of the supernatant of the beads were subjected to SDS-PAGE and analysed using western blotting. Additionally, 20 µg proteins of the initial whole-cell lysate were mixed with 5x Laemmli sample buffer with β-mercaptoethanol, cooked at 95 °C for 5 min and subjected to western blotting (input) to validate the presence of the target protein in the cell lysates.

2.5 Flow Cytometry

Apoptosis analyses were performed using Annexin-V/propidium iodide (PI) staining prior to flow cytometry analysis. Annexin-V reveals a high affinity to bind phosphatidylserine (PS). PS are components of the cell membrane normally directed into the cytoplasm. However, upon induction of apoptosis, PS also appears on the surface of the cellular membrane and can be detected by allophycocyanin (APC)-labelled Annexin-V. PI can intercalate into the DNA and reveals fluorescence but only upon loss of the cellular and nuclear integrity due to late apoptotic or necrotic processes. Hence, simultaneous staining with Annexin-V and PI can distinguish between living (Annexin-V and PI negative), early apoptotic (positive for Annexin-V but negative for PI), late apoptotic (positive for both Annexin-V and PI), and dead cells (positive for PI but negative for Annexin-V) (Vermes et al. 1995, Vermes et al. 2000).

For Annexin-V/PI staining, cells were cultivated in a 6-well-plate and treated with STS to induce apoptosis. Cells were washed with cold PBS, harvested using trypsin, and transferred to a FACS tube. Subsequently, cells were pelleted for 3 min at 1200 rpm and RT and the pellet was resuspended in 500 µl Annexin-V-Binding buffer. Following another centrifugation step for 3 min at 1200 rpm and RT, supernatant was discarded, and cells were mixed with 100 µl Annexin-V-Binding buffer, 5 µl Annexin-V, and 3 µl PI (1 mg/ml). After incubation for 15 min at RT in the dark, 200 µl Annexin-V-Binding buffer was added and mixed

thoroughly. Staining intensity was determined using BD FACSCanto II, analysed using FlowJo, and visualized using GraphPad PRISM. An equal gating strategy was utilized for all samples.

2.6 Histological Staining

All *in vivo* experiments were conducted by different scientists of the Hessmann group. Transplantation, surveillance, and sacrificing of orthotopically transplanted mice (Patil et al. 2020) as well as tissue processing, survival and relative tumor weight analysis were performed by Dr. Shilpa Patil. Surveillance, sacrificing, and tissue processing of *Kras^{G12D}* (*KC*) and *Kras^{G12D};Ezh2$^{fl/fl}$* (*KEC*) mice were conducted by Waltraut Kopp and Benjamin Steuber as described before (Chen et al. 2017, Patil et al. 2020). All mice experiments were accomplished in agreement with the protocols approved by the Institutional Animal Care and Use Committee of the UMG (33.9-42502-04- 14/1633, -15/2057, -19/3085, -17-2407).

For histological staining of tissue, murine pancreas and liver tissue was fixed in formalin, embedded in paraffin, and sections of 4 µm were placed on slides. To perform histological staining, tissue sections were deparaffinized by incubating twice in xylene for 15 minutes followed by hydration through incubation of tissues with descending ethanol concentration for 3 min (99%, 99%, 96%, 80%, 70%, 50%). After washing slides for 1 min in ddH_2O, different staining methods can be continued.

2.6.1 Haematoxylin and Eosin staining

A commonly used staining method is the H&E staining to distinguish between nuclei and cytoplasm and to get a general overview of the structure of the tissue (Titford 2005). Therefore, sectioned and hydrated tissue was incubated for 7 min in haematoxylin solution to stain nuclei followed by 5 min washing under running tap water. Subsequently, slides were incubated for 30 seconds in eosin solution to stain cytoplasm prior to three washing steps. To dehydrate tissue, slides were incubated in ascending ethanol concentrations for 3 min (70%, 80%, 96%, 99%) followed by four incubation steps in xylene for 10 min each. Coverslips were mounted utilizing mounting medium.

2.6.2 Masson's Trichrome

Another staining technique to differentiate between nuclei, cytoplasm and connective tissue is the Masson's trichrome staining (Foot 1933). For Masson`s Trichrome staining the stain kit from Polyscience Europe was used. Briefly, slides with sectioned and hydrated tissue were incubated in Bouin´s Fixative solution overnight. After washing slides for 5 minutes with dH_2O, sections were incubated for 15 minutes in mixed Weigert´s Iron Hematoxylin solution A and B to stain nuclei followed by a washing step in dH_2O. Next, the tissue was incubated in Biebrich Scarlet-Acid Fuchsin solution for 5 minutes to stain the cytoplasm and briefly washed with water. Sections were incubated in phosphotungstic/phosphomolybdic acid for 5 minutes prior to staining with Aniline Blue for 8 minutes to stain collagen and washing in dH_2O. Next, the tissue was incubated in 1% acetic acid for 1 min and washed in H_2O prior to dehydration in ethanol (96%, 99%, 30 seconds each), incubation in xylene for 1 minute, and mounting.

2.6.3 Immunohistochemistry

To recognize and visualize target antigens and proteins in PDAC tissue, immunohistochemistry (IHC) was performed (Coons et al. 1941, Avrameas and Uriel 1966, Nakane and Pierce 1967). Following sectioning and hydrating, tissue was boiled for 15 min in citrate buffer (Table 5). After heat-induced epitope retrieval, tissue was cooled down in citrate buffer for 10 min at RT following 20 min on ice. Next, slides were incubated for 10 min in 3 % H_2O_2 to inhibit the endogenous peroxidase activity. Subsequently, slides were washed in H_2O and transferred into the Sequenza slide system. After the next washing step with PBS-T (Table 5), tissue was blocked for 1 h at RT with 10 % BSA in PBS-T. Incubation of primary antibody diluted in PBS-T was performed overnight at 4 °C. All antibodies and their dilution used in this study are listed in Table 17. For αSMA staining, which is a primary mouse antibody stained on mouse tissue, the M.O.M. immunodetection kit was used according to the manufacturer's protocol. The next day, slides were washed with PBS-T and incubated with secondary antibody for 1 h at RT. Following three additional washing steps with PBS-T, slides were incubated for 1h at RT with the Vectastain ABC kit to allow streptavidin-biotin-complex formation. Next, 3,3'-diaminobenzidine (DAB) staining was performed briefly prior to nuclei staining with Haematoxylin for 5 min and washing for 5 min in H_2O. Finally, slides were incubated in ascending ethanol concentrations for 3 min (70%, 80%, 96%, 99%) to dehydrate followed by four incubation steps in xylene for 10 min each. Coverslips were mounted using mounting medium.

EZH2 staining in human PDAC was performed by Jennifer Appelhans, Institute of Pathology, UMG. Human primary PDAC samples were received from the Institute of Pathology at the UMG. Prior to analysis samples from resected PDAC specimen were Formalin-Fixed-Paraffin-Embedded (FFPE) as described before (Patil et al. 2020). For EZH2 and $p14^{ARF}$ staining in human PDAC, patients were classified in $EZH2^{high/low}$ and $p14^{ARF\ high/low}$ according to their expression based on IHC staining in PDAC tissue. $EZH2^{low}$ was defined as < 7 % positive EZH2 staining and $p14^{ARF\ low}$ as < 13 % positive p14ARF staining.

After the respective staining, slides were viewed and photographed under the microscope. Quantification of (immuno-) histochemistry was performed in ten representative images of each section by measuring positive stained areas or cells, respectively, using ImageJ Fiji.

2.7 Immunofluorescence and Proximity Ligation Assay

Immunofluorescence

For immunofluorescence (IF) staining of $p19^{Arf}$ in murine pancreatic tissue, slides were washed with PB buffer (Table 5) after sectioning and hydration. Antigen retrieval was performed by cooking for 10 min in citrate buffer (Table 5). Following cooling down on ice for 30 min and 3 washing steps with PB for 5 min, tissue was blocked with 10 % normal goat serum (NGS) in PB supplemented with 0.4 % Triton X-100 (PB-T) at 4 °C. After 2 h, the blocking solution was removed and slides were incubated with primary $p19^{Arf}$ antibody overnight at 4 °C in 2 % NGS in PB-T as depicted in Table 18. The next day, slides were washed six times with PB for 5 min and incubated with the secondary anti-rat antibody for 2 h at 4 °C in 2 % NGS in PB-T. Subsequently, slides were washed 5 times for 5 min with PB and nuclei were stained with DAPI (1:1000) for 10 min at RT prior to mounting. Images of stained tissue sections were taken with Leica LAS X software under a Leica DMi8 microscope. Positive staining was counted in six representative images of six different mice per condition using ImageJ Fiji.

Proximity Ligation Assay

To assess protein-protein interaction, proximity ligation assay (PLA) was performed. Therefore, cells were seeded directly onto a coverslip by seeding cells into a coverslip containing well of a 6-well plate. Cells were washed with 4 °C cold PBS and fixed with 4 % paraformaldehyde (PFA) in PB at RT for 20 min. After five washing steps for 5 min with PB, blocking and permeabilization were facilitated by incubation with 10 % normal goat serum (NGS) in PB-T for 2 h at 4 °C. Subsequently, three washing steps for 5 min with PB followed and the primary antibody dissolved in PB-T supplemented with 2 % NGS was incubated overnight at 4 °C. All antibodies and their dilutions used for PLA are listed in Table 19. The next day, the second day of PLA was performed according to the manufacturer's protocol. Cells were observed under a fluorescence microscope and images were taken with Application Suite (LAS) X software. To improve imagining, brightness and contrast were increased in all images identically using Photoshop.

2.8 Statistical Analysis

Data are represented as mean ± standard deviation (SD) and were visualized using GraphPad PRISM version 8.0.2 (Graphpad Software). Significance was calculated using the respective statistical tests depicted in the figure legends. Significance is indicated as * $p \leq 0.05$; ** $p \leq 0.01$; *** $p \leq 0.001$; **** $p \leq 0.0001$; and ns non-significant.

3 Results

The histone methyltransferase EZH2 is regularly found to be overexpressed in PDAC (Chen et al. 2017). Given the tumor supporting activity of EZH2 and the availability of EZH2 inhibitors, the histone methyltransferase moved to the focus of clinical research. However, recent studies suggest a strong context-dependency of epigenetic regulators in general (Tsuda et al. 2021, Citron and Fabris 2020) and EZH2 in particular (Ougolkov et al. 2008, Kim et al. 2013b, Chen et al. 2017, Patil et al. 2020, Bremer et al. 2021). Therefore, the first part of this study aimed at characterizing the context-dependency of EZH2 activity in PDAC progression and at elucidating important prerequisites for EZH2 inhibition as a potential strategy in PDAC treatment.

3.1 EZH2 depletion is not beneficial in orthotopic PDAC models

Orthotopically transplanted Panc-1 Model

In order to unravel the role of EZH2 in PDAC maintenance, we took advantage of an orthotopic transplantation model of human PDAC cells. We used the human pancreatic epithelial cancer cell line Panc-1 and depleted *EZH2* by the CRISPR/Cas9 technique. Cells that underwent the CRISPR/Cas9 technique but still expressed *EZH2* were used as control. These cells are already established in the Hessmann group and have been published previously (Chen et al. 2017, Patil et al. 2020). The successful *EZH2* KO was confirmed by loss of EZH2 expression and reduced H3K27me3 levels as detected by western blot analysis (Figure 6A) (Chen et al. 2017). Subsequently, these *EZH2*-expressing (Cas9 Ctrl) and -depleted (Cas9 *EZH2* KO) cells were transplanted into the pancreas of immunodeficient *NMRI-Foxn1nu* mice (Figure 6B). Transplantation, surveillance, and sacrificing of orthotopically transplanted mice as well as survival and relative tumor weight analysis were performed by Dr. Shilpa Patil, Department of Gastroenterology, Gastrointestinal Oncology and Endocrinology, UMG. EZH2 IHC validated the absence of EZH2 in the *EZH2* KO tumor tissue (Figure 6C).

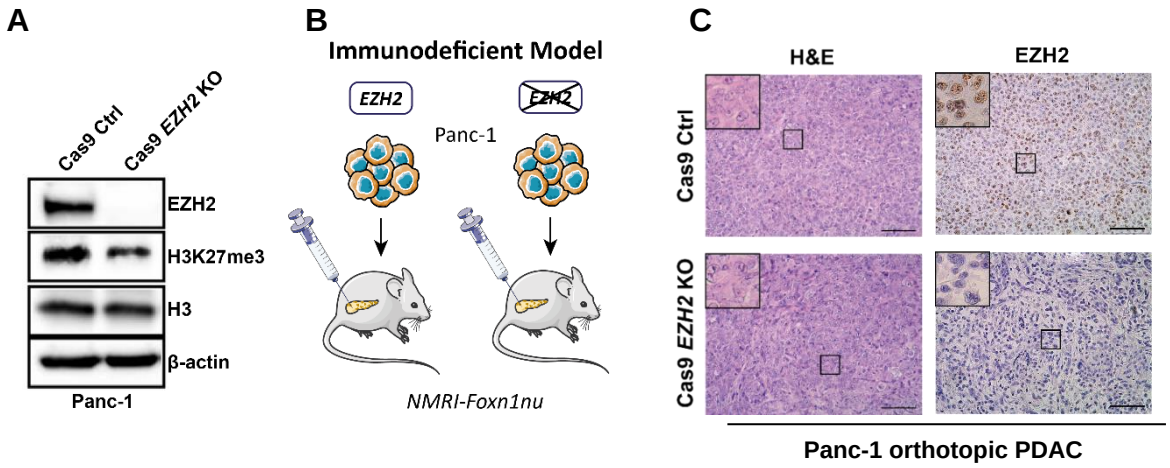

Figure 6: Orthotopic transplantation of human Panc-1 cells into *NMRI-Foxn1nu* mice. A Western blotting analysis of Panc-1 cells, which were subjected to the CRISPR/Cas9 technique resulting in EZH2 proficient (Cas9 Ctrl) and EZH2-deficient (Cas9 *EZH2* KO) cells. Successful knockout of *EZH2* was confirmed by loss of EZH2 and reduction of H3K27me3 levels. H3 and β-actin served as loading controls (Chen et al. 2017). **B** Schematic displaying the transplantation of CRISPR/Cas9-mediated Cas9 Ctrl and *EZH2* KO Panc-1 cells into *NMRI-Foxn1nu* mice. Transplantation was conducted by Dr. Shilpa Patil. **C** Representative images of H&E staining and immunohistochemical staining of EZH2 in orthotopic Panc-1 tumors (Magnification: 100 x, Scale bar 100 µm).

Given the oncogenic activity of EZH2 and the findings that Panc-1 *EZH2* KO cells revealed reduced proliferation and clonogenicity *in vitro* (Chen et al. 2017), we expected an advantageous outcome of *EZH2* depletion. However, *EZH2* depletion did not lead to significant improvements in survival (median survival: Cas9 Ctrl cohort: 70 days, Cas9 *EZH2* KO cohort: 76 days post transplantation) and relative tumor weight (Figure 7A, B). Moreover, H&E staining showed a similar microscopic appearance of EZH2-proficient and -deficient tumors (Figure 6C). Furthermore, immunohistochemical staining of Ki-67 revealed no EZH2 dependent differences in cell proliferation (Figure 6C, D). To get insights into the stromal composition, we stained for αSMA as a marker for fibroblasts (Herman 1993), which are responsible for the production of a desmoplastic microenvironment. Interestingly, αSMA staining was even increased in the absence of EZH2 (Figure 7C, D). In line with these findings, Masson´s Trichrome staining also displayed a higher collagen deposition (blue-stained area) in the absence of EZH2 (Figure 7C, D). However, the activated stroma index, a prognostic marker, which is calculated by dividing the αSMA-stained area by the collagen-stained area (Erkan et al. 2008) was similar in EZH2-proficient and -deficient orthotopic Panc-1 PDAC (Figure 7E). Together, our orthotopic Panc-1 transplantation model revealed no beneficial effect of *EZH2* depletion.

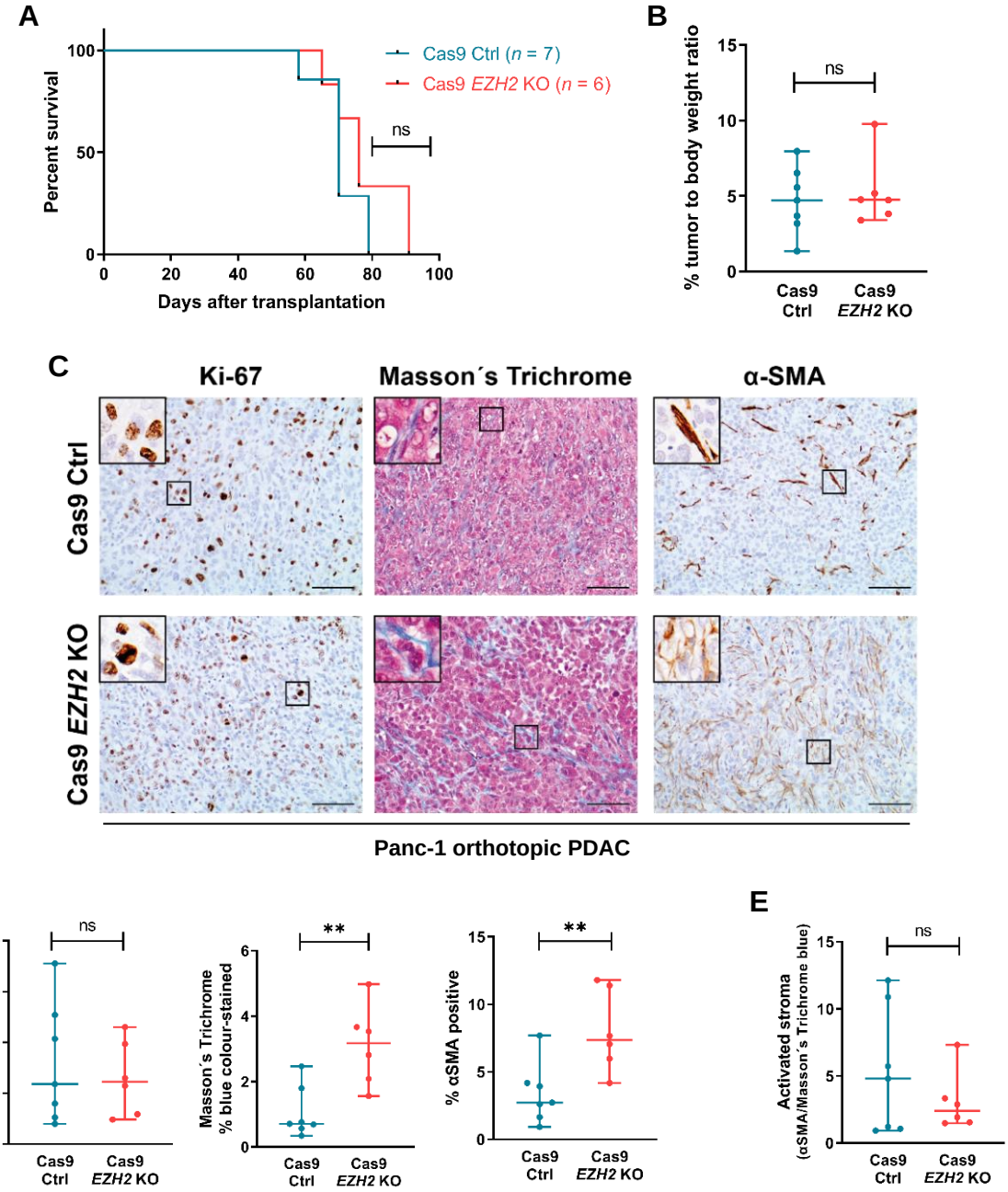

Figure 7: *EZH2* depletion is not beneficial in orthotopic transplanted Panc-1 cells. A-B Kaplan-Meier survival curve (**A**) and relative tumor weight (**B**) of *NMRI-Foxn1nu* mice after transplantation of *EZH2*-proficient (Cas9 Ctrl) and CRISPR/Cas9-mediated *EZH2*-deficient Panc-1 cells. Significance of survival analysis was determined by Log-rank (Mantel-Cox) test, ns, non-significant. Significance of relative body weight was determined by two-tailed unpaired Student´s *t* test, ns, non-significant. Each dot represents one mouse. Analyses were performed by Dr. Shilpa Patil. **C-D** Indicated immunohistochemical and Masson's Trichrome staining (Magnification: 100 x, Scale bar: 100 µm) (**C**) and the respective indicated quantification (**D**). For Masson's Trichrome and αSMA, positively stained areas of ten representative images (100 x) of each tumor were measured. For Ki-67 staining, number of Ki-67 positive cells of ten representative images (100 x) was counted and normalized to all cells. *(Figure legend continued on next page).*

E Activated stroma index calculated by the ratio of αSMA-stained area to collagen-stained area. Each dot represents one mouse. Values represent mean ± SD. Significance was determined by two-tailed unpaired Student´s *t* test; **, p ≤ 0.01; ns, non-significant.

Syngeneic orthotopically transplanted KPC Model

Next, we speculated how much the absence of immune system in *NMRI-Foxn1nu* mice contributes to the unexpected results in our orthotopic Panc-1 model. It has been shown previously that both the immune system and the microenvironment have high relevance for tumor maintenance and progression especially in PDAC (Hessmann et al. 2020, Huber et al. 2020, Karamitopoulou 2019, Murakami et al. 2019). Therefore, we took advantage of a syngeneic PDAC model and transplanted *Kras*^{G12D}*;Trp53*$^{R172H/+}$ (KPC) cells into immuno-competent *C57BL/6J* mice. The KPC model is one of the best established transgenic PDAC murine model systems harbouring both oncogenic *Kras* (*Kras*^{G12D}) and *Trp53* GOF (*Trp53*$^{R172H/+}$) mutation rendering the resulting PDAC highly invasive and metastatic (Hingorani et al. 2005). To analyse the EZH2-specific effect, we generated CRISPR/Cas9-mediated *Ezh2* KO KPC cells. KPC cells that underwent to the CRISPR/Cas9 technique, but still expressed *Ezh2* were used as control. These KPC cells are established in the Hessmann group and have been published before (Patil et al. 2020). The resulting *Ezh2* KO was verified by western blot analysis (Figure 8A). Subsequently, the KPC Cas9 ctrl and KPC Cas9 *Ezh2* KO cells were transplanted into the pancreas of immune-competent *C57BL/6J* mice for the generation od a syngeneic model (Figure 8B). Transplantation, surveillance, and sacrificing of orthotopically transplanted mice as well as survival and relative tumor weight analysis were performed by Dr. Shilpa Patil. EZH2 IHC validated the absence of EZH2 in the *Ezh2* KO tumor (Figure 8C).

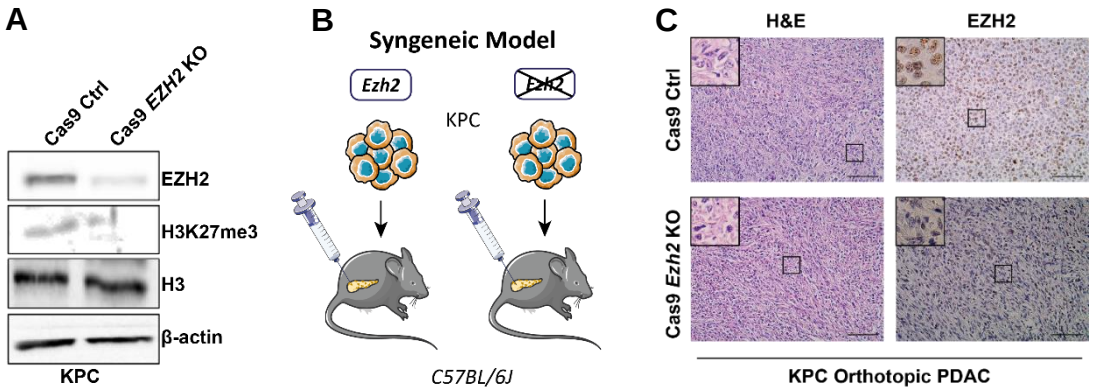

Figure 8: Syngeneic transplantation of murine KPC cells into *C57BL/6J* mice. A Immunoblotting of *Kras*^{G12D}*;Trp53*$^{R172H/+}$ (KPC) cells upon subjection to CRISPR/Cas9 technique resulting in *Ezh2* proficient (Cas9 Ctrl) and *Ezh2*-deficient (Cas9 *Ezh2* KO) cells. Successful knockout of *Ezh2* was confirmed by loss of EZH2 and reduction of H3K27me3 levels. H3 and β-actin served as loading controls. **B** Schematic illustration of syngeneic transplantation of CRISPR/Cas9-mediated Cas9 Ctrl and *Ezh2* KO KPC cells into *C57BL/6J* mice. Transplantation was conducted by Dr. Shilpa Patil. **C** Representative images of H&E staining and immunohistochemical staining of EZH2 in syngeneic *KPC* tumors (Magnification: 100 x, Scale bar 100 µm).

Again, and in accordance with our findings in the aforementioned Panc-1 orthotopic model, a better outcome of EZH2 depletion could not be observed in the syngeneic KPC model. On the contrary, the survival of mice bearing *Ezh2*-deficient tumors was even reduced (median survival: Cas9 ctrl cohort: 23 days, Cas9 *Ezh2* KO cohort: 16 days post transplantation) (Figure 9A). However, we could not identify significant differences in the relative tumor weight (Figure 9B) and H&E staining suggested a similar microscopic phenotype of *Ezh2*-proficient and -deficient orthotopic tumors (Figure 8C). Likewise, cell proliferation as measured by Ki-67 staining, fibroblast activity as indicated by αSMA staining, and collagen deposition as revealed by the blue area in Masson´s Trichrome staining was unaffected by *Ezh2* depletion (Figure 9C, D). Consistently, the calculated activated stroma index was also similar in *Ezh2*-proficient and -deficient tumors (Figure 9E). These findings suggest that it is not the presence of the immune system influencing the outcome of *EZH2* depletion in PDAC but implicate that EZH2 activity is rather influenced by factors other than the immune system.

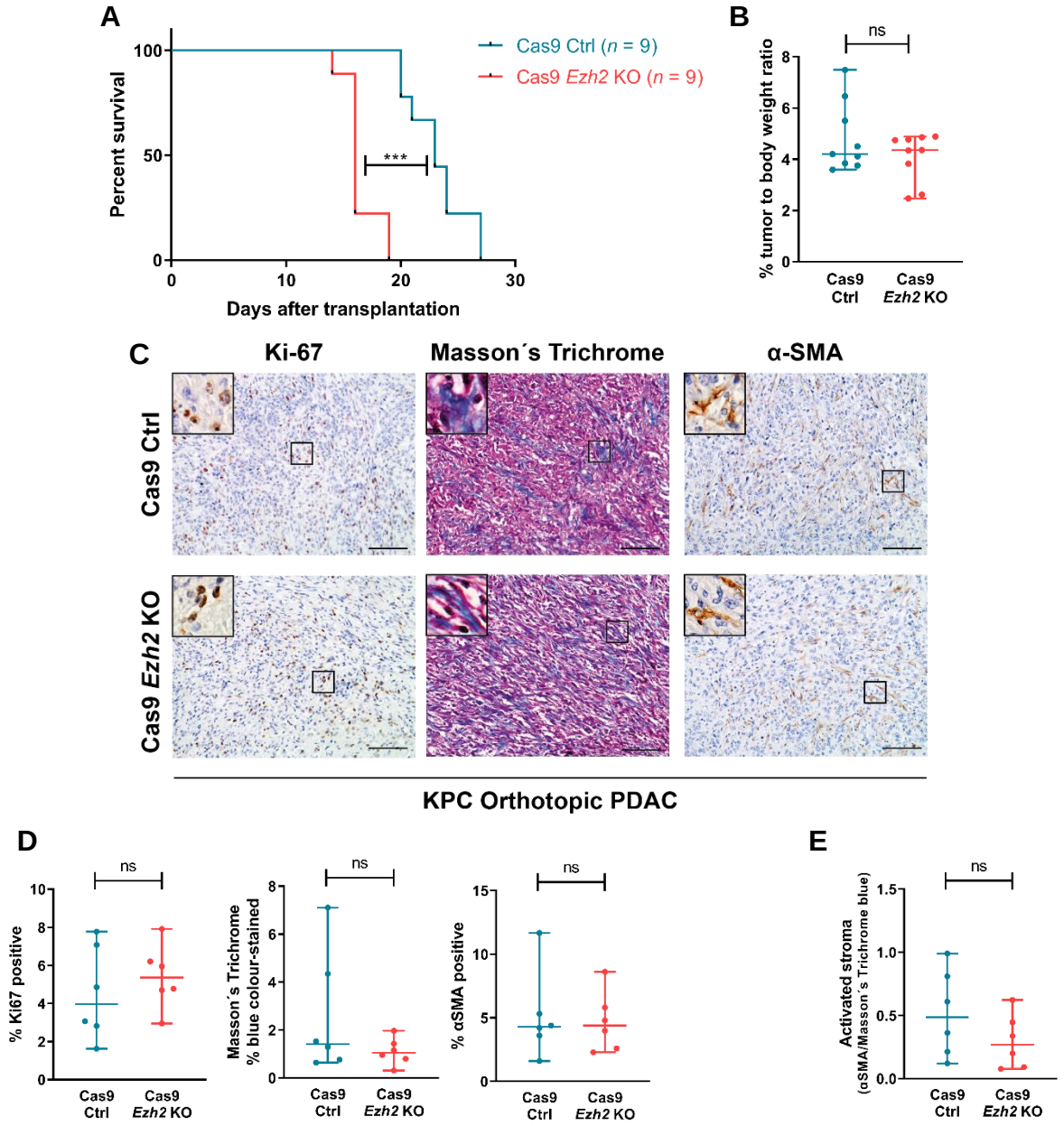

Figure 9: EZH2 depletion does not favour a less aggressive phenotype in a syngeneic transplantation model. A-B Survival curve (**A**) and relative tumor weight (**B**) of *C57BL/6J* mice post transplantation of *Ezh2*-expressing (Cas9 Ctrl) and CRISPR/Cas9-mediated *Ezh2*-deleted $Kras^{G12D}$;$Trp53^{R172H/+}$ (KPC) cells. Significance of survival analysis was determined by Log-rank (Mantel-Cox) test, ***, $p \leq 0.001$. Significance of relative body weight was determined by two-tailed unpaired Student´s *t* test, ns, non-significant. Each dot represents one mouse. Analyses were performed by Dr. Shilpa Patil. **C-D** Indicated immunohistochemical and Masson's Trichrome staining (Magnification: 100 x, Scale bar: 100 µm) (**C**) and the respective quantification (**D**). For Masson's Trichrome and αSMA, positively stained areas of ten representative images (100 x) of each tumor were measured. For Ki-67 staining, number of Ki-67 positive cells of ten representative images (100 x) was counted and normalized to all cells. *(Figure legend continued on next page).*

E Activated stroma index calculated by the ratio of αSMA-stained area to collagen-stained area. Each dot represents one mouse. Values represent mean ± SD. Significance was determined by two-tailed unpaired Student´s *t* test, ns, non-significant.

Consequently, in contrast to our initial hypothesis that EZH2 harbours tumor supporting functions in general, both our immune-deficient human and our immune-competent murine orthotopic PDAC models did not reveal a reduced tumor progression or a beneficial outcome upon *EZH2* depletion in PDAC. Hence, inhibition of EZH2 is not generally beneficial and associated with a better prognosis, but rather context-specific. This suggestion is in accordance with recent findings that EZH2 does not only harbour oncogenic activity (Ougolkov et al. 2008, Kim et al. 2013b), but also shows tumor-suppressive functions (Bremer et al. 2021). Therefore, we aimed at deciphering the context-defining characteristics rendering EZH2 inhibition ineffective to predict the outcome of EZH2 inhibition as a potential PDAC therapy.

3.2 EZH2 dependent target gene regulation is determined by the *Trp53*-status

Global transcriptional effects of EZH2 depletion

We next examined potential context-determining characteristics that are present in our orthotopic models, in which EZH2 depletion does not render PDAC less aggressive and compared it with the previous findings identifying oncogenic EZH2 activity (Patil et al. 2021, Patil et al. 2020). The most prominent difference was the *TP53* status. A favourable outcome of EZH2 inhibition was mostly observed in *TP53* wildtype conditions (Patil et al. 2021, Patil et al. 2020), whereas our orthotopic PDAC models harboured a mutation in *TP53*. Therefore, we hypothesized that the activity of EZH2 is specifically dependent on the *TP53* status. To address this hypothesis, we took advantage of four different murine *Trp53* wildtype (referred to as p53wt) or *Trp53* mutant (referred to as p53mut) PDAC cells, depleted EZH2, and subsequently subjected these cells to RNA sequencing thereby analysing p53-status mediated EZH2-dependent target gene regulation (Figure 10A). To reflect the p53wt situation, we used PDAC cells derived from the well-established $Kras^{G12D}$ (*KC*) and *caNFATc1;*$Kras^{G12D}$ (*NKC*) genetically engineered mouse models (GEMM) (Hingorani et al. 2003, Baumgart et al. 2014). In *KC* mice, the oncogenic pancreas-specific $Kras^{G12D}$ mutation can initiate preinvasive lesions. Potentially, with low incidence, these lesions can develop

into invasive and metastatic PDAC (Hingorani et al. 2003). An additional factor to initiate and accelerate carcinogenesis in a *Trp53* wildtype context and a *Kras*^{G12D} mutant background is the constitutive nuclear expression of Nuclear Factor of Activated T cells 1 (NFATc1), an inflammatory calcineurin-responsive transcription factor. *Kras*^{G12D} combined with constitutive nuclear accumulation of NFATc1 in the pancreas led to the development of all grades of preinvasive lesions and the progression into invasive and metastatic PDAC with a penetrance of nearly 100 % (Baumgart et al. 2014). Comparable to human PDAC, *NKC* mice show typical human PDAC properties, such as cachexia and abdominal extension due to ascites and duodenal obstruction (Baumgart et al. 2014, Chen et al. 2015, Hessmann 2014), rendering NKC cells suitable to study PDAC in a p53wt condition (Patil et al. 2020, Patil et al. 2021). For cells harbouring a mutation in *Trp53*, we used the aforementioned KPC cells as a corresponding model to KC cells. Additionally, we utilized *Kras*^{G12D}*;caNFATc1;Trp53*$^{R172H/+}$ (KNPC) cells as the corresponding model to NKC cells. These cells were derived from *KNPC* mice which developed dedifferentiated PDAC and mostly died within 6-8 weeks. Like *NKC* mice, they also revealed characteristic PDAC symptoms, including cachexia and abdominal ascites. Indeed, as expected compared to the p53wt *NKC* model, the p53mut *KNPC* model exhibited accelerated PDAC development and progression (Singh et al. 2015). To exclude effects that may be specific to one particular p53 mutation, we used p53mut cell lines containing the same *Trp53*$^{R172H/+}$ GOF mutation. To study the EZH2 dependent target gene regulation, we performed triplicates of *Ezh2* knockdown in KC, KPC, and KNPC cells using siRNA prior to RNA-seq analysis. Raw data of RNA-seq of NKC cells after shRNA-mediated *Ezh2* knockdown has been published previously and was used for our studies (Figure 10) (Patil et al. 2020). IN the interest of comparability, it was analysed with the same pipeline and under the same conditions as used for the KC, KPC, and KNPC cells. Successful *Ezh2* knockdown was confirmed by qRT-PCR analysis (Figure 10B).

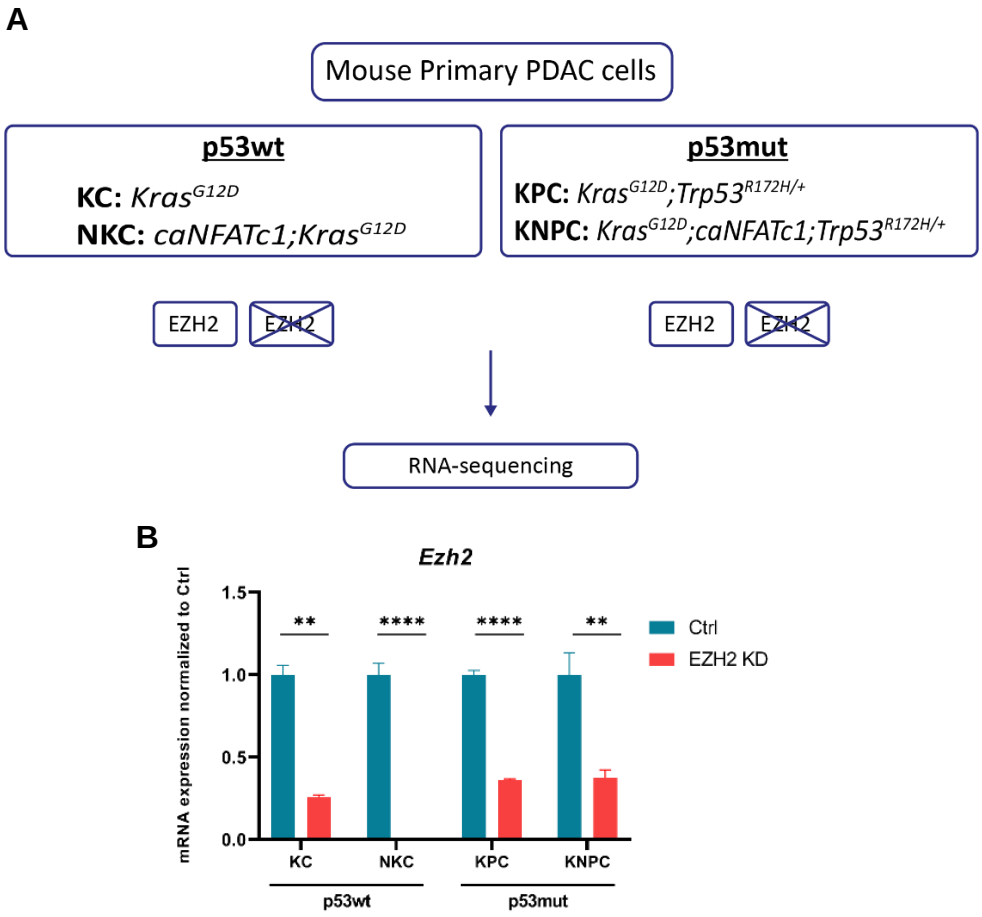

Figure 10: RNA sequencing of murine PDAC cells. A Schematic illustration of the RNA-sequencing procedure in p53wt and p53mut PDAC cells. **B** qPCR in the indicated murine PDAC cells validating the knockdown of EZH2. Values represent mean ± SD. Significance was determined by two-tailed unpaired Student´s t test; **, $p \leq 0.01$; ****, $p \leq 0.0001$.

Initially, quality, similarities of triplicates, and differences among the four conditions (*Ezh2*-proficient vs. *Ezh2*-deficient and p53wt vs. p53mut) were confirmed by principal component analysis (PCA) and sample-to-sample distances (Figure 11A-E). To better display the distances of KNPC cells in the presence and absence of EZH2, which clustered closely together in a joint NKC-KNPC diagram (Figure 11B), PCA was performed separately and validated the clustering of two different conditions (*Ezh2*-proficient vs. *Ezh2*-deficient) (Figure 11C).

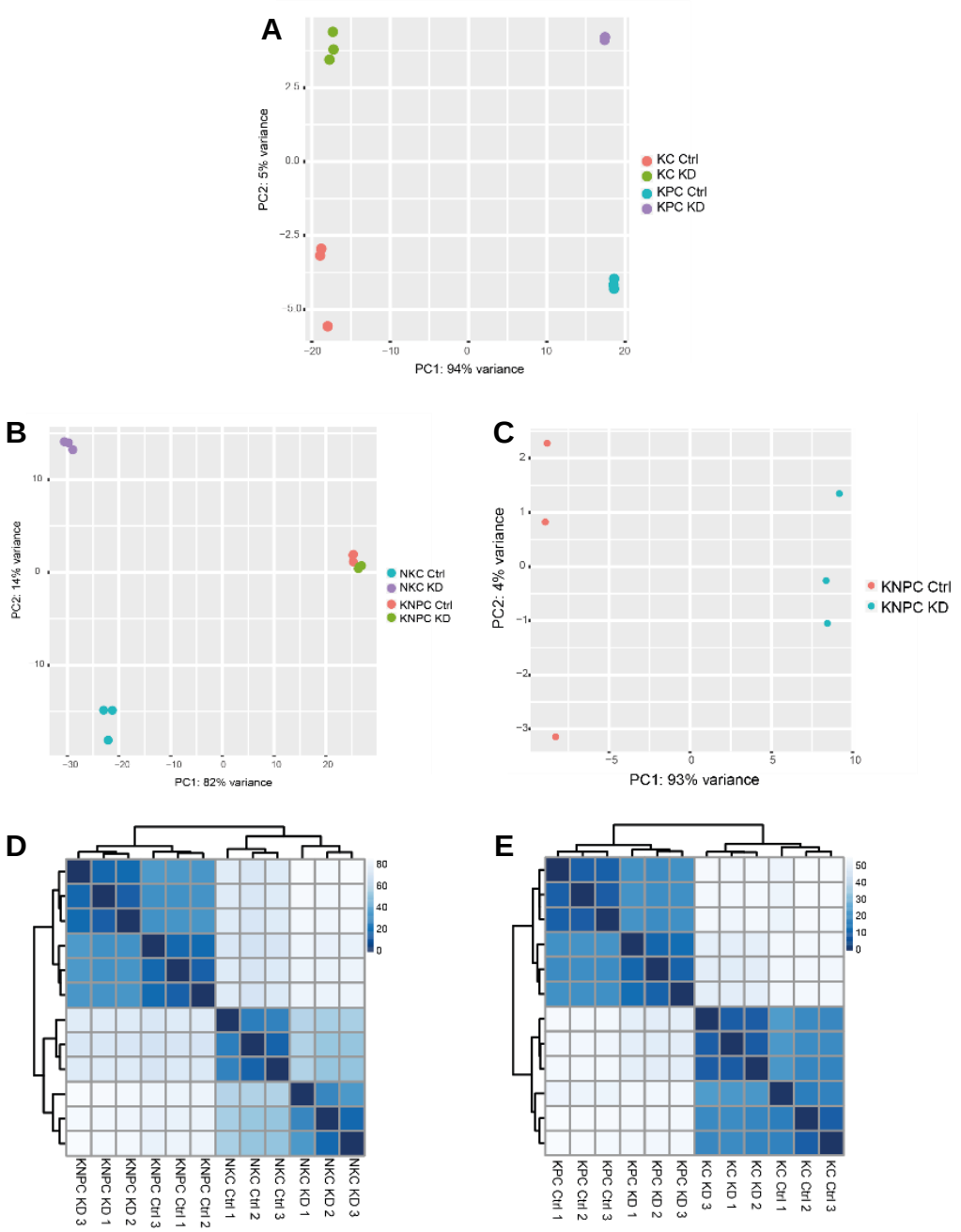

Figure 11: Principal component analysis and sample-to-sample distances of RNA-seq. A-C PCA plots showing the similarities of the triplicates and the differences in the conditions after *Ezh2* knockdown (KD) in KC and KPC (**A**) and NKC and KNPC (**B**) cells. To improve the visualization of the distances between KNPC *Ezh2*-proficient (KNPC Ctrl) and Ezh2-deficient (KNPC KD) cells, PCA was performed separately (**C**). **D-E** Heatmap of sample-to-sample distances of triplicates of KC and KPC (**D**) and NKC and KNPC (**E**) cells upon knockdown of EZH2 after RNA-seq.

To reduce false-positive gene expression, genes with an expression of lower than 0.01 Fragments per kilobase of transcript per million mapped fragments (FPKM) were excluded from analysis resulting in including approximately 70 % of the whole genome. In order to investigate global *Trp53*-status dependent differential gene regulation by EZH2, we displayed the FPKM values of all genes being significantly upregulated (log2FC > 0.5, q < 0.05) in p53wt PDAC cells in a heatmap and investigated the consequences of EZH2 knockdown in the respective p53mut cells (Figure 12).

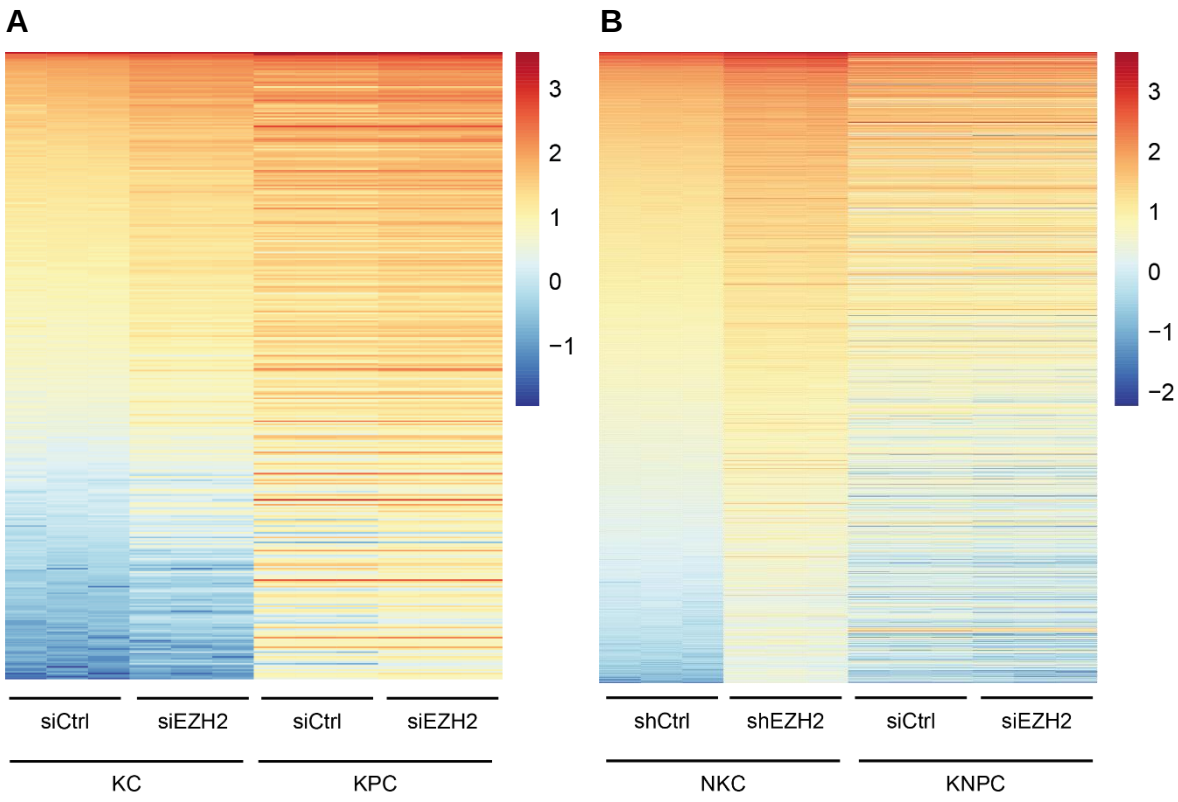

Figure 12: EZH2 regulates target genes differentially in p53wt and p53mut cells. A-B Heatmap displaying the expression of significantly upregulated genes in KC (**A**) and NKC (**B**) upon EZH2 silencing from RNA-seq and its consequences on the expression of these genes in the respective p53mut cells (FPKM > 0.01, log2FC > 0.5, q < 0.05).

In KC cells, we found 384 upregulated genes upon EZH2 knockdown. Interestingly, these genes were mostly not upregulated in KPC cells but rather unaltered or even downregulated (Figure 12A). Even more distinct, in NKC cells, EZH2 knockdown led to the upregulation of 1322 genes. However, these genes were mostly not upregulated in the respective KNPC cells (Figure 12B) suggesting that the *Trp53*-status alters the global EZH2-dependent target gene regulation. To also consider PRC2-independent effects of EZH2, we also looked at

genes being significantly downregulated (log2FC < -0.5, q < 0.05) in p53wt PDAC cells upon knockdown of EZH2 and examined the effects on the expression in the respective p53mut cells (Figure 13). In KC cells, we identified 188 genes that were significantly downregulated upon EZH2 silencing. Interestingly, these genes were mostly not altered in KPC cells (Figure 13A). Similarly, in NKC cells 964 genes were found to be significantly downregulated upon EZH2 knockdown whereas in KNPC cells the expression of these genes remained mostly similar (Figure 13B). Together, these findings suggest that the *Trp53*-status not only impacts the canonical methyltransferase activity of EZH2 but also alters potential non-canonical EZH2 functions or indirect EZH2 effects.

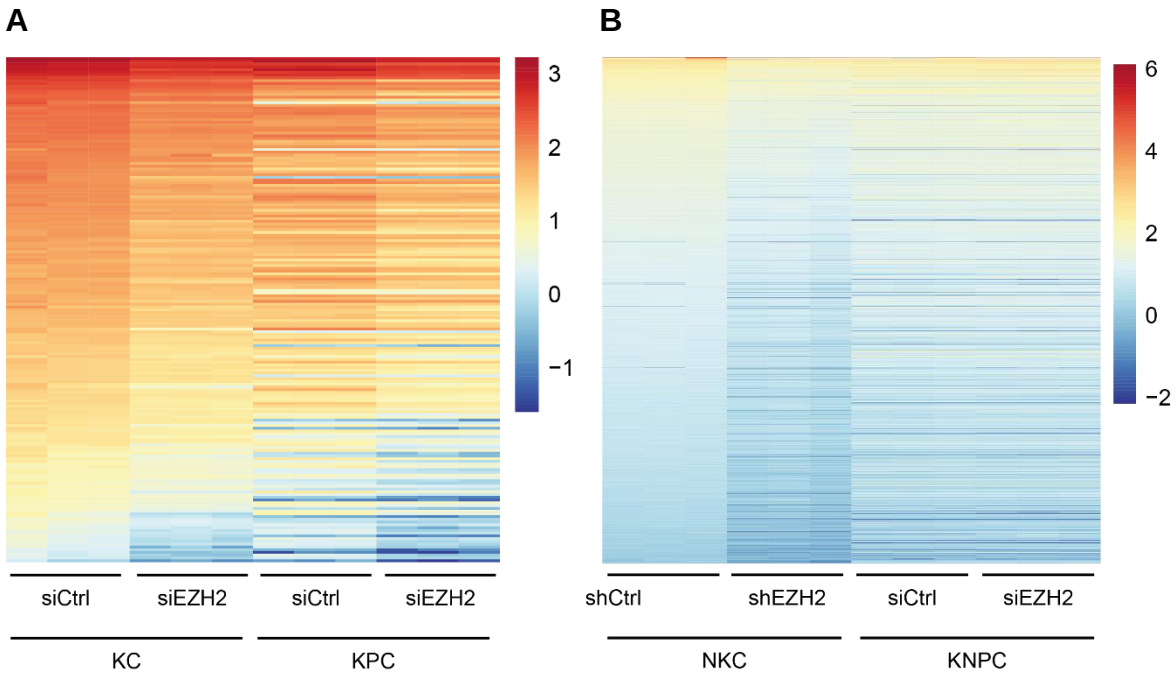

Figure 13: PRC2 independent EZH2 activity in p53wt and p53mut PDAC. A-B Heatmap illustrating significantly downregulated genes (FPKM > 0.01, log2FC < -0.5, q < 0.05) upon knockdown of EZH2 in KC (**A**) and NKC (**B**) cells and its consequences on the expression of these genes in the respective p53mut cells.

EZH2 depletion favours better prognosis restrictively in p53wt PDAC

Next, we assessed whether the *Trp53*-status not only influences the global transcriptional level, but also genes that are associated with a favourable PDAC prognosis to examine if the *Trp53*-status determines the prognostic relevance of EZH2 inhibition. Therefore, we used publicly available transcriptomic data from *The Cancer Genome Atlas* (TCGA) where 857 genes were classified as 'Favorable Prognosis' genes, meaning that high expression

of these genes correlates with better overall survival (Weinstein et al. 2013). In line with previous findings (Patil et al. 2020) our analysis revealed that EZH2 depletion correlates with better prognosis only in p53wt PDAC, but not in p53mut PDAC (Figure 14). As previously published (Patil et al. 2020), the enrichment of favorable prognosis genes is highly significant (Negative Enrichment Score (NES): -1.302, False Discovery Rate (FDR) *q* value: 0.003) upon EZH2 blockade in NKC cells. In KC cells the tendency that EZH2 depletion led to the enrichment of favorable prognosis genes (NES: -1.10, FDR *q* value: 0.16) is also verifiable. However, it is only significant when using an FDR *q* value cutoff of 25 % (Figure 14A). Contrary, in p53mut cells, better prognosis was either unaltered by EZH2 depletion as for KNPC (NES: 1.00, FDR *q* value: 0.44) or even associated with the presence of EZH2 as for KPC (NES: 1.22, FDR *q* value: 0.03) (Figure 14B).

Consequently, consistent with the results of our orthotopic *in vivo* model, in p53mut cells, we could not detect a beneficial outcome of EZH2 depletion, whereas in p53wt PDAC cells we do see an advantageous effect of EZH2 blockade. Together, these findings support our hypothesis that the *TP53*-status determines the regulation of EZH2 target genes with implication in PDAC prognosis.

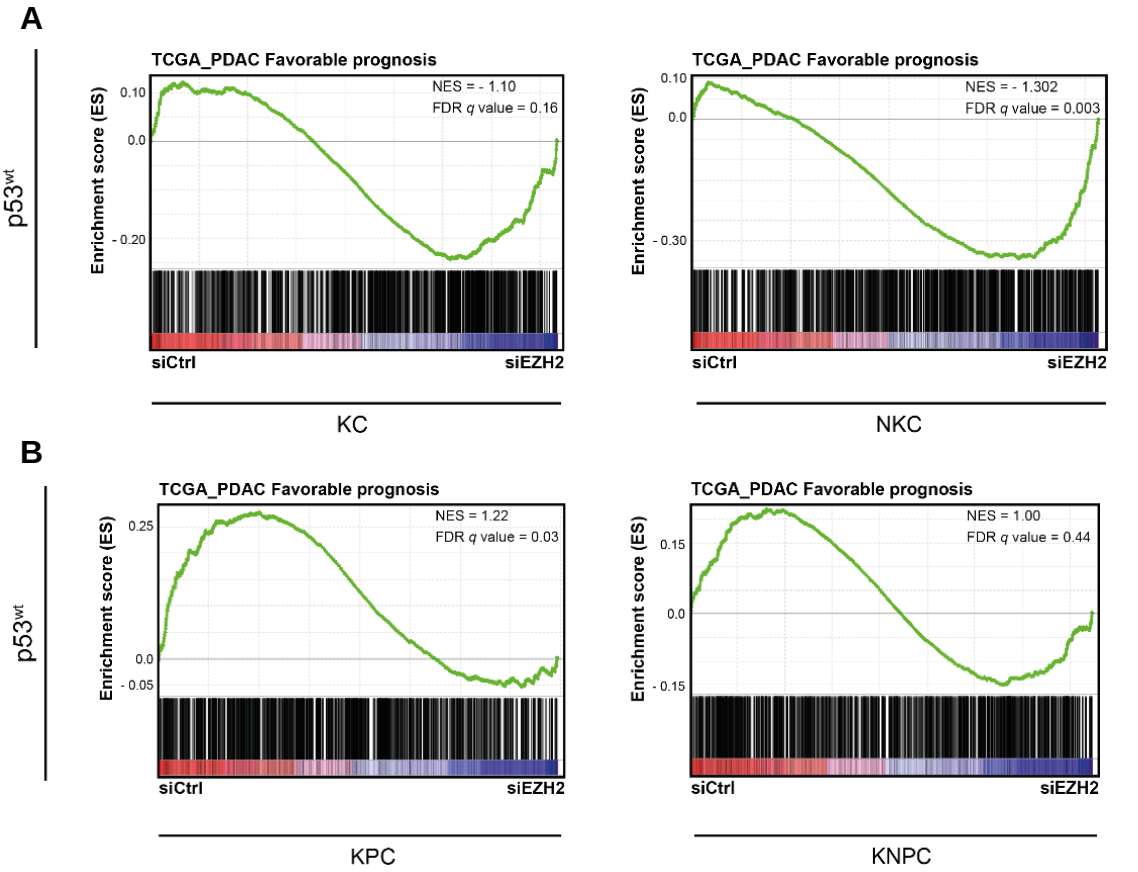

(Figure legend on next page)

Figure 14: EZH2 silencing correlates with better prognosis only in p53wt PDAC. A-B Gene set enrichment analysis (GSEA) in the indicated p53wt (KC, NKC) (**A**) and p53mut (KPC, KNPC) (**B**) PDAC cells display a positive enrichment of 'Favorable prognosis'-associated genes upon knock-down of EZH2 after RNA-sequencing (RNA-seq) only in p53wt PDAC cells (GSEA of NKC as published previously in Patil et al. 2020).

3.3 Inverse effects of apoptotic processes depending on the *TP53* status

EZH2 regulates apoptosis and p53 pathway-related genes

To examine pathways differentially regulated in p53wt and p53mut PDAC, we performed gene ontology (GO) analysis. Our NKC-KNPC model revealed that p53 pathway and apoptosis-associated genes are significantly enriched upon EZH2 depletion restrictively in p53wt NKC cells, whereas in p53mut KNPC cells, they are unaltered (apoptosis) or even down-regulated (p53 pathway) (Figure 15).

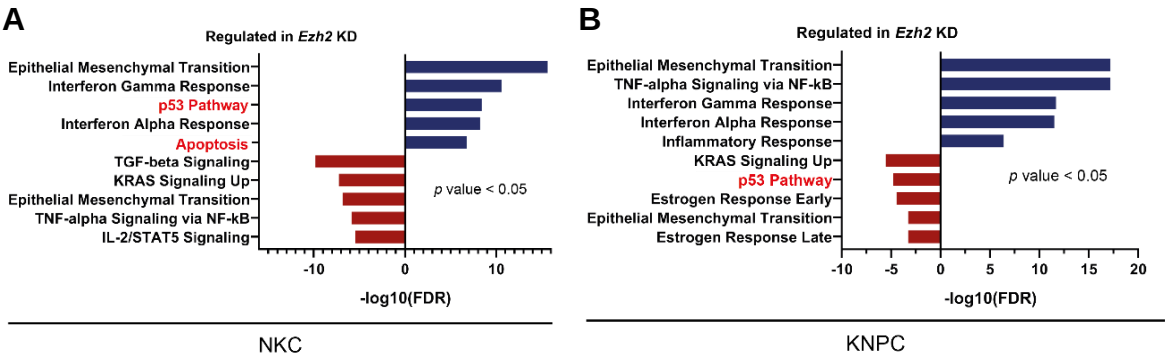

Figure 15: Upregulation of Apoptosis and p53 Pathway associated gene sets are restricted to p53wt NKC cells. A, B Gene ontology (GO) analysis displaying significantly up- and downregulated pathways upon EZH2 silencing in NKC (**A**) and KNPC (**B**) cells ($p < 0.05$). Importantly, p53 Pathway and apoptosis-related genes are only enriched in p53wt NKC cells.

Consistently, in KC cells, we observed significant upregulation of apoptosis and p53 pathway genes while in KPC cells these gene sets were not affected upon EZH2 depletion (Figure 16).

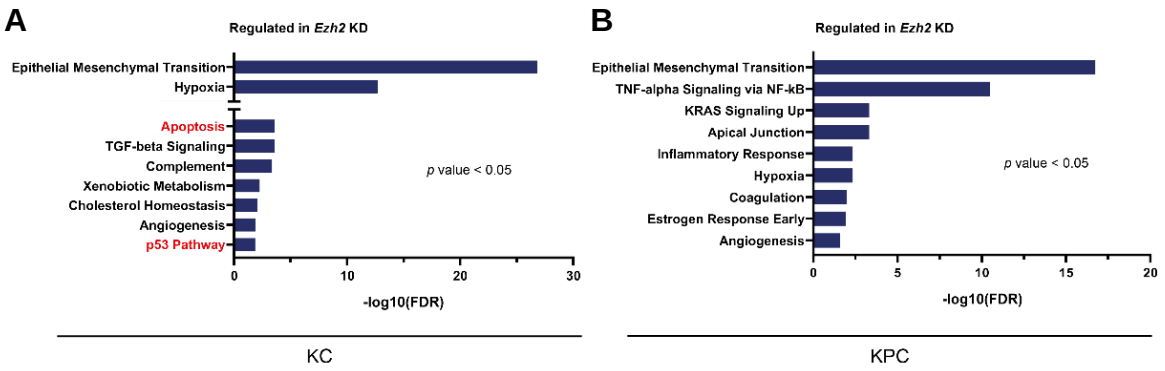

Figure 16: Apoptosis and p53 pathway associated gene sets are only enriched in p53wt PDAC cells. A-B Gene ontology (GO) analysis displaying significantly upregulated pathways upon EZH2 silencing in KC (**A**) and KPC (**B**) cells ($p < 0.05$).

To confirm the significance of the *Trp*53-status on EZH2-dependent target gene regulation and specifically on apoptosis-related and p53 pathway associated genes, we selected 62 genes from the Molecular Signatures Database (MSigDB) (Liberzon et al. 2015) that are pro-apoptotic and/or p53 pathway-related and that were highly upregulated in NKC cells upon knockdown of EZH2 (Figure 17). In line with our previous findings, we found a positive enrichment of these gens upon EZH2 depletion only in p53wt NKC cells, whereas in p53mut KNPC cells these genes were mostly not enriched (Figure 17).

In summary, our data support our hypothesis that the *TP53*-status alters EZH2-dependent target gene regulation and significantly determines the outcome of EZH2 depletion.

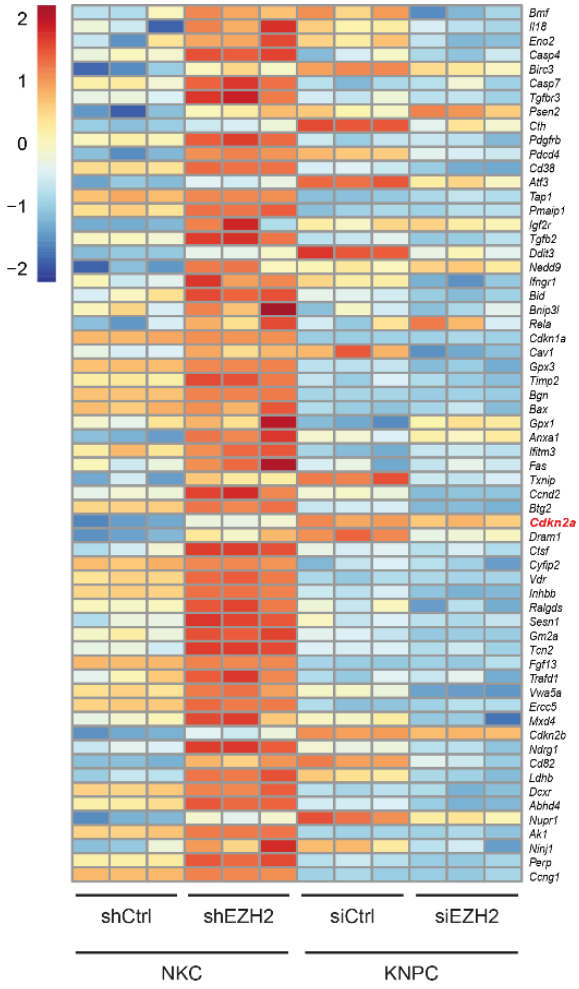

Figure 17: EZH2 blockade results in an enrichment of apoptosis and/or p53 pathway-related genes in NKC cells. Heatmap displaying the expression of 62 selected pro-apoptotic and/or p53 pathway associated genes in NKC and KNPC cells upon EZH2 knockdown after RNA-seq (FPKM > 0.01).

EZH2 depletion favours apoptosis-related gene sets restrictively in p53wt PDAC

Based on our GO analysis that EZH2 depletion resulted in an enrichment of apoptosis-related pathways, we next aimed at exploring, whether the *Trp53* status indeed impacts apoptotic processes. Initially, we performed GSEA and compared our RNA-seq results to apoptosis-related gene sets (Figure 18). In p53wt PDAC cells, we revealed an enrichment of pro-apoptotic genes upon EZH2 knockdown (KC: NES: -1.19, FDR *q* value: 0.13, NKC: NES: -1.41, FDR *q* value: 0.02) (Figure 18A) whereas in p53mut cells apoptotic gene sets were either even enriched in siCtrl condition (KNPC: NES: 1.32, FDR *q* value: 0.05) or not significantly regulated (KPC: NES: 1.01, FDR *q* value: 0.45) (Figure 18B).

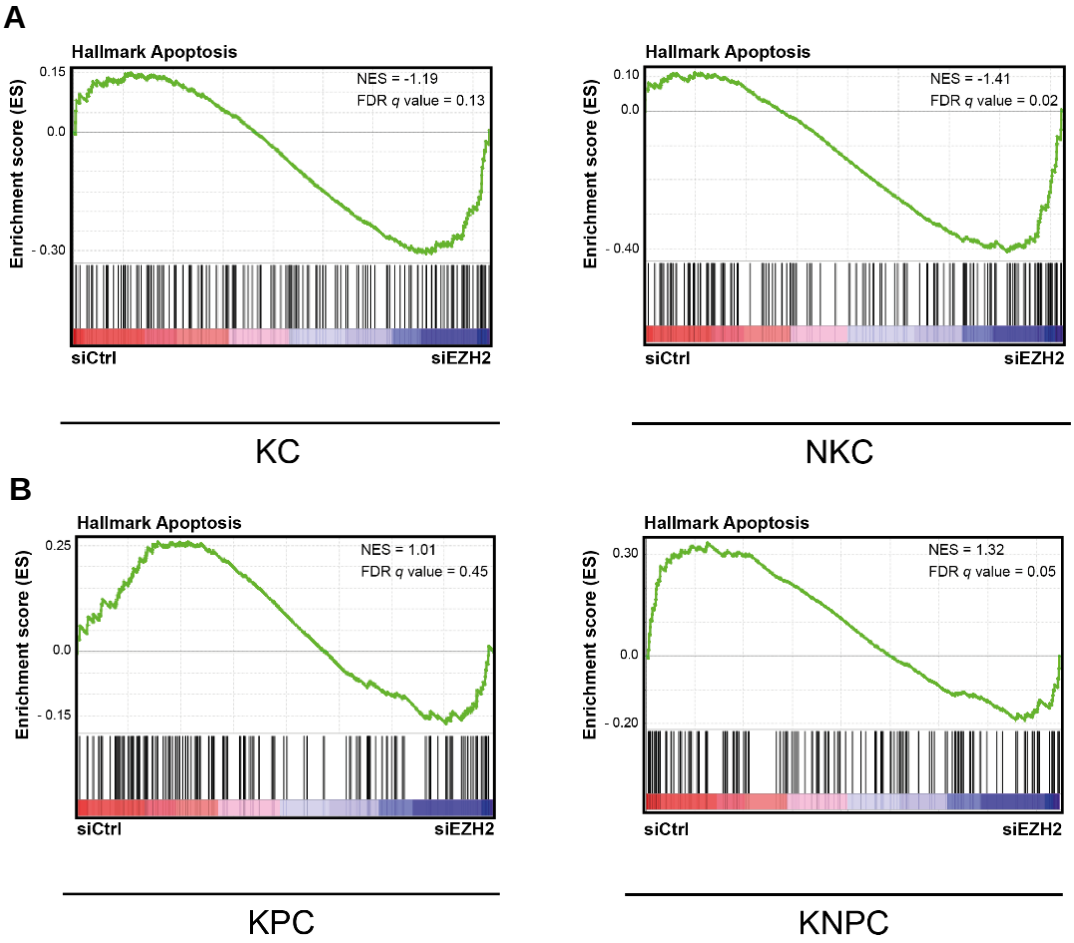

Figure 18: Depletion of EZH2 mediates apoptosis only in p53wt PDAC. A-B Gene set enrichment analysis (GSEA) upon RNA-seq in the indicated p53wt (KC, NKC) (**A**) and p53mut (KPC, KNPC) (**B**) cells upon knockdown of EZH2 revealing enrichment of apoptotic gene sets.

Opposite functional consequences of EZH2 depletion on apoptosis induction depending on the *Trp53*-status

To explore whether the transcriptomic differences also resulted in functional implications, we looked for apoptotic processes both on the protein level using immunoblotting analysis and on the functional level using Annexin-V and propidium iodide (PI) staining followed by flow cytometry. Simultaneous staining of Annexin-V and PI can distinguish between living (Annexin-V and PI negative), early apoptotic (positive for Annexin-V but negative for PI), late apoptotic (positive for both Annexin-V and PI), and dead (positive for PI but negative for Annexin-V) cells. Since EZH2 depletion alone is not sufficient to induce detectable proapoptotic processes on a functional level, we took advantage of the potent protein kinase C inhibitor staurosporine (STS) to effectively induce apoptosis (Couldwell et al. 1994).

Notably, only in p53wt cells, the additional knockdown of EZH2 combined with STS treatments augmented apoptotic processes, as demonstrated by increased cleavage of PARP and caspase 3 (Figure 19A, B). Specifically, the increased cleavage of caspase 3 was very prominent in NKC cells (Figure 19B). Moreover, the portion of early apoptotic cells was significantly increased upon STS treatment and EZH2 depletion (Figure 19A, B). Contrary and in accordance with our GSEA, in p53mut PDAC cells, EZH2 depletion did not accelerate apoptosis induction. In KPC cells, pro-apoptotic cleavage of PARP and caspase 3 as well as the fractions of apoptotic cells upon flow cytometry analysis were similar in the presence and absence of EZH2 (Figure 19C). In KNPC cells, a reduced cleavage of PARP and caspase 3 was at least observed on protein level, however, it did not result in reduced Annexin-V staining (Figure 19D).

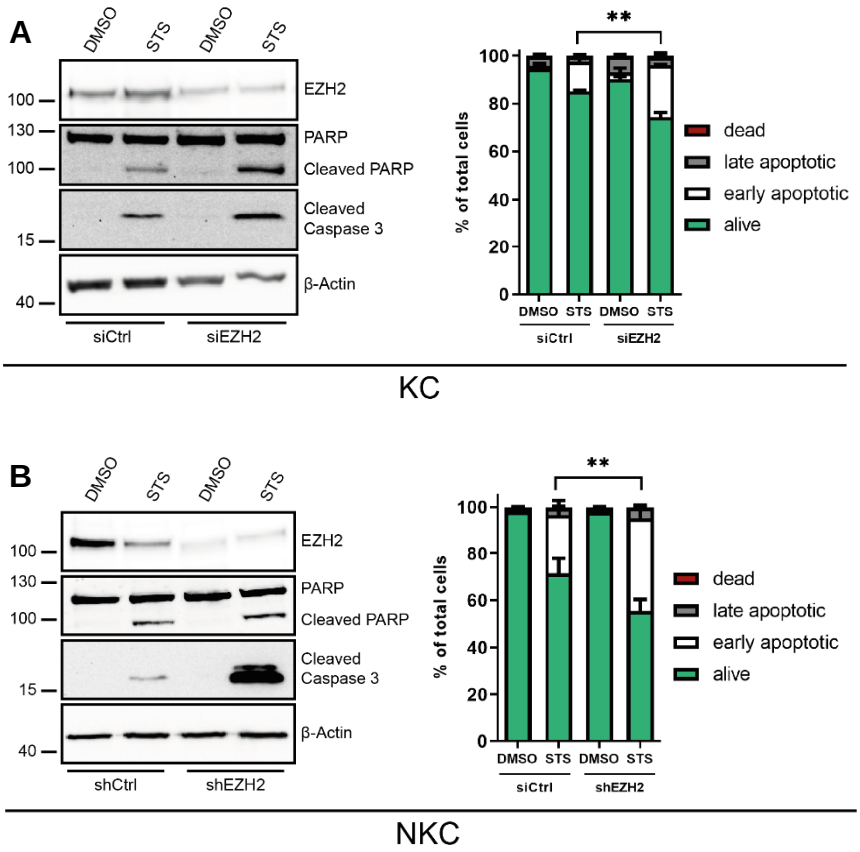

(Figure continued on next page)

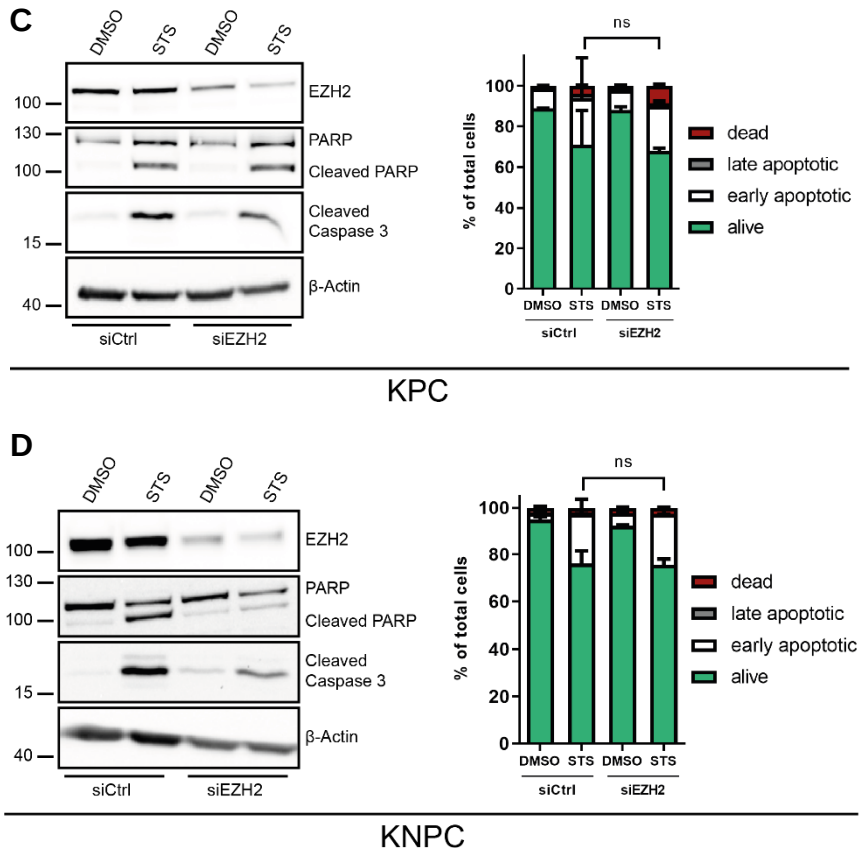

Figure 19: EZH2 depletion augments apoptosis restrictively in p53wt cells. A-D Elucidation of apoptosis induction upon knockdown of EZH2 and simultaneous treatment with 0.5 µM staurosporine (STS) (24 h) in the indicated p53wt (KC (**A**), NKC (**B**)) and p53mut (KPC (**C**), KNPC (**D**)) cells. Western blot analysis of whole cell lysate (left panel) revealing successful EZH2 knockdown and apoptotic response to STS treatment. β-actin served as loading control. DMSO treatment was used as control. Annexin-V/propidium iodide (PI) staining and subsequent analysis by flow cytometry (right panel) to assess apoptosis induction. Data from three independent experiments were analysed and cells were classified as alive (negative for Annexin-V and PI), early apoptotic (positive for Annexin-V, negative for PI), late apoptotic (positive for both Annexin-V and PI), and dead (positive for PI, negative for Annexin-V). Significance was determined by two-tailed unpaired Student´s *t* test; **, p ≤ 0.01; ns, non-significant.

Additionally, to confirm our findings and underline the relevance of the *Trp53* status on the consequences of EZH2 depletion, we combined EZH2 silencing with the chemotherapeutic agent 5-fluorouracil (5-FU) treatment to induce programmed cell death (Shi et al. 2002). Consistent with our previous results, the absence of EZH2 and treatment with the chemotherapeutic drug 5-FU led to enhanced apoptosis induction as identified by increased levels of cleaved PARP and cleaved caspase 3 only in p53wt PDAC cells (Figure 20A). In contrast, in p53mut cells, EZH2 depletion did not increase cleavage of PARP or caspase 3 (Figure 20B).

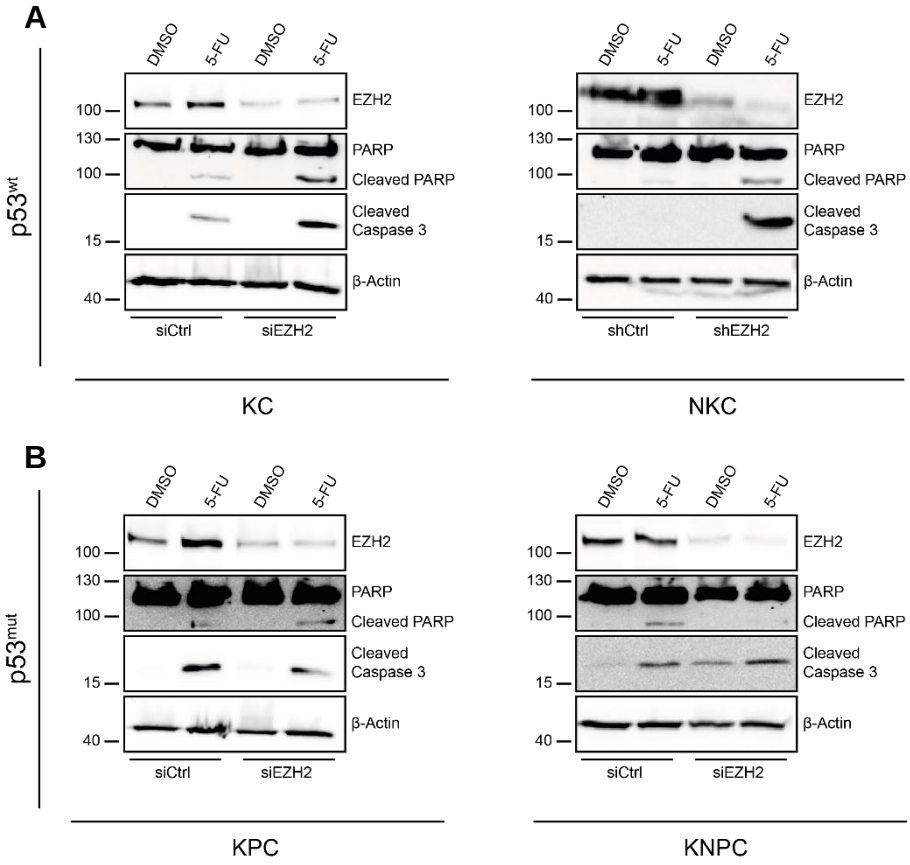

Figure 20: *Trp53* wildtype status accelerates apoptosis upon EZH2 silencing.A-B Western blot analysis to elucidate apoptosis induction upon EZH2 silencing and treatment with 10 µM 5-fluorouracil (5-FU) (24 h) in the indicated p53wt (**A**) and p53mut (**B**) PDAC cells. DMSO treatment was used as control. β-actin served as loading control.

Additionally, to exclude that the observed inverse consequences of EZH2 depletion depending on the *Trp53*-status were due to cell line-specific properties other than the *Trp53*-status, we used a $p53^{null}$ system and transfected re-expressed $p53^{wt}$ or $p53^{mut}$ constructs in *Kras^{G12D};caNFATc1;Trp53$^{\Delta/\Delta}$* ($KNP^{null}C$) cells. $KNP^{null}C$ cells are derived from *Kras^{G12D};caNFATc1;Trp53$^{\Delta/\Delta}$* GEMM and these *KNP^{null}C* mice have comparable phenotypic PDAC characteristics to those of *KNPC* mice (Singh et al. 2015). Upon knockdown of EZH2 and simultaneous treatment with 5-FU, we observed no changes in PARP and caspase 3 cleavage in the $p53^{null}$ condition. More importantly, an augmented activation of caspase 3 and cleavage of PARP in p53wt condition was detectable, whereas in p53mut condition cleavage of caspase 3 was higher in the presence of EZH2, while PARP cleavage remained unchanged. These findings underlined that the oncogenic EZH2 activity with regard to induction of pro-apoptotic markers is strongly p53-status dependent (Figure 21).

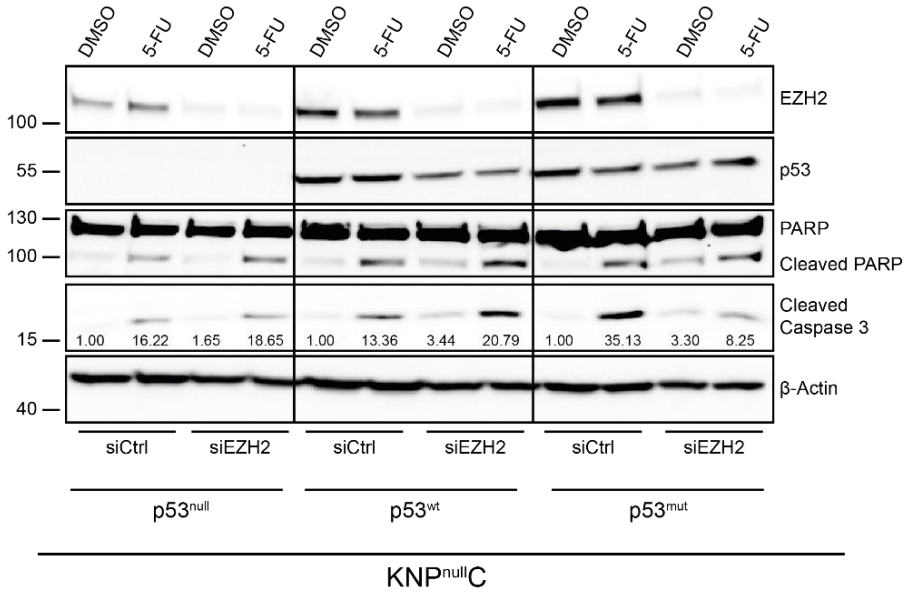

Figure 21: Opposite consequences of EZH2 blockade depending on p53wt expression. *Kras^{G12D};caNFATc1;Trp53$^{\Delta/\Delta}$* ($KNP^{null}C$) cells were transfected with $p53^{wt}$ or $p53^{mut}$ construct to re-express $p53^{wt}$ or $p53^{mut}$, respectively. Subsequently, EZH2 was silenced using siRNA and apoptosis was induced using 10 µM 5-fluorouracil (5-FU) (24 h). Whole cell lysates were conducted to immunoblot analysis to confirm successful EZH2 knockdown and p53 re-expression and to assess apoptotic response to 5-FU treatment. β-actin served as loading control. Densitometric quantification of cleaved caspase 3 detection was performed using ImageJ and is revealed under the respective band.

Similarly, we used human primary PDAC cells with p53wt (GöCDX13) and p53mut (GöCDX5) expression and demonstrated that EZH2 depletion fostered apoptosis induction as revealed by activation of caspase 3 only in the p53wt condition whereas in p53mut cells cleavage of caspase 3 was not detectable (Figure 22).

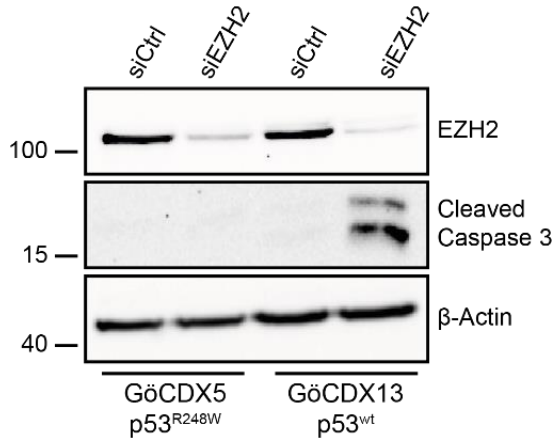

Figure 22: EZH2 depletion induces caspase 3 cleavage only in p53wt human PDAC. Knockdown of EZH2 in primary human PDAC cells with p53mut (GöCDX5) and p53wt (GöCDX13) expression and subsequent western blotting analysis to examine pro-apoptotic cleaved caspase 3 level. β-actin served as loading control.

In summary, our *in vitro* data highlight a strong context-dependency of EZH2 inhibition specifically regarding the *TP53*-status and suggest that depletion of EZH2 might be restrictively advantageous in *TP53* wildtype PDAC, but not in subtypes bearing mutations in *TP53*.

3.4 EZH2 regulates the p53wt protein

Since our RNA-seq analysis in p53wt PDAC cells revealed that EZH2 depletion led not only to the enrichment of apoptotic related gene sets but also to the upregulation of p53 pathway associated gene sets (Figure 15, Figure 16), we aimed to investigate the functional implications of EZH2 knockdown on p53 expression. Surprisingly, on the mRNA level, we could not detect any significant differences upon EZH2 depletion on *Trp53* gene expression both in p53wt and in p53mut PDAC cells (Figure 23A). However, on protein level, we observed an upregulation of p53 upon EZH2 knockdown, restrictively in p53wt PDAC cells (Figure 10B, Figure 23B), suggesting that EZH2 regulates p53wt on a post-translational level.

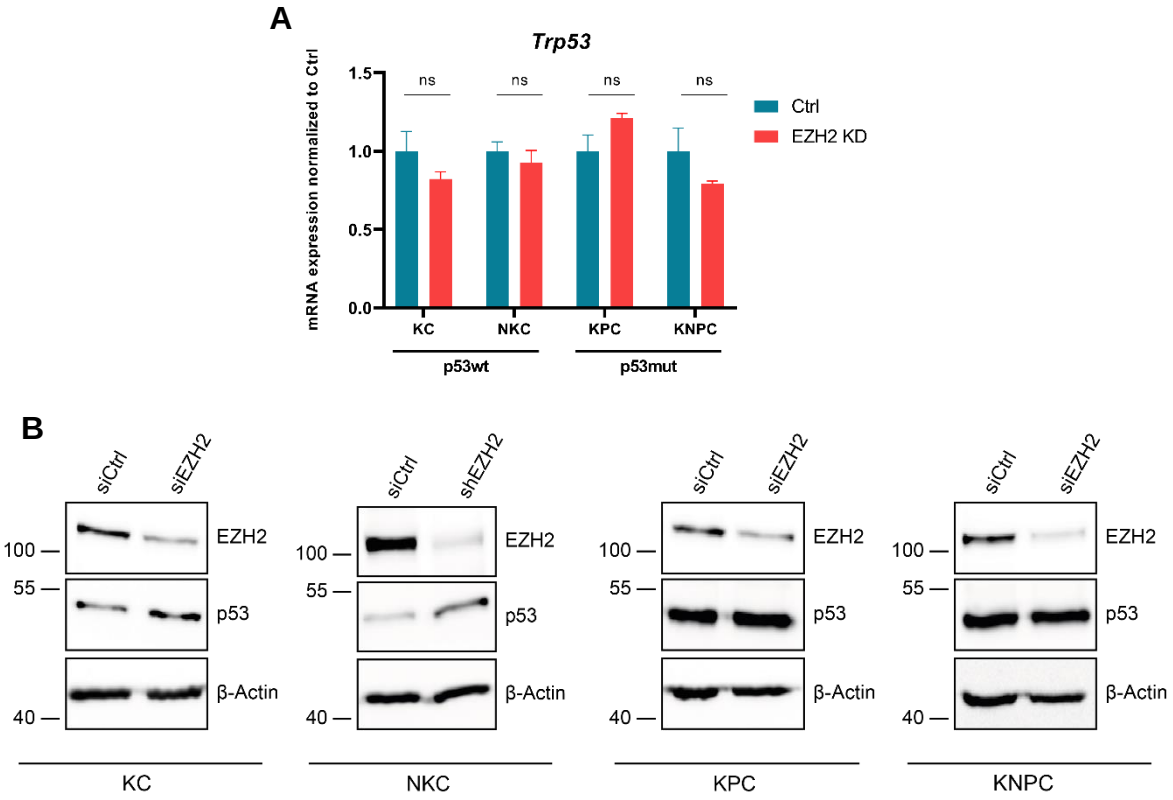

Figure 23: EZH2 regulates p53wt on a post-translational level. A-B qRT-PCR (**A**) and western blot (**B**) analysis in the indicated p53wt and p53mut PDAC cells upon knockdown of EZH2 to assess the consequences on p53 expression. Knockdown of EZH2 on mRNA level was shown previously in Figure 10B. Values represent mean ± SD. Significance was determined by two-tailed unpaired Student´s *t* test, ns, non-significant.

Next, we addressed a potential post-translational EZH2-dependent p53wt regulation. As previously described (see *1.2 The Tumor Suppressor p53*, p. 6) the expression of p53wt is tightly regulated. In unstressed cells, p53wt is quickly destabilized by proteasomal degradation mediated by E3-ligases such as Mouse double minute 2 homolog (Mdm2) (Oliner et al. 1992, Momand et al. 1992). However, this strict regulation is abolished in tumors with mutant p53 resulting in stabilization and accumulation of p53mut protein (Lukashchuk and Vousden 2007, Frum and Grossman 2014). To examine, if EZH2 regulates p53wt on a post-translational level, we interfered with the translational machinery using cycloheximide (Schneider-Poetsch et al. 2010), thus obtaining information on the half-life of the p53wt protein. Indeed, cycloheximide treatment displayed a prolonged half-life of p53wt in EZH2-depleted cells. Densitometric measurements of p53 protein detection confirmed the increased p53wt stability upon EZH2 knockdown (Figure 24).

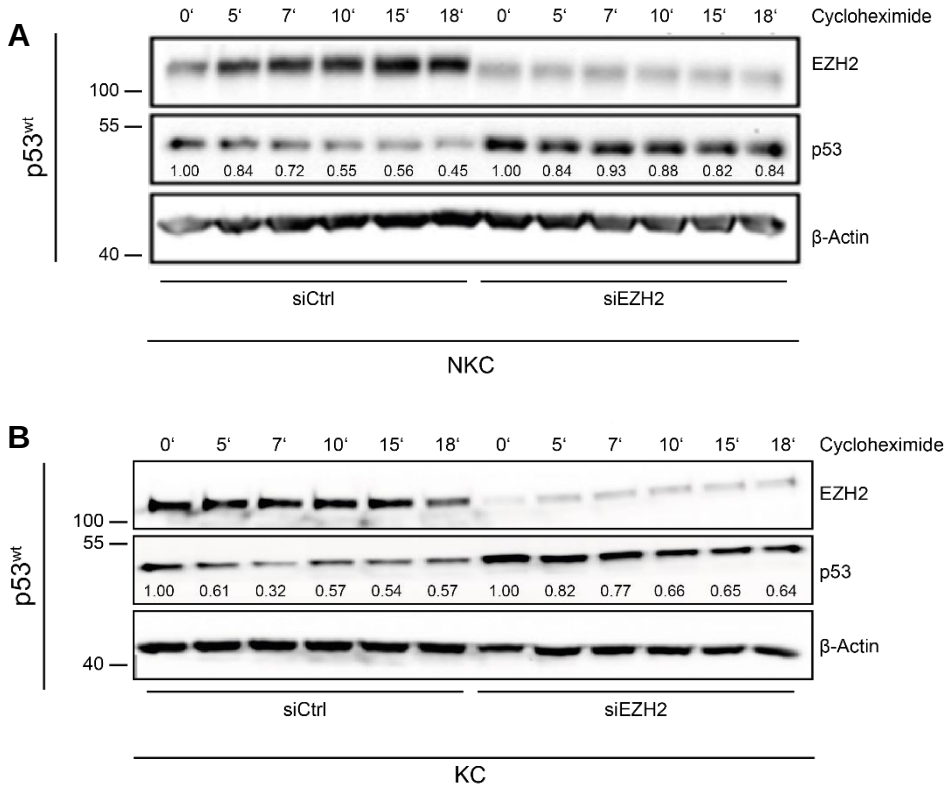

Figure 24: EZH2 decreases stability of p53wt protein. A-B NKC (**A**) and KC (**B**) cells were treated with 20 mg/ml cycloheximide for the indicated time points to prevent re-synthesis of p53 thereby providing information on p53 half-life. Whole cell lysates were subjected to western blot analysis to analyse p53 protein level. Densitometric quantification of p53 detection was performed using ImageJ and normalized to the respective H_2O-treated control. Quantification is revealed under the respective band.

Consistently, our data suggest that EZH2 promotes p53wt degradation (Figure 25). By using the proteasome inhibitor MG132, which blocks proteasomal degradation of p53, we examined the extent of ubiquitinated p53wt (Zhu et al. 2007). Importantly, the p53wt protein is stronger ubiquitinated in the presence of EZH2 (Figure 25), emphasizing that EZH2 accelerates the degradation of p53wt.

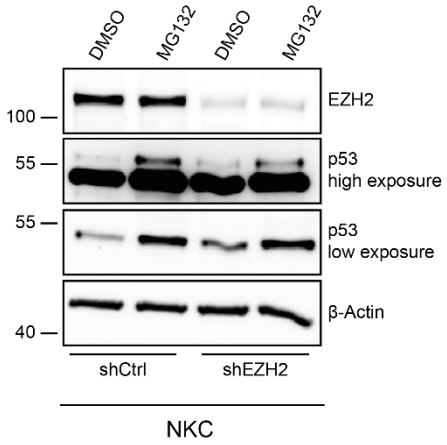

Figure 25: EZH2 promotes p53wt degradation. NKC cells were treated with 10 µM of the proteasome inhibitor MG132 for 1 h and were subjected to western blotting analysis to examine the ubiquitination levels of p53. DMSO treatment was used as negative control. β-actin served as loading control.

3.5 EZH2 regulates p53wt via the *CDKN2A* axis

Cdkn2a is repressed by EZH2

The significant role of $p14^{ARF}$ and its murine equivalent $p19^{Arf}$ has been intensively studied. It is encoded by the *Cdkn2a* gene locus and forms stable complexes with Mdm2 thereby preventing Mdm2 from binding and destructing p53, thus leading to p53 stabilization (Zhang et al. 1998). Notably, *Cdkn2a* also appeared among the 62 selected apoptosis-related and/or p53 pathway-associated genes that are highly enriched in NKC cells upon EZH2 knockdown (Figure 17). Accordingly, we used our RNA-seq data and overlayed all significantly upregulated genes in all four cell types. We identified 35 genes that were only upregulated in p53wt condition (KC, NKC), but not in p53mut cells (KPC, KNPC) (Figure 26A) (*35 genes are listed in Supplementary Table 1*). We performed expression analysis of these genes in independent EZH2 knockdown experiments. Herein, we validated the expected upregulation upon EZH2 knockdown in p53wt cells and revealed that these genes are not upregulated in p53mut cells (Figure 26B-D). Importantly, *Cdkn2a* was detected among these 35 genes that were significantly upregulated only in p53wt, but not in p53mut PDAC cells (Figure 26D). Hence, FPKM values from RNA-seq analysis displayed that in p53wt cells *Cdkn2a* reads are significantly enriched upon EZH2 knockdown normalized to control condition whereas in p53mut cells *Cdkn2a* reads remain similar upon normalization to control condition (Figure 26C).

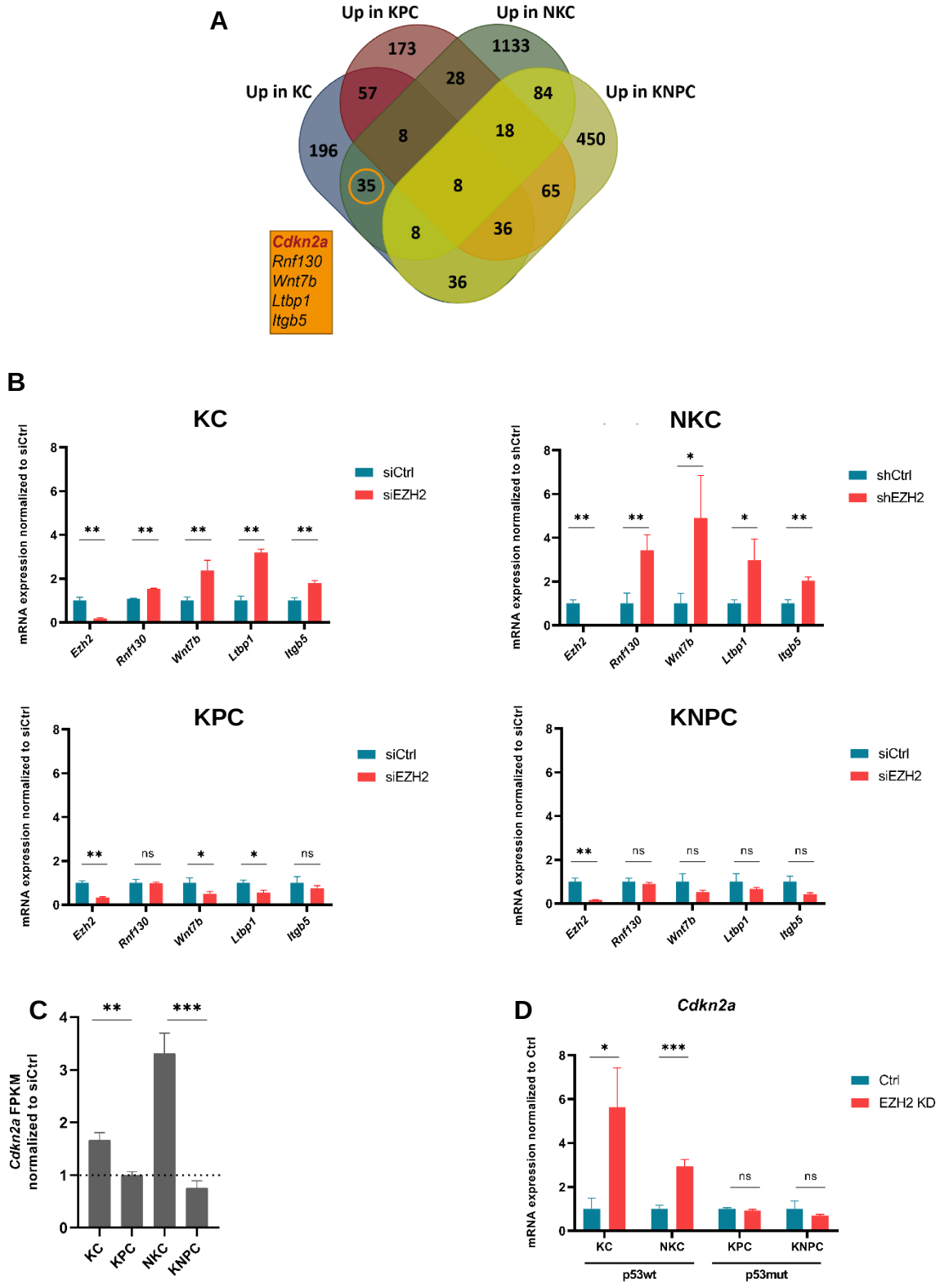

Figure 26: Selection of genes, that are restrictively repressed by EZH2 in p53wt but not in p53mut cells. A Venn diagram showing the intersection of significantly upregulated genes (FPKM > 0.01, log2FC > 0.5, q < 0.05) in the indicated p53wt and p53mut PDAC cells upon knockdown of EZH2 upon RNA-seq. *(Figure legend continued on next page).*

Box reveals a selection of five of 35 genes that are only upregulated in p53wt but not in p53mut cells. **B** qRT-PCR to validate the gene expression level of the selected and indicated genes. **C** Gene expression of *Cdkn2a* upon EZH2 knockdown in the indicated cells. **D** *Cdkn2a* FPKM counts normalized to control condition in the indicated PDAC cells. Values represent mean ± SD. Significance was determined by two-tailed unpaired Student´s *t* test; *, $p \leq 0.05$; **, $p \leq 0.01$; ***, $p \leq 0.001$; ns, non-significant.

Cdkn2a is a direct target gene of EZH2

Our RNA-seq data imply that EZH2 silences *Cdkn2a* in p53wt cells. To identify if *Cdkn2a* displays a direct EZH2 target gene in PDAC as indicated previously (Comet et al. 2016, Pinton et al. 2021, Yamagishi and Uchimaru 2017, Kotake et al. 2007, Sparmann and van Lohuizen 2006), we performed chromatin immunoprecipitation (ChIP) analysis followed by qRT-PCR in NKC cells. ChIP experiments were conducted by Dr. Shilpa Patil and following qRT-PCR analysis by Lennart Versemann. Since EZH2 predominantly binds to the transcriptional start site (TSS)/promoter regions of genes (Patil et al. 2020), we examined if *Cdkn2a* TSS is bound by EZH2. Indeed, ChIP experiments displayed a strong EZH2 binding at the *Cdkn2a* TSS (Figure 27A). To examine if EZH2 knockdown also results in transcriptional activation of *Cdkn2a*, we analysed H3K4me3 occupancy at the *Cdkn2a* TSS. The trimethylation of histone 3 at lysine 4 (H3K4me3) loosens the packaging of DNA, resulting in increased accessibility of genes, thereby facilitating the activation of transcription (Barski et al. 2007). In line with increased expression of *Cdkn2a* upon EZH2 knockdown (Figure 26C), we identified enriched H3K4 trimethylation at the *Cdkn2a* gene upon knockdown of EZH2 (Figure 27B), suggesting that the gene activation of *Cdkn2a* is increased upon EZH2 depletion. Hence, these data are in accordance with EZH2-dependent transcriptional repression of *Cdkn2a* in PDAC.

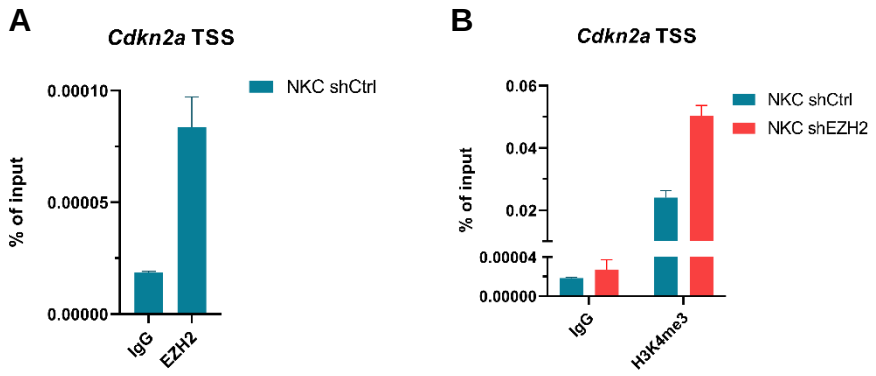

Figure 27: *Cdkn2a* is a direct EZH2 target gene and repressed by EZH2. A-B Chromatin immunoprecipitation (ChIP) and subsequent qRT-PCR in NKC cells reveals binding of EZH2 at the *Cdkn2a* transcriptional start site (TSS) region (**A**) and increased H3K4me3 occupancy ipon EZH2 knockdown at the *Cdkn2a* gene (**B**).

Functional consequences of p19^{Arf} knockdown in EZH2 deficient PDAC cells

Next, we aimed for examining the functional relevance of the discovered EZH2 dependent *Cdkn2a* silencing on the stability and the half-life of p53wt. Therefore, we transiently knocked down p19^{Arf} in EZH2-deficient NKC cells and blocked the translational machinery by treating the cells with cycloheximide. Indeed, the stability and the half-life of p53wt were clearly reduced upon p19^{Arf} knockdown (Figure 28), suggesting that the EZH2-dependent *Cdkn2a* repression is critically involved in EZH2-dependent p53wt regulation. Hence, we identified that EZH2 mediates p53wt degradation via repressing *Cdkn2a* expression, thus resulting in reduced p19^{Arf} synthesis.

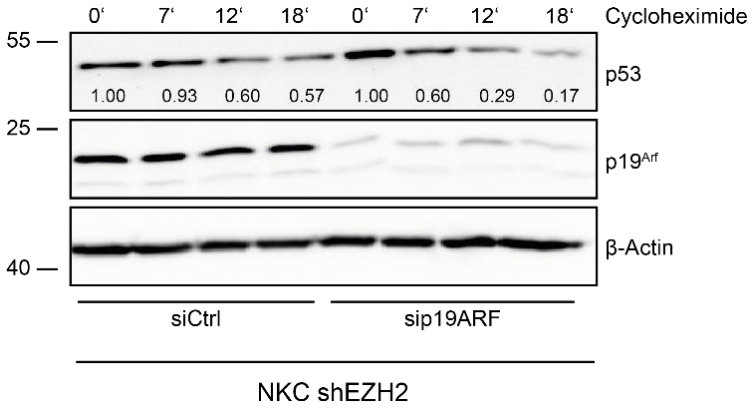

Figure 28: EZH2 alters p53wt half-life indirectly via p19^{Arf} encoded by *Cdkn2a*.

(Figure legend continued on next page).

Whole cell lysate of NKC shEZH2 cells upon knockdown of p19^{Arf} and treatment with cycloheximide (20 mg/ml) for the indicated periods were subjected to western blot analysis to reveal the influence of p19^{Arf} on p53 half-life upon EZH2 deficiency. Densitometric quantification of p53 detection was performed using ImageJ and is depicted under the respective band. p19^{Arf} knockdown was validated. β-actin served as loading control.

To elucidate if the EZH2 dependent regulation of p19^{Arf} is also causative for reduced apoptosis induction in the presence of EZH2 in p53wt PDAC cells, we silenced p19^{Arf} in NKC cells lacking EZH2 and simultaneously treated the cells with STS or 5-FU (Figure 29). Importantly, cleavage of PARP and caspase 3 was significantly decreased upon p19^{Arf} knockdown, implying that apoptotic processes were reduced upon the loss of p19^{Arf} in EZH2 deficient PDAC. Accordingly, the EZH2-dependent regulation of *Cdkn2a* expression is also involved in the suppression of apoptotic processes.

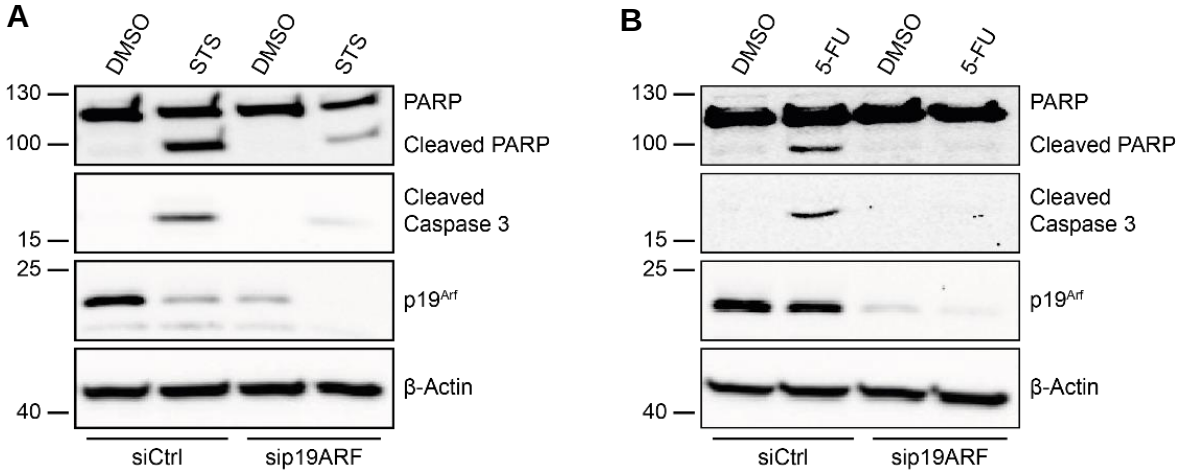

Figure 29: P19^{Arf} knockdown decreases drug-induced apoptosis upon EZH2 deficiency. A-B Western blot analysis in NKC shEZH2 cells upon knockdown of p19^{Arf} and treatment with staurosporine (STS) (0.5 µM) (**A**) or 5-fluorouracil (5-FU) (10 µM) (**B**) for 24 h revealing successful p19^{Arf} knockdown and level of apoptosis-related marker to STS or 5-FU, respectively. DMSO treatment was used as control. β-actin served as loading control.

In summary, the herein identified EZH2-dependent *Cdkn2a* repression has functional consequences for the EZH2 dependent p53wt degradation and the inhibition of apoptosis in p53wt PDAC cells.

3.6 PDAC formation despite low EZH2 expression

PDAC formation despite EZH2 depletion by evading p19^{Arf} upregulation in GEMM

Next, we investigated the significance of the EZH2-dependent *Cdkn2a* regulation on the EZH2-dependent PDAC development and maintenance *in vivo*. Therefore, we utilized a *Kras^{G12D};Ezh2$^{fl/fl}$* (*KEC*) GEMM with pancreas-specific homozygous *Ezh2* deficiency (Chen et al. 2017, Mallen-St Clair et al. 2012) and compared it to *KC* mice (Figure 30A) which are *Trp53* wildtype. Surveillance and sacrificing of mice were conducted by members of the Hessmann group. Tumor incidence, relative tumor weight, and survival analysis were performed by Dr. Shilpa Patil. Notably, *Ezh2* depletion led to decreased number and severity of PDAC precursor lesions (Figure 30B).

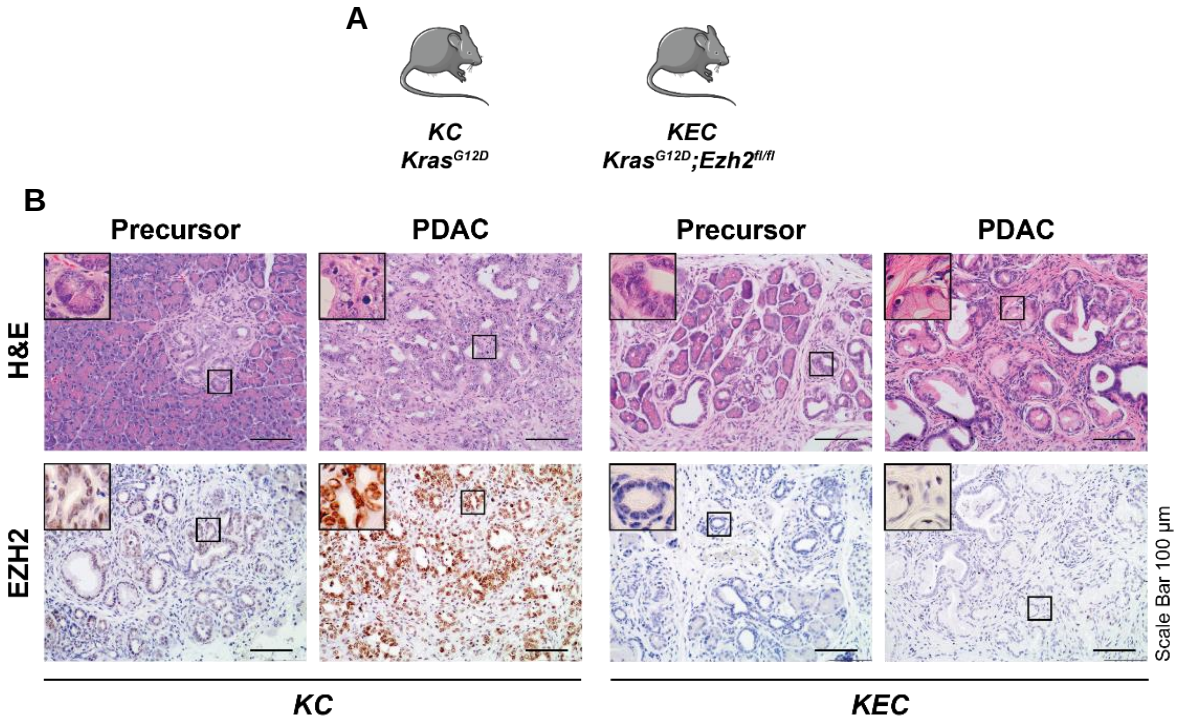

Figure 30: Homozygous *Ezh2* depletion reduces precursor lesions and PDAC. A Schematic illustration of *Kras^{G12D}* (*KC*) and *Kras^{G12D};Ezh$^{fl/fl}$* (*KEC*) GEMM. **B** H&E staining of precursor lesions and PDAC of the indicated genotypes. EZH2 IHC confirms the presence of EZH2 in *KC* tissue and the absence in *KEC* tissue. Magnification 100 x, Scale bar 100 µm.

In line with our hypothesis that EZH2 deficiency leads to upregulation of p19^{Arf}, we detected higher levels of p19^{Arf} in *KEC* precursor tissue as identified by western blot analysis and immunofluorescence (Figure 31, Figure 32).

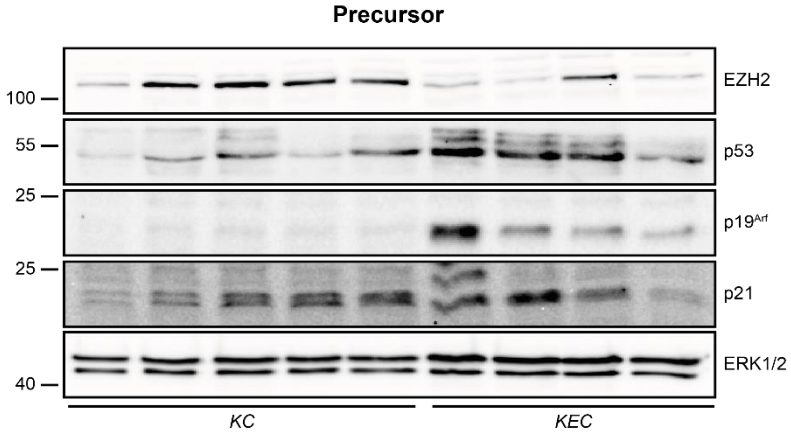

Figure 31: Lack of EZH2 leads to increased p19^{Arf} level in precursor lesions. Protein samples were extracted from pancreatic tissue from *KC* and *KEC* mice (12 weeks old) harbouring PDAC precursor lesions and subjected to immunoblot analysis. Lack of EZH2 was successfully confirmed and leads to increased levels of p53 and p19^{Arf}. ERK1/2 served as loading control.

Consistent with increased p19^{Arf} levels, p53 levels were increased in *KEC*, although p21 expression was not increased in all the lysates (Figure 31). However, our findings suggest that despite *Kras* mutation, EZH2 depletion led to the activation or maintenance of tumor-suppressive mechanisms by increasing p19^{Arf} and p53 expression.

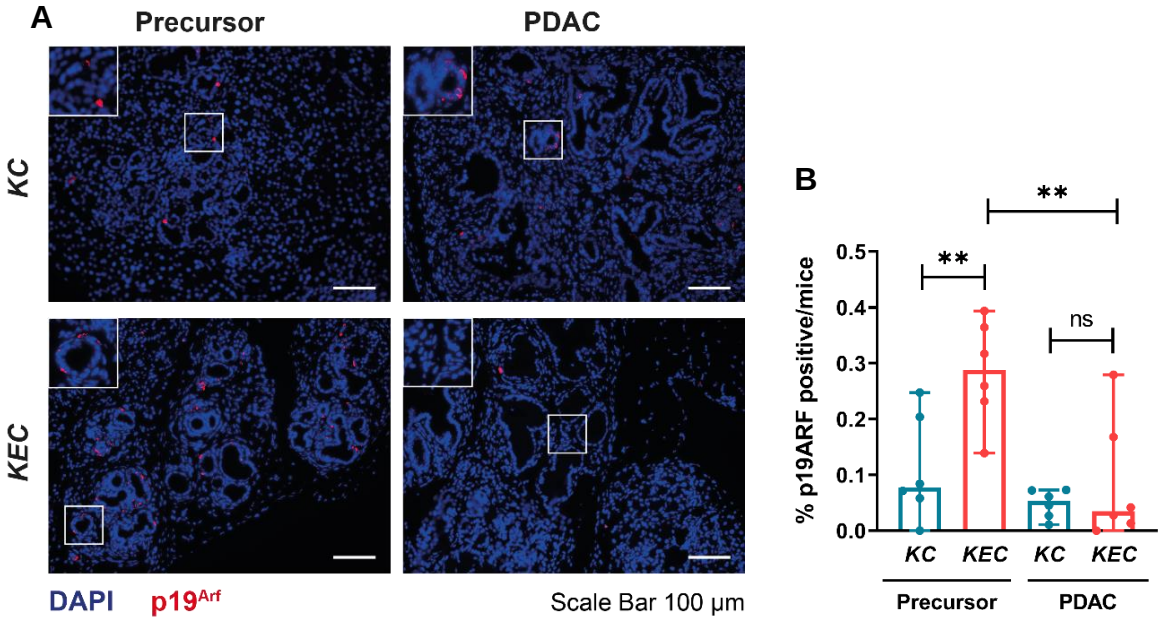

Figure 32: Tumors that develop despite the absence of EZH2 reveal low p19^{Arf} levels. A Immunofluorescence staining of p19^{Arf} (red) of precursor lesions and PDAC of *KC* and *KEC* mice. *(Figure legend continued on next page).*

DAPI (blue) staining was performed to visualize nuclei. Single-channel photographs of DAPI or p19^{Arf}, respectively, were merged. Magnification 100 x, Scale bar, 100 µm. **B** Bar graph showing quantification of p19^{Arf} staining. Positive staining was counted in six representative images of six different mice per condition using ImageJ Fiji. One dot represents one mouse. Significance was determined using two-tailed unpaired Student´s *t* test, **, p ≤ 0.01, ns, non-significant.

Consistent with our findings of at least partially sustained tumor failsafe mechanisms in the *Ezh2*-deficient pancreas, *KEC* mice that were allowed to age until reaching endpoint criteria revealed a significantly reduced tumor incidence (*KC*: 81 % vs *KEC*: 42 %) (Figure 33A) and tumors of these mice showed a significantly smaller tumor weight normalized to body weight (Figure 33B). Surprisingly, the tumor-specific survival of *KEC* mice was not prolonged compared to *KC* mice (Figure 33C).

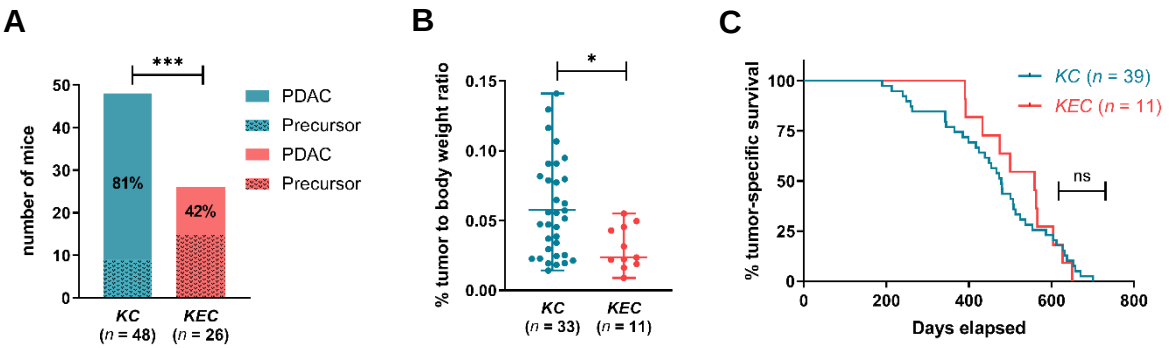

Figure 33: *Ezh2* depletion reduces tumor incidence and relative tumor weight but does not alter survival *in vivo*. A Bar graph revealing reduced PDAC incidence in *KEC* survival mice compared to *KC* survival mice. Significance was determined using Fisher's exact test. ***, p ≤ 0.001. **B** Relative tumor weight of *KC* and *KEC* mice. Each dot represents one mouse, significance was determined using two-tailed unpaired Student´s *t* test, *, p ≤ 0.05. **C** Kaplan-Meier plot of *KC* and *KEC* mice to illustrate no significant differences in tumor-specific survival. Significance was determined by log-rank (Mantel-Cox) test. ns, non-significant.

Therefore, we speculated that *KEC* mice that do develop PDAC were able to bypass the activation of tumor-suppressive mechanisms and do not upregulate p19^{Arf} and p53 expression in precursor lesions (Figure 31). Accordingly, we compared immunofluorescence and western blot analysis of PDAC tissue of *KC* and *KEC* (Figure 32, Figure 34). Contrary to our observations in precursor lesions but in line with our hypothesis, we found similar and only very little p19^{Arf} expression in both *KEC* and *KC* PDAC (Figure 32, Figure 34). Moreover, p53 and its downstream target p21 were not upregulated in *KEC* tumor compared to

KC PDAC (Figure 34), suggesting that *KEC* mice that do develop PDAC despite *Ezh2* deficiency can evade the upregulation of $p19^{Arf}$ and p53 and subsequent induction of tumor fail-safe mechanisms.

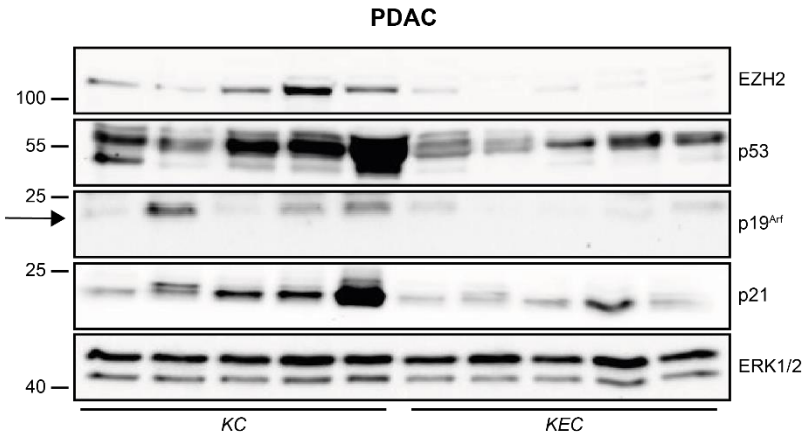

Figure 34: PDAC that is formed even without *Ezh2* shows low $p19^{Arf}$ levels. Western blot analysis was performed with PDAC tissue lysates from KC and KEC mice. Lack of EZH2 was successfully confirmed but does not result in increased leads p53, p21, and $p19^{Arf}$ level. Arrow indicates an unspecific band for $p19^{Arf}$. ERK1/2 served as loading control.

Human PDAC formation despite low EZH2 expression by evading $p14^{ARF}$ upregulation

Finally, we examined whether these observations could be translated to human PDAC. Therefore, we selected 17 human PDAC patients with resectable tumors that have been characterited as *TP53* wildtype (as detected by gene panel-sequencing in cooperation with the Institute of Human Genetics, UMG). 14 out of these 17 patients carried an additional *CDKN2A* wildtype expression (Figure 35A). Subsequently, we performed IHC staining of EZH2 and $p14^{ARF}$ in the 14 *TP53* and *CDKN2A* wildtype resected PDAC samples, quantified the staining, and grouped the patients according to their EZH2- and $p14^{ARF}$- expression into $EZH2^{high/low}$ and $p14^{ARF\ high/low}$ (Figure 35). EZH2 staining was performed by Jennifer Appelhans, Department of Pathology, UMG. Generally, the EZH2 levels in all 14 resected PDACs were relatively low supporting previous findings that high EZH2 levels and activity correlates with advanced tumor progression and dedifferentiation (Ougolkov et al. 2008, Patil et al. 2020). Remarkably, the majority (78 %) of these 14 patients revealed nearly no EZH2 expression (< 7 % positive EZH2 staining). Within this $EZH2^{low}$ group, we identified eight patients with low $p14^{ARF}$ expression (< 13 % positive $p14^{ARF}$ staining) and only three patients with high $p14^{ARF}$ expression. In accordance with the function of EZH2 as a transcriptional repressor of *CDKN2A*, there was no patient with high $p14^{ARF}$ expression in the $EZH2^{high}$

group, but three patients with low p14^{ARF} expression (Figure 35C, D). Hence, our data suggest that in established human PDAC EZH2 expression levels do not significantly affect p14^{ARF} expression. In the absence of genetic alterations of the *CDKN2A* gene, these findings argue for the existence of EZH2-independent epigenetic mechanisms that contribute to *CDKN2A* wildtype repression in EZH2^{low} PDAC subtypes.

Consequently, our findings that EZH2 deficient PDAC can evolve through bypassing the upregulation of p14^{ARF}/p19^{Arf} might also be evident in human PDAC. This underlines the significance of an intact p14^{ARF}-p53wt signalling cascade for the therapeutic efficacy of EZH2 inhibition in PDAC treatment.

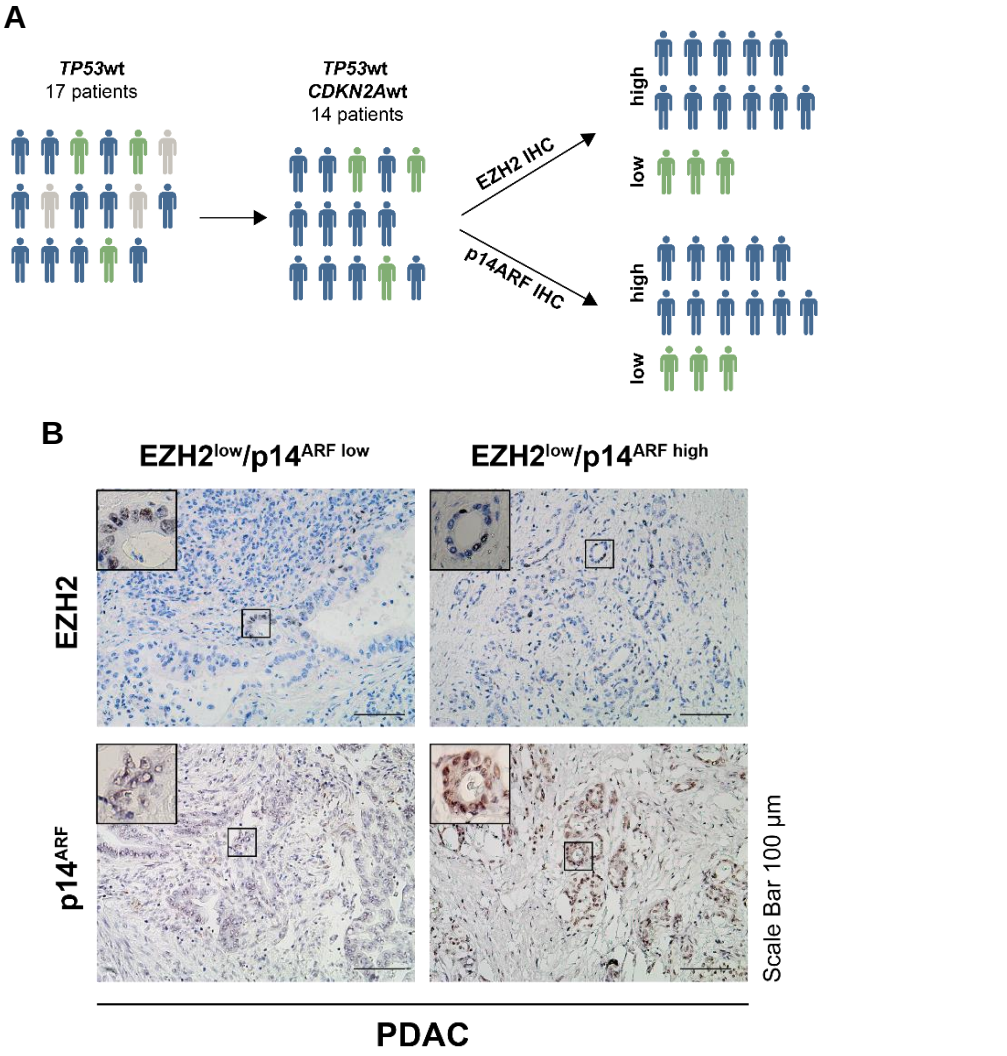

(Figure continued on next page)

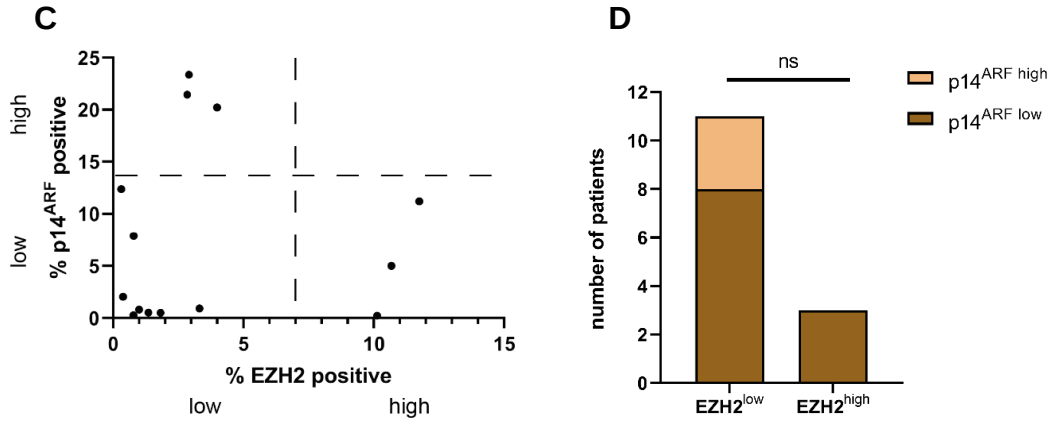

Figure 35: Human PDAC with low EZH2 expression mostly reveals low p14^{ARF} levels. A Schematic displaying the process of how *TP53* wildtype human PDAC patients were classified depending on their EZH2 and p14^{ARF} expression. **B** Representative images of EZH2 and p14^{ARF} IHC in human PDAC grouped in EZH2^{low}/p14ARF ^{low} or EZH2^{low}/p14$^{ARF\ high}$, respectively. Magnification 100 x, Scale bar, 100 µm. **C** Quantification of EZH2 and p14^{ARF} staining. Dotted line indicates classification in 'low' and 'high' expression. Positive staining was counted in ten representative images using ImageJ Fiji. One dot represents one patient. **D** Bar graph showing number of patients in the respective group indicating that number of $^{p14ARF\ high}$ patients in EZH2^{low} group does not significantly differ from number of p14$^{ARF\ high}$ patients in EZH2^{high} group.

Together, we identified a *TP53*-status dependent EZH2 functions in pancreatic cancer. Our findings suggest that EZH2 inhibition might be a beneficial strategy in *TP53* wildtype PDAC subtypes with an intact *CDKN2A*-*TP53*wt axis but not in *TP53*mut PDAC subtypes.

3.7 EZH2-p53 complex formation in PDAC

Native EZH2-p53-binding in PDAC

Besides the canonical function of EZH2 acting as a methyltransferase and mediating trimethylation of H3K27 leading to gene repression, it is also known that EZH2 has non-canonical histone-methyltransferase-independent and chromatin-independent functions. In castration-resistant prostate cancer, for instance, EZH2 interacts with the androgen receptor (Xu et al. 2012) and in breast cancer, EZH2 regulates and activates the NF-κB signalling pathway (Lee et al. 2012, Lawrence and Baldwin 2016). Recently, we also identified non-canonical functions of EZH2 in PDAC by its chromatin-independent interaction with NFATc1 (Patil et al. 2021).

Given these non-canonical functions evident in several tumor entities, we speculated if EZH2 also harbours additional histone-methyltransferase-independent functions in PDAC. Hence, in the second part of this thesis, we aimed at elucidating potential histone-methyltransferase-independent mechanisms by which EZH2 potentially regulates p53. Specifically, we aimed at examining a direct EZH2-p53-binding in PDAC since EZH2 can interact with different proteins as demonstrated in other cancer types (Xu et al. 2012, Wienken et al. 2016). Therefore, we performed immunoprecipitation (IP) studies in different murine and human p53wt and p53mut PDAC cells. Indeed, we could reveal a physical binding between EZH2 and p53wt and p53mut in murine KC, NKC, KPC, and KNPC but also in human p53wt GöPDX13 upon precipitation for EZH2 (Figure 36).

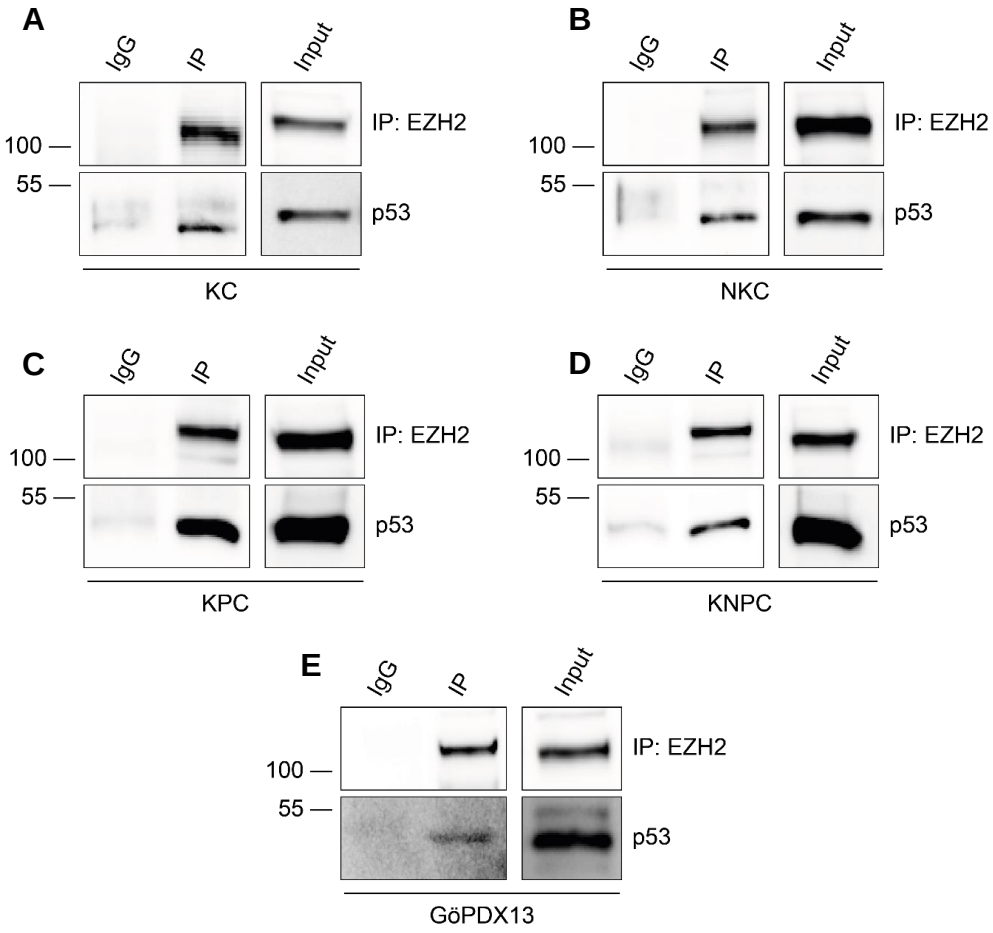

Figure 36: EZH2 and p53 form a stable complex. A-E Immunoprecipitation (IP) of EZH2 in murine KC (**A**), NKC (**B**), KPC (**C**), KNPC (**D**), and human GöPDX13 (**E**) PDAC cells indicates a physical interaction of EZH2 and p53. Normal rabbit immunoglobulin G (IgG) was used as negative control. Input of whole cell lysates was subjected to western blot analysis and reveals presence of respective proteins in lysates.

The physical interaction of EZH2 and p53 was confirmed by proximity ligation assay in NKC cells when visualized under the fluorescence microscope (Figure 37). Two different primary antibodies recognized EZH2 and p53, respectively. Due to its near proximity, secondary antibodies containing oligonucleotides could start rolling circle DNA synthesis. Upon DNA amplification, fluorescence-labelled complementary DNA probes were added leading to high fluorescent signals (red). DAPI (blue) staining was used to visualize the nucleus. For negative control, only primary p53 antibody was added (Figure 37).

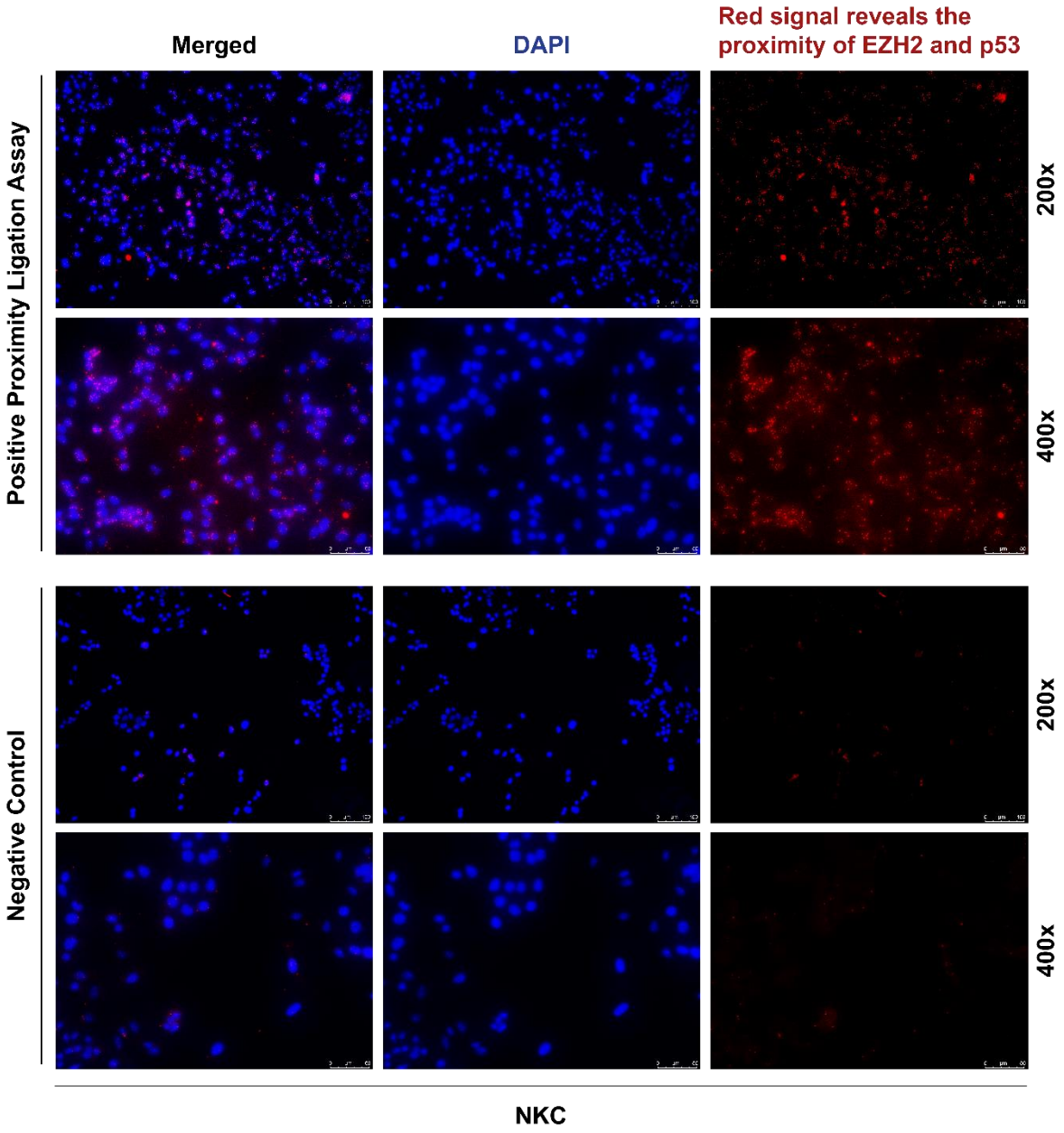

Figure 37: EZH2 and p53 physically interact with each other. Proximity ligation assay (PLA) in NKC cells to confirm EZH2-p53-complex formation. Top: Two primary antibodies raised in different species recognize the target antigens (EZH2 and p53). Red signal reveals the proximity of EZH2 and p53. Bottom: Negative control without EZH2 primary antibody. Scale bar 200 x, 100 µm. Scale bar 400 x, 50 µm. To improve visualization, contrast and brightness were increased in all images identical using Photoshop.

P53 DNA-binding domain is involved in the interaction with EZH2

To examine the specific domain of p53 interacting with EZH2, we took advantage of various human p53 variants lacking different protein domains cloned in a pCEP4 expression vector and re-expressed these p53 variants in the previously introduced KNP^{null}C cells (Pietenpol et al. 1994). The p53wt protein comprises 393 amino acids (aa) and five key domains. In the N-terminal, the p53wt protein consists of a transactivation domain (TAD), subdivided in TAD1 and TAD2, followed by a proline-rich region (PRR). The DNA-binding domain (DBD) is in the centre of the protein followed by a flexible linker region. In the C-terminal, the p53 protein comprises an oligomerization domain (OD) and the C-terminal regulatory domain (CTD) (see *1.2 The Tumor Suppressor p53,* p. 6). Besides the p53wt construct, we also re-expressed three additional p53 variants. The VP1680-p53 variant lacks the TAD (aa 1-79) and contains a foreign TAD from herpes simplex virus VP16 (aa 410-489) instead. In the p53-343CC variant, the CTD (aa 343-393) is replaced by a foreign coiled-coil (CC) domain of the yeast transcription factor Gcn4. Finally, in the VP1680-p53-343CC variant, both the TAD and the CTD are replaced by VP1680 and 343CC, respectively (Pietenpol et al. 1994) (Figure 38A). Upon re-expression of these variants in KNP^{null}C cells, we confirmed the expression of the resulting proteins using western blot analysis (Figure 38B). Subsequently, we performed IP analysis and precipitated for the p53 variants to investigate whether EZH2 is bound to these p53 variants. Although the p53-pulldown was not equal for all p53 variants, we detected that EZH2 is bound to all these variants even if not to the same extent (Figure 38B). In general, we could detect a good binding of EZH2 with p53wt, the VP1680-p53, and the p53-343CC protein, however, the binding of EZH2 with the double mutated VP1680-p53-343CC protein seemed to be the weakest. Since all variants share an intact full-length DNA-binding domain and EZH2 binding was at least partially observed for all variants, our findings suggested that the DNA-binding domain of p53 is involved in the interaction with EZH2 (Figure 38B).

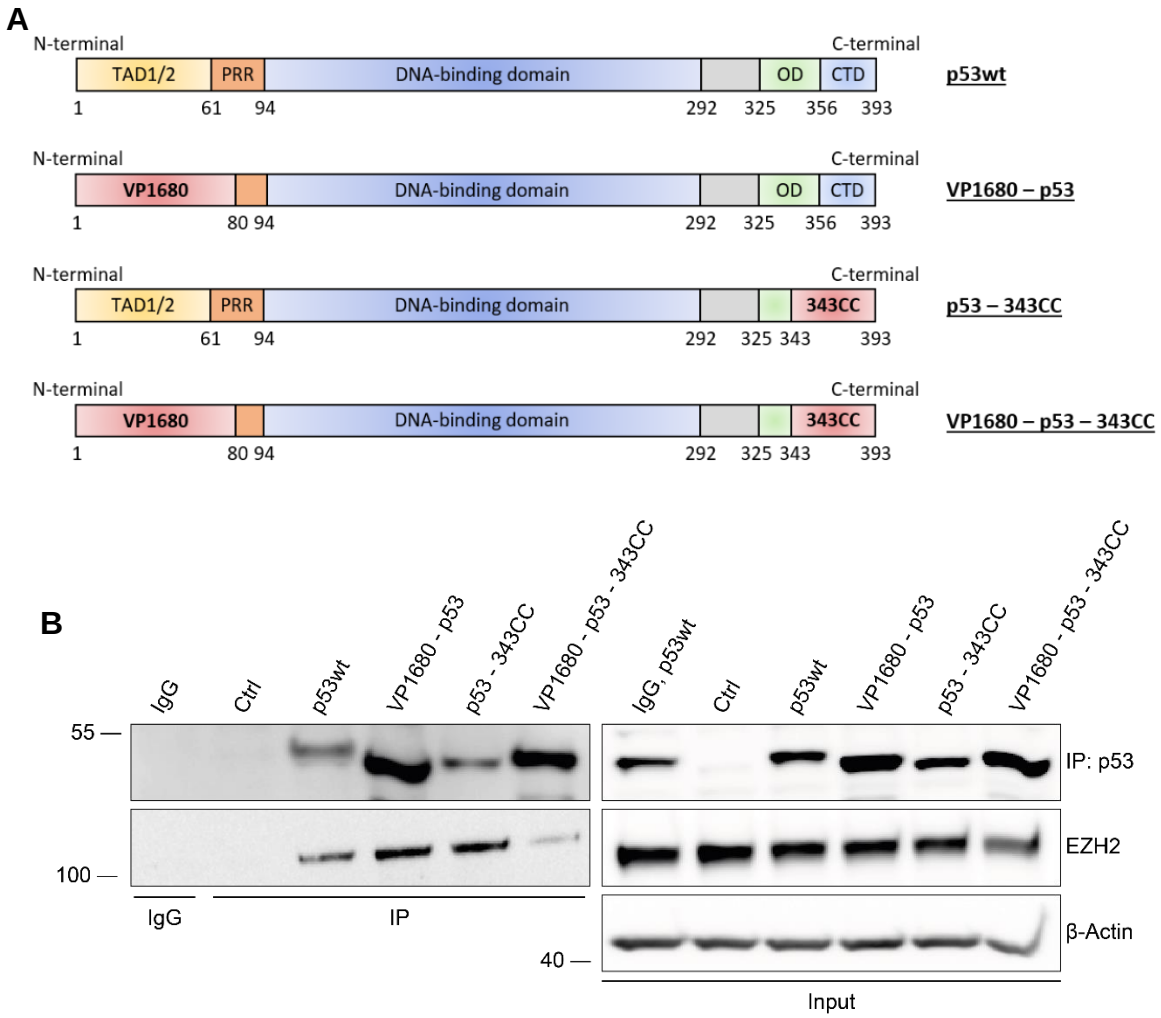

Figure 38: DNA-binding domain of p53 interacts with EZH2. A Schematic illustration of the structure of different human p53 variants cloned in a pCEP4 expression vector (Pietenpol et al. 1994). The wildtype protein p53 consists of 393 amino acids (aa). N-terminal p53 contains the transactivation domain (TAD), which can be subdivided in TAD1 and TAD2, and the proline-rich region (PRR), followed by the central DNA-binding domain, a flexible linker region (grey), an oligomerization domain (OD), and the C-terminal regulatory domain (CTD). For the VP1680-p53 vector, the TAD1/2 of p53 was replaced by a foreign TAD from herpes simplex virus VP16 (aa 410-489). The p53-343CC vector contains instead of the CTD domain a foreign truncated coiled-coil (CC) domain of the yeast transcription factor Gcn4. In the VP1680-p53-343CC vector, both the TAD1/2 and the C-terminal CTD are replaced by foreign VP1680 and 343CC, respectively (Pietenpol et al. 1994). **B** Whole cell lysates of $p53^{null}$ $KNP^{null}C$ cells upon re-expression of different p53 variants followed by immunoprecipitation (IP) of p53 and subsequent western blot analysis to identify the specific domain of p53 physically interacting with EZH2. Normal mouse immunoglobulin G (IgG) was used as negative control, p53 IP samples were detected using an HRP-linked p53 antibody. Input of whole cell lysates was subjected to western blotting analysis and reveals successful re-expression of p53 and presence of EZH2. Empty vector transfection was used as control (Ctrl) condition. β-actin served as loading control.

PRC2 complex members are involved in the EZH2-p53-complex

Next, we aimed at unravelling if the other PRC2-complex members Suz12 and Eed are also involved in the EZH2-p53-complex. Therefore, we precipitated for p53 in NKC cells and stained for EZH2, Suz12, and Eed in western blot analysis (Figure 39A). Importantly, the IP approach confirmed the existence of the EZH2-p53 complex with endogenous p53 and EZH2 upon p53 pulldown, thus confirming our previous findings upon EZH2 pulldown and from PLA (Figure 36, Figure 37). Notably, besides EZH2 we also detected Suz12 and Eed bound to p53 (Figure 39A), suggesting that the PRC2 complex members participate in the EZH2-p53 complex. Furthermore, we examined the significance of the presence of Suz12 and Eed for the EZH2-p53 complex. We silenced Suz12 or Eed using siRNA, pulled down EZH2, and observed the p53 levels bound to EZH2 by western blot analysis (Figure 39B). Our IP approaches revealed that the amount of p53 co-precipitated by EZH2-pulldown was reduced, but did not completely vanish upon silencing the other PRC2 complex members. Since the precipitated EZH2 varied among the three conditions, we quantified and normalized p53 to the respective levels of the EZH2 bait protein and the siCtrl condition using ImageJ revealing that the knockdown of the PRC2 complex members led to a reduction of the EZH2-p53 binding. Upon silencing of Suz12 or Eed the amount of p53 bound to EZH2 was reduced by approximately one-third (Figure 39B). Hence, our observations suggest that Suz12 and Eed do not only participate but also partially stabilize the complex formation of p53 and EZH2.

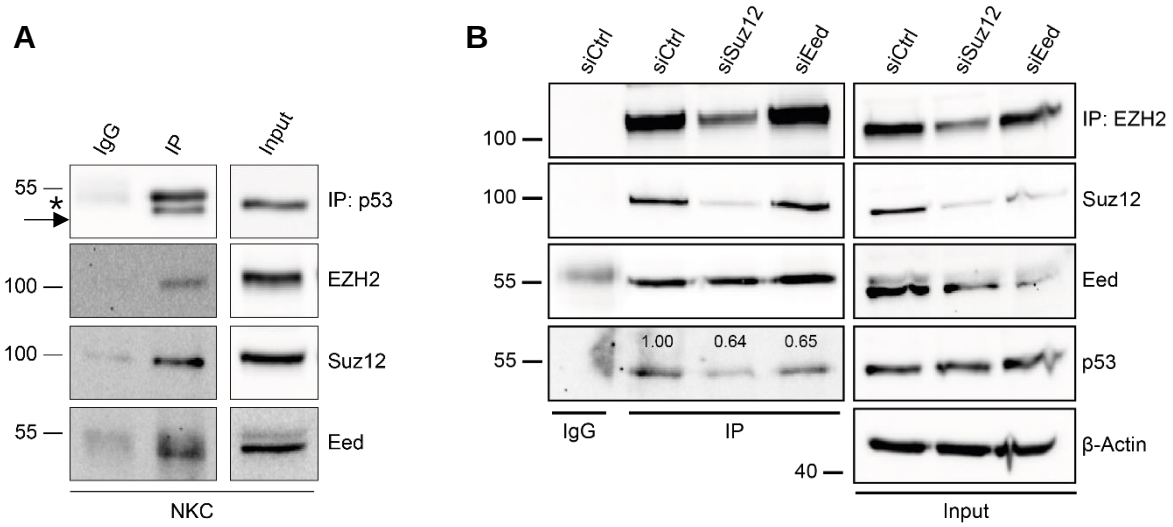

Figure 39: PRC2 complex members participate in the EZH2-p53-complex. A Immunoprecipitation (IP) of p53 in NKC cells to examine potential protein-protein binding of p53 and PRC2-complex member EZH2, Suz2, and Eed. (*) marks the (upper) band representing immunoglobulin heavy chain (~ 50 kDa), (→) marks the (lower) band representing p53. Normal mouse immunoglobulin G (IgG) was used as negative control. Input of whole cell lysates was subjected to western blot analysis and reveals the presence of respective proteins in lysates. **B** Whole cell lysates of NKC cells upon knockdown of Suz12 or Eed, respectively, and subsequent pulldown of EZH2 followed by western blot analysis. Rabbit IgG was used as negative control and p53 IP samples were detected using an HRP-linked p53 antibody. Upon densitometric quantification of EZH2 and p53 using ImageJ, p53 was normalized to the respective EZH2 band and siCtrl condition and is depicted above the respective p53 band. Input of whole cell lysates was subjected to immunoblot analysis displaying successful silencing of Suz12 and Eed, respectively, and presence of EZH2 and p53. β-actin served as loading control.

EZH2-p53 complex is MDM2 and methyltransferase-independent

Previously, it has been shown that EZH2 and Mdm2 directly form a complex in osteosarcoma cells in the absence of p53 (Wienken et al. 2016). Since Mdm2 also binds to p53 (Kussie et al. 1996) we asked whether the herein detected EZH2-p53 interaction might require Mdm2 expression. Consequently, we investigated if Mdm2 participates in the EZH2-p53 complex and if Mdm2-knockdown can disrupt the EZH2-p53-binding. However, our findings revealed that Mdm2 did not physically interact with EZH2 in PDAC and that the EZH2-p53 binding was therefore Mdm2 independent (Figure 40).

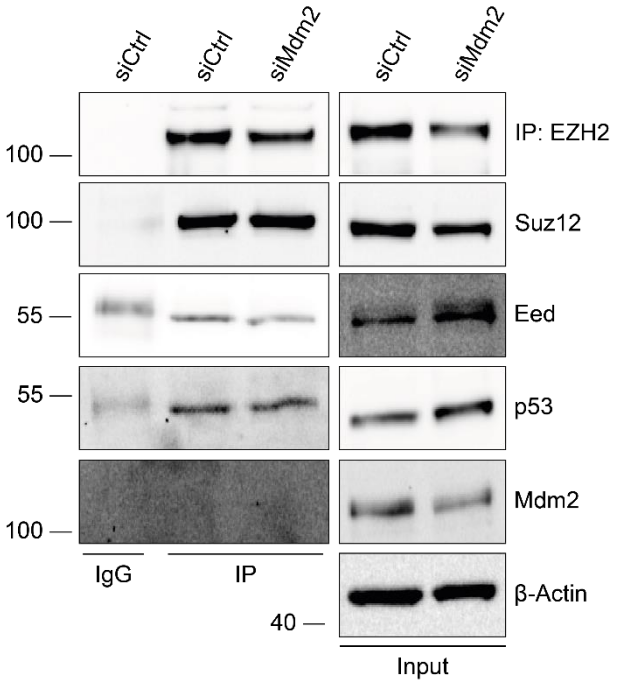

Figure 40: Mdm2-independent EZH2-p53 complex formation. Transient knockdown of Mdm2 using siRNA followed by immunoprecipitation (IP) of EZH2 and subsequent western blot analysis in NKC cells. Normal rabbit immunoglobulin G (IgG) was used as negative control. Input of whole cell lysates was subjected to western blot analysis revealing successful Mdm2 knockdown and presence of respective proteins in lysates. β-actin served as loading control.

Next, we investigated if the EZH2-p53 complex is methyltransferase-dependent. Therefore, we treated NKC cells with the potent methyltransferase inhibitor Tazemetostat (EPZ-6438) (Lue and Amengual 2018) prior to EZH2 pulldown and western blot analysis. Reduction of H3K27me3 levels revealed successful Tazemetostat treatment (Figure 41A). Importantly, before and after inhibition of EZH2 methyltransferase we detected similar amounts of p53 bound to EZH2 suggesting that the physical interaction is methyltransferase independent (Figure 41B).

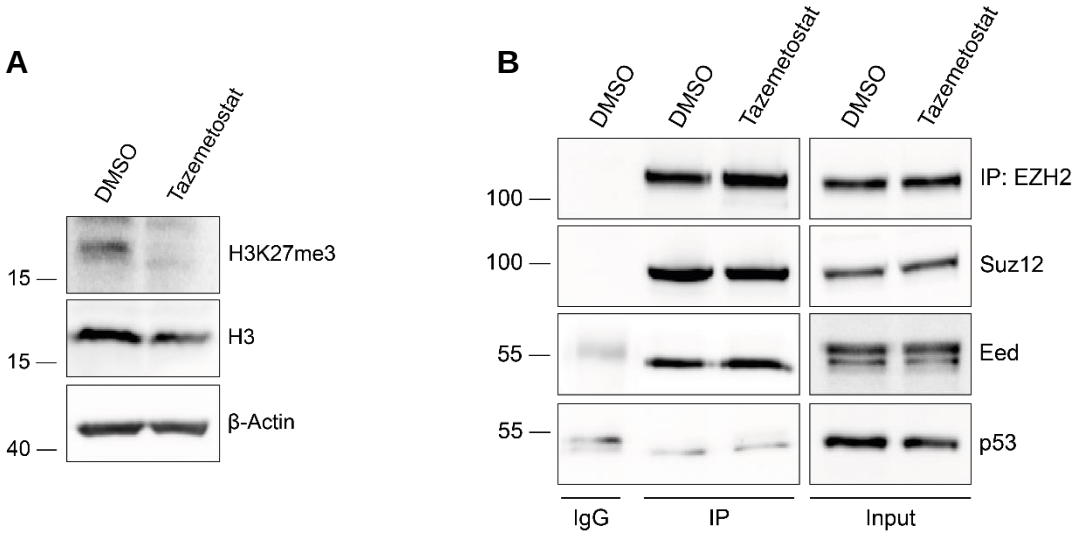

Figure 41: Methyltransferase-independent EZH2-p53-binding. A NKC cells were treated with Tazemetostat (EPZ-6438) (750 nM for 72 hrs) to inhibit EZH2 methyltransferase activity. Successful treatment was verified by H3K27me3 decrease demonstrated upon western blot analysis. DMSO was used as treatment control. H3 and β-actin served as loading control. **B** EZH2-immunoprecipitation (IP) upon treatment with Tazemetostat revealing methyltransferase activity-independent EZH2-p53-complex formation. Normal rabbit immunoglobulin G (IgG) was used as negative control. Input of whole cell lysates was subjected to western blot analysis and shows the presence of respective proteins in lysates.

In summary, our findings revealed a mechanistic binding between EZH2 and p53 in different PDAC cell lines irrespective of the *TP53*-status. Moreover, we identified that the DNA-binding domain of p53 is involved in the interaction with EZH2 and that the EZH2-p53 binding is methyltransferase and Mdm2 independent. We also discovered that the other two PRC2 complex members, Suz12 and Eed, are relevant for the EZH2-p53 interaction.

4 Discussion

4.1 *TP53*-status determines oncogenic EZH2 activity

EZH2 is the catalytic domain of the epigenetic regulator PRC2 mediating trimethylation on H3K27 resulting in silencing of target genes through local chromatin condensation (Pasini et al. 2004). EZH2 is regularly overexpressed in various solid cancer types including breast, prostate, and lung cancer, and is regularly associated with poor prognosis and advanced tumor stages (Kleer et al. 2003, Varambally et al. 2002, Matsukawa et al. 2006, Liu et al. 2016). Previous findings reveal that dysregulated EZH2 activity has a pivotal role in tumor initiation, progression, and invasion (Koh et al. 2011, Garipov et al. 2013, Richter et al. 2009). Given these oncogenic features of EZH2 and the availability of EZH2 inhibitors, the histone methyltransferase is being explored in clinical research in several cancer types.

In PDAC, EZH2 is frequently highly expressed and associated with dedifferentiated high tumor grading and worse survival implicating its oncogenic functions (Chen et al. 2017, Ougolkov et al. 2008, Patil et al. 2020). Recently, our group has shown that EZH2 favours pro-tumorigenic processes by regulating proliferation, clonogenicity, cellular plasticity, and dedifferentiation *in vitro* as well as mediating PDAC development and progression *in vivo*. (Patil et al. 2020, Chen et al. 2017). Moreover, EZH2 expression and activity were associated with a more aggressive and invasive PDAC phenotype. Mechanistically, EZH2 silences *GATA6* expression thereby counteracting less aggressive classical PDAC subtype identity (Patil et al. 2020).

Given these tumor-promoting activities of EZH2, we expected a beneficial outcome of *EZH2* depletion in our orthotopic PDAC models. Surprisingly, and in contradiction to our initial hypothesis, we could not reveal advantageous effects of *EZH2* depletion in these two orthotopic PDAC models. It is noteworthy, that neither mice survival nor typical tumor characteristics, including proliferation marker and tumor stroma composition displayed a beneficial effect upon *EZH2* depletion. However, the aforementioned oncogenic EZH2 activity, including the regulation of clonogenicity and cellular plasticity identified *in vitro* (Patil et al. 2020, Chen et al. 2017) implies a crucial role of EZH2 in PDAC maintenance which needs to be elucidated. Given the central impact of the immune system and the microenvironment on tumor maintenance and progression especially in PDAC (Hessmann et al. 2020, Huber et al. 2020, Karamitopoulou 2019, Murakami et al. 2019), we initially explained the unexpected findings from our immune-deficient Panc-1 PDAC model with the absence of the immune system. However, we could also not confirm the previously identified oncogenic EZH2

activity in the presence of the immune system in our syngeneic KPC PDAC model. Notably, the survival of mice bearing *Ezh2*-deficient tumors was even diminished.

It is well known that epigenetic processes are generally highly tissue- and context-dependent and that a specific cellular or genetic background can determine if the influence of epigenetic processes is rather oncogenic or tumor-suppressive. Several EZH2 studies have revealed its oncogenic as well as tumor-suppressive functions indicating the context-dependent roles of EZH2 (Ougolkov et al. 2008, Chen et al. 2017, Patil et al. 2020, Vanharanta et al. 2013, Bremer et al. 2021). One example of tumor-suppressive EZH2 activity was found in T cell acute lymphoblastic leukemia (T-ALL), an immature hematopoietic malignancy. In T-ALL, oncogenic NOTCH1 signaling results in the loss of EZH2 activity, thereby promoting T-ALL progression (Ntziachristos et al. 2012). Moreover, tumor-suppressive functions of PRC2 were found in clear cell renal carcinoma (Vanharanta et al. 2013). It was shown that the hypoxia-inducible factor (HIF)-driven chemokine receptor 4 (CXCR4) expression was activated through the loss of PRC2-dependent H3K27me3 in support of chemotactic cell invasion resulting in increased metastasis formation (Vanharanta et al. 2013). Furthermore, recent studies revealed that in colorectal cancer high EZH2 expression significantly correlated with favorable prognosis also implying its tumor-suppressive functions (Bremer et al. 2021).

However, the context-specificity of EZH2 is not only shown in other tumor entities but is also evident in the pancreas. Previous studies have reported tumor-suppressive EZH2 activity in pancreatic regeneration (Mallen-St Clair et al. 2012, Chen et al. 2017). This was demonstrated by the findings that loss of EZH2 leads to impaired pancreatic regeneration upon acinar cell injury, suggesting that EZH2 prevents acinar cells from malignant transformation (Mallen-St Clair et al. 2012, Chen et al. 2017). Interestingly, constitutive active KRAS signaling switches the tumor-suppressive activity of EZH2 into tumor promotive activities and accelerates pancreatic carcinogenesis demonstrating the context-dependency of EZH2 activity (Chen et al. 2017). Mechanistically, the *KRAS*-driven EZH2-dependent acceleration of pancreatic tumorigenesis is mediated by NFATc1, the inflammatory calcineurin-responsive transcription factor. It was shown that in the *KRAS* wildtype background, EZH2 represses *Nfatc1,* thereby enabling acinar cell redifferentiation and avoiding organ atrophy. However, under the influence of oncogenic KRAS activation, the EZH2-dependent *Nfatc1* repression was abrogated and PDAC progression was fostered (Chen et al. 2017). This *KRAS*-dependent EZH2 activity demonstrates that the genetic background highly impacts the activity of EZH2 and determines whether EZH2 mediates oncogenic or tumor-suppressive functions. Consequently, the specific cellular and genetic context highly contribute to the

context-dependent activity of EZH2. It can only be speculated why the EZH2 activity reveals this strong context-dependency. Eventually, there might be context-dependent EZH2 interaction partners recruiting EZH2 to different target genes, thus influencing their expression. Moreover, also non-canonical EZH2 function might contribute to the strong context-dependency. Hence, EZH2 might also alter the activity of crucial context-dependent transcription factors, thereby changing their target gene regulation.

To examine the context-dependent activity of EZH2 in PDAC, we aimed at deciphering the specific context-defining characteristics rendering EZH2 inhibition in our orthotopic PDAC models ineffective to generally predict the outcome of EZH2 inhibition as a potential PDAC therapy. Hence, we compared the specific genetic background of our model where we could not detect a strong oncogenic activity of EZH2 with studies stating pro-tumorigenic EZH2 functions. Indeed, we could identify a very pronounced difference. In our orthotopic model, we used *TP53*mut PDAC, whereas previously published studies used *TP53*wt PDAC models (Patil et al. 2020).

The tumor-suppressor gene *TP53* encoding for p53 is a frequent target of mutations in cancer, including PDAC (Bailey et al. 2016). These *TP53* mutations lead to the loss of typical tumor suppressor functions like the regulation of cell cycle progression and apoptosis. Additionally, it mediates oncogenic gain-of-function such as supporting cell invasion, cell migration, and induction of genomic instability (Brosh and Rotter 2009, Freed-Pastor and Prives 2012, Alexandrova et al. 2017, Mantovani et al. 2019). Consequently, the *TP53*-status highly impacts the functional behavior of cancer cells.

Our unexpected findings that EZH2 blockade is not beneficial in our orthotopic PDAC models demonstrate the strong context-dependency of EZH2 activity. We reveal that specifically the *TP53*-status determines the oncogenic activity of EZH2 and the consequences of EZH2 inhibition. Interestingly, our findings are in accordance with results from a transgenic mouse model of Non-Small-Cell-Lung-Cancer (NSCLC). In this model, inhibition of PRC2 hindered tumor formation in a *TP53*wt background, whereas in NSCLC harbouring a *TP53* mutation PRC2 blockade even accelerated tumor formation (Serresi et al. 2016).

TP53-status determines EZH2-dependent target gene regulation

Based on these findings that the *TP53*-status determines oncogenic EZH2 activity, we aimed at elucidating the impact of the *TP53*-status on EZH2-dependent target gene regulation by comparing transcriptomic analysis in the presence and absence of EZH2 with respect to the *TP53*-status. In accordance with our findings that the *TP53*-status determines the outcome of EZH2 depletion in our orthotopic PDAC models, we could also reveal that the *TP53*-status differentially influences and determines global EZH2-dependent target gene regulation. Notably, specifically p53-pathway and apoptosis-related gene signatures are differentially regulated by EZH2 depending on the *TP53*-status. Our findings demonstrate that EZH2 loss led to the enrichment of these gene signatures only in *TP53*wt PDAC cells, whereas in *TP53*mut PDAC cells these gene signatures were either unaltered or even diminished. Importantly, EZH2 knockdown correlates with transcriptional programs indicating favorable prognosis restrictively in *TP53*wt PDAC cells. Notably, we could demonstrate these *TP53*-status-dependent transcriptional EZH2 activities in two different genetic backgrounds. Both in the presence and absence of constitutively active NFATc1, the *TP53*-status differentially influences EZH2 activity, thus underlining the strong *TP53*-status dependency of EZH2 activity. To further investigate potential reasons for the identified *TP53*-status-dependent transcriptional EZH2 activity, genome-wide binding and expression analysis could be performed to examine distinct differences in EZH2 target gene regulation. Based on our findings, it can be speculated that ChIP-seq analysis in *TP53*wt and *TP53*mut PDAC cells might identify different direct EZH2 target genes altering the outcome of EZH2 inhibition. Eventually, *TP53*-status-dependent competing factors might influence the EZH2 binding, thereby altering its target gene repression.

TP53-status determines the outcome of EZH2 depletion

Given the enrichment of apoptosis-related pathways in our GO and GSEA analysis upon knockdown of EZH2 restrictively in p53wt PDAC cells, we aimed at exploring whether the *TP53*-status also functionally impacts apoptotic processes. Indeed, our study provides preclinical evidence demonstrating augmented apoptosis induction only in *TP53*wt PDAC upon additional convenient apoptosis-inducing strategy, whereas in *TP53*mut PDAC, induction of apoptotic processes was unaltered or even diminished upon apoptosis-inducing treatment and simultaneous EZH2 blockade. Therefore, our preclinical data suggest a therapeutic potential of EZH2 inhibition in PDAC, selectively in patients with a *TP53*wt-status, thus underlining the clinical relevance of our results. Hence, our findings demonstrate the

significance of molecular stratification approaches to outbid the potential of EZH2 inhibition as a therapeutic strategy in PDAC treatment.

One huge challenge in PDAC therapy is the acquirement of drug resistance mediated by cellular plasticity installed by epigenetic processes allowing PDAC cells to adapt to internal and external cues escape cancer therapy (Singh et al. 2015). Therefore, epigenetic therapy aims to conquer drug resistance and sensitize PDAC to chemotherapy. Hence, the combination of targeted epigenetic therapy with classical chemotherapy could expand and improve cancer therapy resulting in increased treatment success. Generally, targeting epigenetic processes in cancer therapy are highly efficient and has gained approval in several less heterogeneous malignancies, including lymphoma and multiple myeloma. The EZH2 inhibitor tazemetostat (EPZ-6438), for instance, is approved for adult patients with relapsed or refractory follicular lymphoma and for non-resectable epithelioid sarcoma (Hoy 2020). However, epigenetic treatment strategies in PDAC remain challenging due to the heterogeneous and diverse genetic alterations in PDAC (Hessmann et al. 2017). Nevertheless, current preclinical and clinical studies using pharmacological inhibition of epigenetic processes reveal promising therapeutic strategies. Several clinical trials are ongoing examining the clinical use of epigenetic inhibitors even if the effective use in PDAC is far from being clinical routine (Hessmann et al. 2020, Versemann et al. 2022). Importantly, given the heterogeneous genetic alterations occurring in PDAC (Waddell et al. 2015, Bailey et al. 2016), deeper mechanistic and functional insights into context-determining conditions need to be elucidated to safely introduce epigenetic inhibitors and predict their clinical outcome.

Like the aforementioned studies in NSCLC (Serresi et al. 2016), our findings in PDAC reveal that interfering with EZH2 expression is predominately beneficial in *TP53*wt tumors providing preclinical evidence demonstrating that a specific genetic background in general and the *TP53*-status, in particular, regulates EZH2 function. In line with the findings that the *TP53*-status determines the outcome of EZH2 inhibition, there are studies in gastric cancer using 3-deazaneplanocin A (DZNep) to inhibit EZH2. DZNep is an S-adenosyl-L homocysteine hydrolase inhibitor mediating EZH2 inhibition of the methyltransferase activity and protein depletion. The depletion of EZH2 results in cancer cell growth inhibition and apoptosis activation in several tumor entities, including breast, prostate, lung, gastric, and brain cancer (Gonzalez et al. 2009, Fan et al. 2011, Tan et al. 2007, Cheng et al. 2012). In gastric cancer, it was shown that the effectiveness of DZNep treatment correlates with the *TP53*wt status as well demonstrated by the findings that *TP53*wt cells are more sensitive toward DZNep treatment (Cheng et al. 2012). Mechanistically, better responsiveness of *TP53*wt gastric cancer cells was caused by increased p53 stability leading to the activation of

canonical p53 targets such as p21 and Fas revealing the significance of an intact p53 signaling for the tumor-suppressive functions mediated by EZH2 inhibition (Cheng et al. 2012). Therefore, also in *TP53*wt PDAC, EZH2 inhibitors such as DZNep could be tested *in vivo* studies to examine whether the proposed beneficial outcome of EZH2 inhibition can be also observed *in vivo*.

4.2 The role of EZH2 in the regulation of p53

In accordance with the findings in gastric cancer, we also identified the pivotal role of functional p53 signaling in PDAC for appropriate apoptosis induction. Interestingly, our findings identified a mechanism suggesting post-translational EZH2-dependent p53 regulation. We identified that *Cdkn2a* encoding for $p14^{ARF}$ in humans and $p19^{Arf}$ in mice is a direct target of EZH2 in *TP53*wt PDAC leading to EZH2-dependent silencing of *Cdkn2a* (Figure 42). In line with previous results, our findings support that *Cdkn2a* is repressed by EZH2 (Comet et al. 2016, Pinton et al. 2021, Yamagishi and Uchimaru 2017, Kotake et al. 2007, Sparmann and van Lohuizen 2006) but also that EZH2 targets differ depending on the specific genetic background, again supporting the strong context-dependency of EZH2 activity. Given the crucial role of $p14^{ARF}$/$p19^{Arf}$ in inhibition of the p53-antagonist Mdm2, EZH2 regulates p53 indirectly by repressing $p14^{ARF}$/$p19^{Arf}$ leading to increased Mdm2-dependent p53 destabilization. Therefore, our studies identified one mechanism by which EZH2 indirectly regulates the p53wt protein stability by epigenetically repressing *Cdkn2a* (Figure 42).

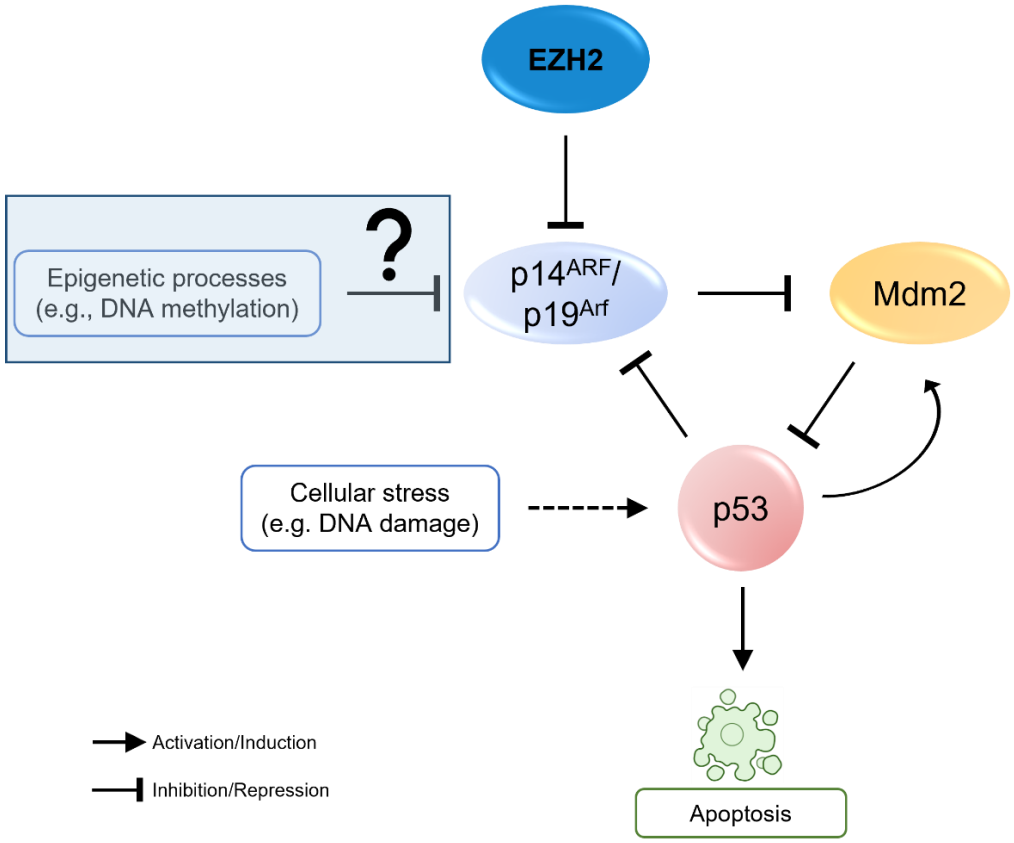

Figure 42: Proposed mechanism of the involvement of EZH2 influencing the functional triangle of p53, Mdm2, and p14^{ARF}/p19^{Arf}. EZH2 represses *CDKN2A*, thereby abrogating p14^{ARF}/p19^{Arf}-dependent inhibition of Mdm2-mediated p53 degradation. Destabilized p53 cannot induce tumor-suppressive functions, such as apoptosis. Given that *TP53*wt PDAC can evolve despite low EZH2 levels by evading p14^{ARF}/p19^{Arf} upregulation, it can be hypothesized that additional EZH2-independent epigenetic mechanisms potentially contribute to *CDKN2A* repression in these PDAC subtypes.

Importantly, EZH2-dependent *Cdkn2a* repression has functional consequences for the EZH2-dependent p53wt destabilization demonstrated by the reduction of apoptosis in p53wt PDAC cells. Interestingly, it has been shown that p19^{Arf} also has multiple p53-independent tumor-suppressive effects. This was displayed by mouse models that are deficient for p19^{Arf}, p53, and Mdm2 showing a higher susceptibility to developing tumors than mice lacking only p53 and Mdm2 (Weber et al. 2000). Moreover, previous studies have shown that p14^{ARF}/p19^{Arf} mediates tumor-suppressive p53-independent functions by suppression of MYC-induced hyperproliferation, ribosomal RNA processing, and NF-κB transactivation (Qi et al. 2004, Sugimoto et al. 2003, Rocha et al. 2003). Besides inhibition of MYC-induced hyperproliferation, p14^{ARF}/p19^{Arf} can additionally foster MYC-induced apoptosis induction (Qi et al. 2004). Given these p53-independent tumor suppressor functions of p14^{ARF}/p19^{Arf}, it can be speculated that EZH2 inhibition in *TP53*wt PDAC with a functional p14^{ARF}/p19^{Arf} expression mediates tumor-suppressive consequences through p53-dependent and p53-

independent processes, thereby increasing the tumor-suppressive effect of EZH2 inhibition in *TP53*wt PDAC.

Besides these p53-independent $p14^{ARF}$/$p19^{Arf}$ functions in other tumor entities, our study demonstrates the significance of an intact *CDKN2A*-*TP53*wt axis to induce tumor fail-safe mechanisms in PDAC. However, this *CDKN2A*-*TP53*wt axis is frequently disrupted. Accordingly, PDAC formation occurs despite low EZH2 expression also in *TP53*wt PDAC. Hence, these *TP53*wt $EZH2^{low}$ PDAC can evolve by evading $p14^{ARF}$/$p19^{Arf}$ upregulation suggesting the existence of EZH2-independent epigenetic mechanisms that contribute to *CDKN2A* wildtype repression in $EZH2^{low}$ PDAC subtypes. Interestingly, hypermethylation of *CDKN2A* was frequently observed in various tumor entities, including head and neck squamous cell carcinoma (HNSCC), colorectal cancer, and esophageal cancer resulting in *CDKN2A* silencing correlating with tumor progression, poor prognosis, and therapy prediction (Zhou et al. 2018, Maeda et al. 2003, Zhou et al. 2017). Notably, also in PDAC *CDKN2A* was found to be hypermethylated (Fukushima et al. 2002, Peng et al. 2006, Baylin and Jones 2011, Park et al. 2012) suggesting that in PDAC as well hypermethylation of *CDKN2A* is involved in silencing $p14^{ARF}$/$p19^{Arf}$ expression thereby disrupting the *CDKN2A*-*TP53*wt axis. Conclusively, our study provides preclinical evidence demonstrating that EZH2 inhibition might be restrictively beneficial in *TP53* wildtype PDAC subtypes harboring an intact *CDKN2A*-*TP53*wt axis.

4.3 Functional consequences of the EZH2-p53 interaction

Although EZH2 is predominantly known for its canonical epigenetic function leading to gene repression, EZH2 additionally comprises different non-canonical functions involved in dysregulated signaling pathways in various cancer types, including breast cancer, prostate cancer, glioblastoma, pancreatic cancer, and leukemia (Shi et al. 2007, Lee et al. 2011, Xu et al. 2012, Kim et al. 2013b, Patil et al. 2021, Wang et al. 2022). Interestingly, the identification of oncogenic non-canonical EZH2 activity was causative for the development of specific EZH2 degraders, such as MS1943 and MS177, using the proteolysis-targeting chimera (PROTAC) technique to develop small molecules that are able to deplete and degrade EZH2. Preclinical studies reveal a higher potency of these EZH2 degraders than small molecules that only inhibit the methyltransferase-activity of EZH2, such as tazemetostat (EPZ-6438) supporting the existence and significance of non-canonical functions of EZH2 (Ma et al. 2020, Wang et al. 2022).

As one investigated non-canonical function, EZH2 can act as a transcriptional (co-) activator and accelerates tumor cell proliferation by binding to different transcription factors (Lee et al. 2011, Shi et al. 2007). In estrogen receptor-positive breast cancer, for instance, EZH2 directly binds to estrogen receptor alpha (ERα) and β-catenin thereby activating the transcription of oncogenic MYC and cyclin D3 (Shi et al. 2007). In estrogen receptor-negative breast cancer, EZH2 interacts with RelA and RelB, which are members of the NF-κB transcription factor family, and induces the transcription of NF-κB target genes leading to cell proliferation (Lee et al. 2011). Furthermore, in colon cancer, EZH2 forms a complex with PCNA-associated factor (PAF) and β-catenin resulting in oncogenic activation of the Wnt signaling pathway (Jung et al. 2013). Very recently, Wang et al. showed that in acute leukemia EZH2 physically interacts with MYC and p300 leading to tumor-promoting gene activation (Wang et al. 2022). Furthermore, EZH2 can also mediate non-canonical transcriptional activating functions in a PRC2-independent manner (Xu et al. 2012). In castration-resistant prostate cancer, AKT1 phosphorylates serine 21 of EZH2 leading to the separation of EZH2 from the PRC2 complex. Subsequently, EZH2 directly binds to the androgen receptor and the complex activates the target gene transcription of the oncogenic androgen receptor (Xu et al. 2012).

Besides its transcriptional (co-) activating function, EZH2 can also modify and methylate non-histone proteins, both PRC2-dependent and -independent, thereby controlling various cellular functions (He et al. 2012, Lee et al. 2012, Kim et al. 2013b). In glioblastoma, for instance, upon AKT1-mediated phosphorylation of EZH2 at serine 21, EZH2 methylates STAT3 in a PRC2-independent manner resulting in the activation of STAT3 (Kim et al. 2013b). Moreover, EZH2 can also methylate different transcription factors in a PRC2-dependent manner, as exemplified by post-translational methylation of RORα and GATA4 (He et al. 2012, Lee et al. 2012). Additionally, our group recently revealed that in PDAC EZH2 biochemically interacts with NFATc1. This complex formation was suggested to have chromatin-independent functions, as both proteins do not regulate joint transcriptional processes (Patil et al. 2021). Interestingly, in line with previous findings in castration-resistant prostate cancer (Xu et al. 2012) and glioblastoma (Kim et al. 2013b), phosphorylation of EZH2 at serine 21 was required to form the stable EZH2-NFATc1 complex (Patil et al. 2021).

Given these reported non-canonical functions of EZH2 and the ability of EZH2 to physically interact with other proteins, we also aimed at examining potential non-canonical functions of EZH2 in PDAC and were specifically interested in exploring whether EZH2 and p53 directly interact with each other. Indeed, our findings demonstrate a biochemical interaction of EZH2 and p53 in different PDAC cell lines irrespective of the p53 mutation status. We reveal that the other PRC2 complex members, Suz12 and Eed, participate in the EZH2-p53 interaction and that the complex is methyltransferase-independent (Figure 43).

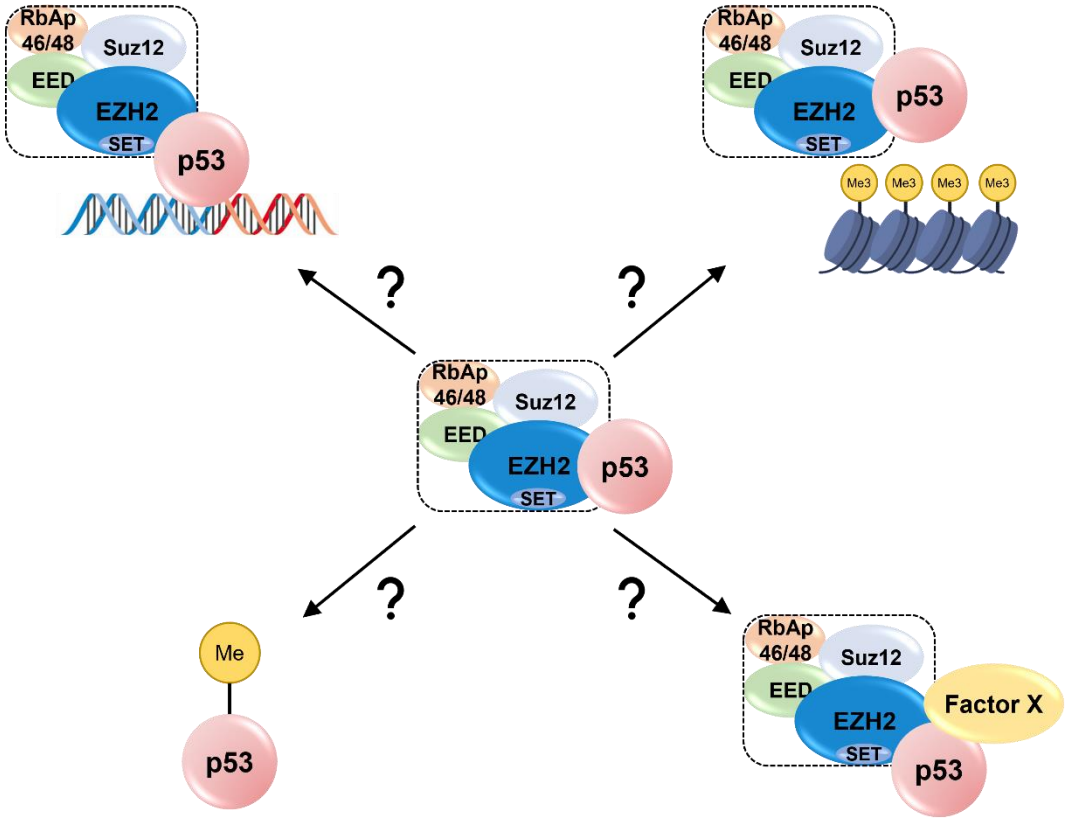

Figure 43: Proposed EZH2-p53 complex and its hypothesized consequences. We identified a physical binding of EZH2 and p53. This EZH2-p53 complex also involves the other PRC2 complex members (EED, SUZ12) but it is methyltransferase-independent. However, the understanding of the functional implications and consequences of this complex remains incomplete. It can be speculated that the EZH2-p53 complex influences the target gene regulation of both proteins. Moreover, additional factors can be involved in the complex and determine its activity. Furthermore, EZH2 might methylate p53, thereby altering its activity.

Several studies have shown that p53 has numerous binding partners and identified the specific domain of p53 binding to the respective interaction partner (Lane and Crawford 1979, Kussie et al. 1996, Wolf et al. 2018). The N-terminal TAD of p53, for instance, binds to many proteins, including its antagonist Mdm2 and the members of the transcriptional machinery as exemplified by TATA box binding protein (TBP) and TBP-associated factors (TAF) components of transcription factor II D (TFIID) (Thut et al. 1995, Lu and Levine 1995, Kussie et al. 1996, Trinidad et al. 2013). The DBD interacts with simian virus 40 (SV40) large T antigen (Lane and Crawford 1979, Jenkins et al. 1984) and cellular proteins, such as p73, 53BP1, and 53BP2 (Wolf et al. 2018, Ruppert and Stillman 1993, Iwabuchi et al. 1994, Gorina and Pavletich 1996). The C-terminal domains of p53 are known for their oligomerization and several interactions with cellular and viral proteins, including the DNA repair mediating helicase CSB (Ko and Prives 1996, Levine 1997) and hepatitis B virus X protein (Wang et al. 1994).

Although these studies could clearly identify the specific domain of p53 interacting with its cooperation partner, further investigation is required to also identify the p53 domain interacting with EZH2. Generally, we could detect the binding of EZH2 with different p53 variants lacking different p53 domains, but we could not identify the specific p53 protein domain binding to EZH2. Nevertheless, our findings provide first evidence that the DBD of p53 interacts with EZH2. However, it is also possible that EZH2 binds to different domains of p53. Hence, if one domain of p53 is lost or replaced artificially, another domain of p53 might compensate and can bind to EZH2.

Besides these precise mechanistic features of the EZH2-p53 complex, the reasons, functional implications, and consequences of the identified EZH2-p53 binding still remain unclear. Initially, based on our findings that EZH2 regulates p53 post-translationally and that p53 and EZH2 physically interact with each other, we hypothesized that EZH2 increases p53wt degradation by participating and stabilizing the Mdm2-p53wt-destruction complex. Supportively, previous studies revealed a direct interaction of EZH2 and Mdm2, although it was observed in the absence of p53 (Wienken et al. 2016). However, we could not detect Mdm2 in the EZH2-p53 complex and could therefore not confirm this hypothesis.

Moreover, based on the findings in other tumor entities that posttranslational modifications, such as phosphorylation of EZH2 at serine 21, are involved in non-canonical EZH2 functions (Xu et al. 2012, Kim et al. 2013b), it can be hypothesized that also in PDAC posttranslational modifications might play a role for the existence of the EZH2-p53 complex or its hitherto unknown functional activity. Interestingly, phosphorylated serine 21 of EZH2 was generally identified in PDAC (Patil et al. 2021) suggesting that it is eventually also involved

in the EZH2-p53 interaction. To examine whether this modification indeed impacts the EZH2-p53 complex, IP experiments could be performed with antibodies specifically targeting the phosphorylated EZH2. Overexpression of either wildtype EZH2, constitutively serine 21-phosphorylated EZH2, or a phosphorylation-dead mutant and subsequent IP might unravel the role of this modification for the EZH2-p53 complex.

For potential functional consequences, it can be speculated that the EZH2-p53 complex influences the target gene regulation of both proteins. Hence, p53 might influence EZH2-dependent target gene regulation by determining EZH2 recruitment to different target genes or EZH2 might impact the p53 transcriptional activity through capturing p53, thereby mediating and determining p53 target gene regulation. One method to study potential transcriptional-dependent functions is the investigation of jointly or independently regulated target genes of EZH2 and p53 by ChIP-seq analysis.

Since both EZH2 and p53 are also known to interact with other proteins, the involvement of other factors might contribute to the identified EZH2-p53 complex, thereby influencing and determining the precise activity. Mass spectrometry-based strategies can be performed to analyse further interactions with other proteins. Moreover, it can be hypothesized that the EZH2-p53 complex mediates transcription independent functions. EZH2 might modify p53 by post-translational methylation, thereby altering its activity (Figure 43). Previous studies have shown that p53 is highly controlled by several post-translational modifications, including lysine methylation (Scoumanne and Chen 2008, Huang et al. 2010, West and Gozani 2011). One example that methylation of p53 can interfere with its tumor-suppressive function was shown by the methylation of p53 by G9a and GLP. Normally, G9a and GLP mediate mono- and di-methylation of H3K9 leading to transcriptional silencing. However, it was shown that G9a and GLP can also methylate p53 at lysine 373 resulting in damping or even inactivating p53 which was induced in response to DNA damage (Huang et al. 2010). Therefore, the existence of this specific methylation site and a potential EZH2-dependency could also be investigated in PDAC by using antibodies specifically against this methylated p53 protein.

Taken together, although the detailed mechanistic and functional consequences resulting from the EZH2-p53 complex need to be elucidated, the existence of the EZH2-p53 complex demonstrates the dynamic complexity of the cooperation of regulatory proteins in PDAC.

4.4 Concluding Remarks

Given the reversibility of epigenetic alterations and the availability of epigenetic inhibitors, epigenetic treatment strategies moved to the focus of translational medicine in cancer therapy. However, epigenetic alterations are highly context-dependent, and epigenetic processes can be both tumor-supportive and tumor-suppressive. Hence, to identify and examine the specific context-determining conditions of epigenetic processes is extremely crucial to predict the consequences of their inhibition through targeted therapy. Consequently, the benefit of epigenetic treatment strategies to tackle PDAC highly depends on unraveling these context-determining conditions.

In conclusion, our study demonstrates that specifically the *TP53* status determines the oncogenic EZH2 activity in PDAC. We reveal that EZH2-dependent target gene regulation is determined by the *TP53*-status and that EZH2 inhibition correlates with a better prognosis in *TP53*wt PDAC. We demonstrate preclinical evidence that the inhibition of EZH2 is only beneficial in *TP53*wt PDAC. Additionally, we identified a mechanism by which EZH2 regulates p53wt post-translationally through repression of *CDKN2A* leading to $p14^{ARF}$/$p19^{Arf}$-dependent de-repression of Mdm2, the antagonist of p53, resulting in the destabilization of p53. Moreover, in this work, we examined that PDAC formation was possible despite *TP53*wt-status and low EZH2 expression through EZH2-independent *CDKN2A* repression, demonstrating the importance of an intact *CDKN2A*-*TP53*wt axis for a beneficial outcome of EZH2 inhibition. Conclusively, stratification for a functional *CDKN2A*-*TP53*wt axis is required for a successful application of EZH2 inhibition in PDAC treatment. Furthermore, we identified uncharted non-canonical functions of EZH2 in PDAC and revealed the existence of a physical EZH2-p53-complex, thus implying that also non-canonical EZH2 functions ma influence PDAC progression.

V References

Adamska A., Domenichini A. and Falasca M. 2017. Pancreatic Ductal Adenocarcinoma: Current and Evolving Therapies. International journal of molecular sciences 18.

Afgan E. ET AL. 2016. The Galaxy platform for accessible, reproducible and collaborative biomedical analyses: 2016 update. Nucleic acids research 44: W3-w10.

Alexandrov L. B., Nik-Zainal S., Siu H. C., Leung S. Y. and Stratton M. R. 2015. A mutational signature in gastric cancer suggests therapeutic strategies. Nat Commun 6: 8683.

Alexandrova E. M., Mirza S. A., Xu S., Schulz-Heddergott R., Marchenko N. D. and Moll U. M. 2017. p53 loss-of-heterozygosity is a necessary prerequisite for mutant p53 stabilization and gain-of-function in vivo. Cell death & disease 8: e2661.

Anders S. and Huber W. 2010. Differential expression analysis for sequence count data. Genome biology 11: R106.

Anders S., Pyl P. T. and Huber W. 2015. HTSeq--a Python framework to work with high-throughput sequencing data. Bioinformatics (Oxford, England) 31: 166-169.

Andricovich J., Perkail S., Kai Y., Casasanta N., Peng W. and Tzatsos A. 2018. Loss of KDM6A Activates Super-Enhancers to Induce Gender-Specific Squamous-like Pancreatic Cancer and Confers Sensitivity to BET Inhibitors. Cancer cell 33: 512-526.e518.

Arya A. K., Bhadada S. K., Singh P., Sachdeva N., Saikia U. N., Dahiya D., Behera A., Bhansali A. and Rao S. D. 2017. Promoter hypermethylation inactivates CDKN2A, CDKN2B and RASSF1A genes in sporadic parathyroid adenomas. Scientific Reports 7: 3123.

Aubrey B. J., Kelly G. L., Janic A., Herold M. J. and Strasser A. 2018. How does p53 induce apoptosis and how does this relate to p53-mediated tumour suppression? Cell Death & Differentiation 25: 104-113.

Aung K. L. ET AL. 2018. Genomics-Driven Precision Medicine for Advanced Pancreatic Cancer: Early Results from the COMPASS Trial. Clinical Cancer Research 24: 1344-1354.

Avan A., Crea F., Paolicchi E., Funel N., Galvani E., Marquez V. E., Honeywell R. J., Danesi R., Peters G. J. and Giovannetti E. 2012. Molecular mechanisms involved in the synergistic interaction of the EZH2 inhibitor 3-deazaneplanocin A with gemcitabine in pancreatic cancer cells. Molecular cancer therapeutics 11: 1735-1746.

Avrameas S. and Uriel J. 1966. [Method of antigen and antibody labelling with enzymes and its immunodiffusion application]. Comptes rendus hebdomadaires des seances de l'Academie des sciences Serie D: Sciences naturelles 262: 2543-2545.

Bailey P. ET AL. 2016. Genomic analyses identify molecular subtypes of pancreatic cancer. Nature 531: 47-52.

Barski A., Cuddapah S., Cui K., Roh T. Y., Schones D. E., Wang Z., Wei G., Chepelev I. and Zhao K. 2007. High-resolution profiling of histone methylations in the human genome. Cell 129: 823-837.

Baumgart S. ET AL. 2014. Inflammation-induced NFATc1-STAT3 transcription complex promotes pancreatic cancer initiation by KrasG12D. Cancer discovery 4: 688-701.

Baylin S. B. and Jones P. A. 2011. A decade of exploring the cancer epigenome - biological and translational implications. Nat Rev Cancer 11: 726-734.

Beger H. G. 2018. The pancreas : an integrated textbook of basic science, medicine, and surgery.

Bettaieb A., Paul C., Plenchette S., Shan J., Chouchane L. and Ghiringhelli F. 2017. Precision medicine in breast cancer: reality or utopia? Journal of translational medicine 15: 139.

Biankin A. V. ET AL. 2012. Pancreatic cancer genomes reveal aberrations in axon guidance pathway genes. Nature 491: 399-405.
Bitler B. G. ET AL. 2015. Synthetic lethality by targeting EZH2 methyltransferase activity in ARID1A-mutated cancers. Nat Med 21: 231-238.
Bouaoun L., Sonkin D., Ardin M., Hollstein M., Byrnes G., Zavadil J. and Olivier M. 2016. TP53 Variations in Human Cancers: New Lessons from the IARC TP53 Database and Genomics Data. Human mutation 37: 865-876.
Bradford M. M. 1976. A rapid and sensitive method for the quantitation of microgram quantities of protein utilizing the principle of protein-dye binding. Analytical biochemistry 72: 248-254.
Bremer S. C. B. ET AL. 2021. Enhancer of Zeste Homolog 2 in Colorectal Cancer Development and Progression. Digestion 102: 227-235.
Brooks C. L. and Gu W. 2010. New insights into p53 activation. Cell research 20: 614-621.
Brosh R. and Rotter V. 2009. When mutants gain new powers: news from the mutant p53 field. Nat Rev Cancer 9: 701-713.
Burris H. A. ET AL. 1997. Improvements in survival and clinical benefit with gemcitabine as first-line therapy for patients with advanced pancreas cancer: a randomized trial. Journal of Clinical Oncology 15: 2403-2413.
Campbell S. L., Khosravi-Far R., Rossman K. L., Clark G. J. and Der C. J. 1998. Increasing complexity of Ras signaling. Oncogene 17: 1395-1413.
Cao R., Wang L., Wang H., Xia L., Erdjument-Bromage H., Tempst P., Jones R. S. and Zhang Y. 2002. Role of Histone H3 Lysine 27 Methylation in Polycomb-Group Silencing. Science (New York, NY) 298: 1039-1043.
Cao R. and Zhang Y. 2004. SUZ12 is required for both the histone methyltransferase activity and the silencing function of the EED-EZH2 complex. Mol Cell 15: 57-67.
Chan-Seng-Yue M. ET AL. 2020. Transcription phenotypes of pancreatic cancer are driven by genomic events during tumor evolution. Nat Genet 52: 231-240.
Chen E. Y., Tan C. M., Kou Y., Duan Q., Wang Z., Meirelles G. V., Clark N. R. and Ma'ayan A. 2013. Enrichr: interactive and collaborative HTML5 gene list enrichment analysis tool. BMC bioinformatics 14: 128.
Chen N. M. ET AL. 2017. Context-Dependent Epigenetic Regulation of Nuclear Factor of Activated T Cells 1 in Pancreatic Plasticity. Gastroenterology 152: 1507-1520.e1515.
Chen N. M. ET AL. 2015. NFATc1 Links EGFR Signaling to Induction of Sox9 Transcription and Acinar-Ductal Transdifferentiation in the Pancreas. Gastroenterology 148: 1024-1034 e1029.
Cheng L. L. ET AL. 2012. TP53 genomic status regulates sensitivity of gastric cancer cells to the histone methylation inhibitor 3-deazaneplanocin A (DZNep). Clin Cancer Res 18: 4201-4212.
Chi J., Chung S. Y., Parakrama R., Fayyaz F., Jose J. and Saif M. W. 2021. The role of PARP inhibitors in BRCA mutated pancreatic cancer. Therapeutic advances in gastroenterology 14: 17562848211014818.
Citron F. and Fabris L. 2020. Targeting Epigenetic Dependencies in Solid Tumors: Evolutionary Landscape Beyond Germ Layers Origin. Cancers (Basel) 12.
Collisson E. A. ET AL. 2011. Subtypes of pancreatic ductal adenocarcinoma and their differing responses to therapy. Nat Med 17: 500-503.
Comet I., Riising E. M., Leblanc B. and Helin K. 2016. Maintaining cell identity: PRC2-mediated regulation of transcription and cancer. Nat Rev Cancer 16: 803-810.
Conroy T. ET AL. 2011. FOLFIRINOX versus gemcitabine for metastatic pancreatic cancer. The New England journal of medicine 364: 1817-1825.
Coons A. H., Creech H. J. and Jones R. N. 1941. Immunological Properties of an Antibody Containing a Fluorescent Group. Proceedings of the Society for Experimental Biology and Medicine 47: 200-202.

Couldwell W. T., Hinton D. R., He S., Chen T. C., Sebat I., Weiss M. H. and Law R. E. 1994. Protein kinase C inhibitors induce apoptosis in human malignant glioma cell lines. FEBS letters 345: 43-46.
Dambacher S., Hahn M. and Schotta G. 2010. Epigenetic regulation of development by histone lysine methylation. Heredity 105: 24-37.
Davidson J., Shen Z., Gong X. and Pollack J. R. 2018. SWI/SNF aberrations sensitize pancreatic cancer cells to DNA crosslinking agents. Oncotarget 9: 9608-9617.
De La O. J., Emerson L. L., Goodman J. L., Froebe S. C., Illum B. E., Curtis A. B. and Murtaugh L. C. 2008. Notch and Kras reprogram pancreatic acinar cells to ductal intraepithelial neoplasia. Proc Natl Acad Sci U S A 105: 18907-18912.
Deer E. L., Gonzalez-Hernandez J., Coursen J. D., Shea J. E., Ngatia J., Scaife C. L., Firpo M. A. and Mulvihill S. J. 2010. Phenotype and genotype of pancreatic cancer cell lines. Pancreas 39: 425-435.
Di Agostino S., Strano S., Emiliozzi V., Zerbini V., Mottolese M., Sacchi A., Blandino G. and Piaggio G. 2006. Gain of function of mutant p53: the mutant p53/NF-Y protein complex reveals an aberrant transcriptional mechanism of cell cycle regulation. Cancer cell 10: 191-202.
Di Lorenzo A. and Bedford M. T. 2011. Histone arginine methylation. FEBS letters 585: 2024-2031.
DiGiuseppe J. A., Redston M. S., Yeo C. J., Kern S. E. and Hruban R. H. 1995. p53-independent expression of the cyclin-dependent kinase inhibitor p21 in pancreatic carcinoma. The American journal of pathology 147: 884-888.
Donehower L. A., Harvey M., Slagle B. L., McArthur M. J., Montgomery C. A., Jr., Butel J. S. and Bradley A. 1992. Mice deficient for p53 are developmentally normal but susceptible to spontaneous tumours. Nature 356: 215-221.
Dupont S. ET AL. 2009. FAM/USP9x, a deubiquitinating enzyme essential for TGFbeta signaling, controls Smad4 monoubiquitination. Cell 136: 123-135.
Elmore S. 2007. Apoptosis: a review of programmed cell death. Toxicol Pathol 35: 495-516.
Erkan M., Michalski C. W., Rieder S., Reiser-Erkan C., Abiatari I., Kolb A., Giese N. A., Esposito I., Friess H. and Kleeff J. 2008. The activated stroma index is a novel and independent prognostic marker in pancreatic ductal adenocarcinoma. Clinical gastroenterology and hepatology : the official clinical practice journal of the American Gastroenterological Association 6: 1155-1161.
Fan T., Jiang S., Chung N., Alikhan A., Ni C., Lee C. C. and Hornyak T. J. 2011. EZH2-dependent suppression of a cellular senescence phenotype in melanoma cells by inhibition of p21/CDKN1A expression. Molecular cancer research : MCR 9: 418-429.
Fischer M. 2017. Census and evaluation of p53 target genes. Oncogene 36: 3943-3956.
Foot N. C. 1933. The Masson Trichrome Staining Methods in Routine Laboratory Use. Stain Technology 8: 101-110.
Fraumeni J. F., Jr. and Li F. P. 1969. Hodgkin's disease in childhood: an epidemiologic study. Journal of the National Cancer Institute 42: 681-691.
Freed-Pastor W. A. and Prives C. 2012. Mutant p53: one name, many proteins. Genes & development 26: 1268-1286.
Frum R. A. and Grossman S. R. 2014. Mechanisms of mutant p53 stabilization in cancer. Sub-cellular biochemistry 85: 187-197.
Fukushima N., Sato N., Ueki T., Rosty C., Walter K. M., Wilentz R. E., Yeo C. J., Hruban R. H. and Goggins M. 2002. Aberrant methylation of preproenkephalin and p16 genes in pancreatic intraepithelial neoplasia and pancreatic ductal adenocarcinoma. The American journal of pathology 160: 1573-1581.
Garcia P. L. ET AL. 2016. The BET bromodomain inhibitor JQ1 suppresses growth of pancreatic ductal adenocarcinoma in patient-derived xenograft models. Oncogene 35: 833-845.

Garipov A., Li H., Bitler B. G., Thapa R. J., Balachandran S. and Zhang R. 2013. NF-YA underlies EZH2 upregulation and is essential for proliferation of human epithelial ovarian cancer cells. Molecular cancer research : MCR 11: 360-369.
Ghosh S. and Chan C.-K. K. 2016. Analysis of RNA-Seq Data Using TopHat and Cufflinks. In: EDWARDS, D. (Ed.) Plant Bioinformatics: Methods and Protocols, New York, NY: Springer New York, p. 339-361.
Gidekel Friedlander S. Y., Chu G. C., Snyder E. L., Girnius N., Dibelius G., Crowley D., Vasile E., DePinho R. A. and Jacks T. 2009. Context-dependent transformation of adult pancreatic cells by oncogenic K-Ras. Cancer cell 16: 379-389.
Glozak M. A. and Seto E. 2007. Histone deacetylases and cancer. Oncogene 26: 5420-5432.
Golan T. ET AL. 2019. Maintenance Olaparib for Germline BRCA-Mutated Metastatic Pancreatic Cancer. The New England journal of medicine 381: 317-327.
Gonzalez M. E., Li X., Toy K., DuPrie M., Ventura A. C., Banerjee M., Ljungman M., Merajver S. D. and Kleer C. G. 2009. Downregulation of EZH2 decreases growth of estrogen receptor-negative invasive breast carcinoma and requires BRCA1. Oncogene 28: 843-853.
Gorina S. and Pavletich N. P. 1996. Structure of the p53 tumor suppressor bound to the ankyrin and SH3 domains of 53BP2. Science (New York, NY) 274: 1001-1005.
Habbe N. ET AL. 2008. Spontaneous induction of murine pancreatic intraepithelial neoplasia (mPanIN) by acinar cell targeting of oncogenic Kras in adult mice. Proc Natl Acad Sci U S A 105: 18913-18918.
Hackeng W. M., Hruban R. H., Offerhaus G. J. and Brosens L. A. 2016. Surgical and molecular pathology of pancreatic neoplasms. Diagnostic pathology 11: 47.
Hahn S. A. ET AL. 1996. DPC4, a candidate tumor suppressor gene at human chromosome 18q21.1. Science (New York, NY) 271: 350-353.
Hamdan F. H. and Johnsen S. A. 2018. DeltaNp63-dependent super enhancers define molecular identity in pancreatic cancer by an interconnected transcription factor network. Proceedings of the National Academy of Sciences 115: E12343-E12352.
Hasan N. and Ahuja N. 2019. The Emerging Roles of ATP-Dependent Chromatin Remodeling Complexes in Pancreatic Cancer. Cancers (Basel) 11.
He A., Shen X., Ma Q., Cao J., von Gise A., Zhou P., Wang G., Marquez V. E., Orkin S. H. and Pu W. T. 2012. PRC2 directly methylates GATA4 and represses its transcriptional activity. Genes & development 26: 37-42.
Herman I. M. 1993. Actin isoforms. Current Opinion in Cell Biology 5: 48-55.
Hessmann E. 2014. NFAT in Pancreatic Carcinogenesis. Journal of Carcinogenesis & Mutagenesis 05.
Hessmann E., Buchholz S. M., Demir I. E., Singh S. K., Gress T. M., Ellenrieder V. and Neesse A. 2020. Microenvironmental Determinants of Pancreatic Cancer. Physiological Reviews 100: 1707-1751.
Hessmann E., Johnsen S. A., Siveke J. T. and Ellenrieder V. 2017. Epigenetic treatment of pancreatic cancer: is there a therapeutic perspective on the horizon? Gut 66: 168-179.
Higuchi R., Fockler C., Dollinger G. and Watson R. 1993. Kinetic PCR Analysis: Real-time Monitoring of DNA Amplification Reactions. Bio/Technology 11: 1026-1030.
Hingorani S. R. ET AL. 2003. Preinvasive and invasive ductal pancreatic cancer and its early detection in the mouse. Cancer cell 4: 437-450.
Hingorani S. R., Wang L., Multani A. S., Combs C., Deramaudt T. B., Hruban R. H., Rustgi A. K., Chang S. and Tuveson D. A. 2005. Trp53R172H and KrasG12D cooperate to promote chromosomal instability and widely metastatic pancreatic ductal adenocarcinoma in mice. Cancer cell 7: 469-483.
Hishinuma S., Ogata Y., Tomikawa M., Ozawa I., Hirabayashi K. and Igarashi S. 2006. Patterns of recurrence after curative resection of pancreatic cancer, based on

autopsy findings. Journal of gastrointestinal surgery : official journal of the Society for Surgery of the Alimentary Tract 10: 511-518.
Honda R. and Yasuda H. 1999. Association of p19(ARF) with Mdm2 inhibits ubiquitin ligase activity of Mdm2 for tumor suppressor p53. The EMBO journal 18: 22-27.
Hoy S. M. 2020. Tazemetostat: First Approval. Drugs 80: 513-521.
Hruban R. H., Goggins M., Parsons J. and Kern S. E. 2000. Progression model for pancreatic cancer. Clin Cancer Res 6: 2969-2972.
Hruban R. H., Maitra A., Schulick R., Laheru D., Herman J., Kern S. E. and Goggins M. 2008. Emerging molecular biology of pancreatic cancer. Gastrointestinal cancer research : GCR 2: S10-15.
Huang J., Dorsey J., Chuikov S., Zhang X., Jenuwein T., Reinberg D. and Berger S. L. 2010. G9a and Glp methylate lysine 373 in the tumor suppressor p53. The Journal of biological chemistry 285: 9636-9641.
Huber M., Brehm C. U., Gress T. M., Buchholz M., Alashkar Alhamwe B., von Strandmann E. P., Slater E. P., Bartsch J. W., Bauer C. and Lauth M. 2020. The Immune Microenvironment in Pancreatic Cancer. International journal of molecular sciences 21.
Huppi K., Martin S. E. and Caplen N. J. 2005. Defining and assaying RNAi in mammalian cells. Mol Cell 17: 1-10.
Huqun, Ishikawa R., Zhang J., Miyazawa H., Goto Y., Shimizu Y., Hagiwara K. and Koyama N. 2012. Enhancer of zeste homolog 2 is a novel prognostic biomarker in nonsmall cell lung cancer. Cancer 118: 1599-1606.
Iguchi E., Safgren S. L., Marks D. L., Olson R. L. and Fernandez-Zapico M. E. 2016. Pancreatic Cancer, A Mis-interpreter of the Epigenetic Language. The Yale journal of biology and medicine 89: 575-590.
Iwabuchi K., Bartel P. L., Li B., Marraccino R. and Fields S. 1994. Two cellular proteins that bind to wild-type but not mutant p53. Proc Natl Acad Sci U S A 91: 6098-6102.
Iwakuma T. and Lozano G. 2003. MDM2, an introduction. Molecular cancer research : MCR 1: 993-1000.
Jenkins J. R., Rudge K. and Currie G. A. 1984. Cellular immortalization by a cDNA clone encoding the transformation-associated phosphoprotein p53. Nature 312: 651-654.
Joerger A. C. and Fersht A. R. 2010. The tumor suppressor p53: from structures to drug discovery. Cold Spring Harb Perspect Biol 2: a000919.
Jones S. ET AL. 2008. Core signaling pathways in human pancreatic cancers revealed by global genomic analyses. Science (New York, NY) 321: 1801-1806.
Jones S. N., Roe A. E., Donehower L. A. and Bradley A. 1995. Rescue of embryonic lethality in Mdm2-deficient mice by absence of p53. Nature 378: 206-208.
Jung H. Y., Jun S., Lee M., Kim H. C., Wang X., Ji H., McCrea P. D. and Park J. I. 2013. PAF and EZH2 induce Wnt/β-catenin signaling hyperactivation. Mol Cell 52: 193-205.
Kamijo T., Weber J. D., Zambetti G., Zindy F., Roussel M. F. and Sherr C. J. 1998. Functional and physical interactions of the ARF tumor suppressor with p53 and Mdm2. Proc Natl Acad Sci U S A 95: 8292-8297.
Kamisawa T., Wood L. D., Itoi T. and Takaori K. 2016. Pancreatic cancer. Lancet (London, England) 388: 73-85.
Karamitopoulou E. 2019. Tumour microenvironment of pancreatic cancer: immune landscape is dictated by molecular and histopathological features. British Journal of Cancer 121: 5-14.
Kerr J. F., Wyllie A. H. and Currie A. R. 1972. Apoptosis: a basic biological phenomenon with wide-ranging implications in tissue kinetics. Br J Cancer 26: 239-257.
Kim D., Pertea G., Trapnell C., Pimentel H., Kelley R. and Salzberg S. L. 2013a. TopHat2: accurate alignment of transcriptomes in the presence of insertions, deletions and gene fusions. Genome biology 14: R36.

Kim E. ET AL. 2013b. Phosphorylation of EZH2 activates STAT3 signaling via STAT3 methylation and promotes tumorigenicity of glioblastoma stem-like cells. Cancer cell 23: 839-852.
Kim K. H. ET AL. 2015. SWI/SNF-mutant cancers depend on catalytic and non-catalytic activity of EZH2. Nat Med 21: 1491-1496.
Kim M. P. and Gallick G. E. 2008. Gemcitabine resistance in pancreatic cancer: picking the key players. Clin Cancer Res 14: 1284-1285.
Kischkel F. C., Hellbardt S., Behrmann I., Germer M., Pawlita M., Krammer P. H. and Peter M. E. 1995. Cytotoxicity-dependent APO-1 (Fas/CD95)-associated proteins form a death-inducing signaling complex (DISC) with the receptor. The EMBO journal 14: 5579-5588.
Kleer C. G. ET AL. 2003. EZH2 is a marker of aggressive breast cancer and promotes neoplastic transformation of breast epithelial cells. Proc Natl Acad Sci U S A 100: 11606-11611.
Ko L. J. and Prives C. 1996. p53: puzzle and paradigm. Genes & development 10: 1054-1072.
Koh C. M., Iwata T., Zheng Q., Bethel C., Yegnasubramanian S. and De Marzo A. M. 2011. Myc enforces overexpression of EZH2 in early prostatic neoplasia via transcriptional and post-transcriptional mechanisms. Oncotarget 2: 669-683.
Kohi S., Sato N., Cheng X. B., Koga A., Higure A. and Hirata K. 2016. A novel epigenetic mechanism regulating hyaluronan production in pancreatic cancer cells. Clinical & experimental metastasis 33: 225-230.
Kolde R. 2019. pheatmap: Pretty Heatmaps. R package version 1.0. 12. R Packag version 10 8.
Kopp J. L. ET AL. 2012. Identification of Sox9-dependent acinar-to-ductal reprogramming as the principal mechanism for initiation of pancreatic ductal adenocarcinoma. Cancer cell 22: 737-750.
Kotake Y., Cao R., Viatour P., Sage J., Zhang Y. and Xiong Y. 2007. pRB family proteins are required for H3K27 trimethylation and Polycomb repression complexes binding to and silencing p16INK4alpha tumor suppressor gene. Genes & development 21: 49-54.
Krantz B. A. and O'Reilly E. M. 2018. Biomarker-Based Therapy in Pancreatic Ductal Adenocarcinoma: An Emerging Reality? Clin Cancer Res 24: 2241-2250.
Kruse J. P. and Gu W. 2008. SnapShot: p53 posttranslational modifications. Cell 133: 930-930.e931.
Kuleshov M. V. ET AL. 2016. Enrichr: a comprehensive gene set enrichment analysis web server 2016 update. Nucleic acids research 44: W90-97.
Kulis M. and Esteller M. 2010. 2 - DNA Methylation and Cancer. In*:* HERCEG, Z. and USHIJIMA, T. (Eds.) Advances in Genetics: Academic Press, p. 27-56.
Kung C.-P. and Weber J. D. 2022. It's Getting Complicated—A Fresh Look at p53-MDM2-ARF Triangle in Tumorigenesis and Cancer Therapy. Frontiers in Cell and Developmental Biology 10.
Kussie P. H., Gorina S., Marechal V., Elenbaas B., Moreau J., Levine A. J. and Pavletich N. P. 1996. Structure of the MDM2 oncoprotein bound to the p53 tumor suppressor transactivation domain. Science (New York, NY) 274: 948-953.
Laemmli U. K. 1970. Cleavage of structural proteins during the assembly of the head of bacteriophage T4. Nature 227: 680-685.
Lakin N. D. and Jackson S. P. 1999. Regulation of p53 in response to DNA damage. Oncogene 18: 7644-7655.
Lane D. P. 1992. Cancer. p53, guardian of the genome. Nature 358: 15-16.
Lane D. P. and Crawford L. V. 1979. T antigen is bound to a host protein in SY40-transformed cells. Nature 278: 261-263.
Lawrence C. L. and Baldwin A. S. 2016. Non-Canonical EZH2 Transcriptionally Activates RelB in Triple Negative Breast Cancer. PloS one 11: e0165005.

Lee J. M. ET AL. 2012. EZH2 generates a methyl degron that is recognized by the DCAF1/DDB1/CUL4 E3 ubiquitin ligase complex. Mol Cell 48: 572-586.
Lee S. T., Li Z., Wu Z., Aau M., Guan P., Karuturi R. K., Liou Y. C. and Yu Q. 2011. Context-specific regulation of NF-κB target gene expression by EZH2 in breast cancers. Mol Cell 43: 798-810.
Levine A. J. 1997. p53, the cellular gatekeeper for growth and division. Cell 88: 323-331.
Liberzon A., Birger C., Thorvaldsdóttir H., Ghandi M., Mesirov J. P. and Tamayo P. 2015. The Molecular Signatures Database (MSigDB) hallmark gene set collection. Cell systems 1: 417-425.
Lin J.-C., Liu T.-P. and Yang P.-M. 2020. CDKN2A-Inactivated Pancreatic Ductal Adenocarcinoma Exhibits Therapeutic Sensitivity to Paclitaxel: A Bioinformatics Study. J Clin Med 9: 4019.
Linnekamp J. F., Wang X., Medema J. P. and Vermeulen L. 2015. Colorectal cancer heterogeneity and targeted therapy: a case for molecular disease subtypes. Cancer Res 75: 245-249.
Liu H. ET AL. 2016. EZH2-mediated Puma gene repression regulates non-small cell lung cancer cell proliferation and cisplatin-induced apoptosis. Oncotarget 7: 56338-56354.
Livak K. J. and Schmittgen T. D. 2001. Analysis of relative gene expression data using real-time quantitative PCR and the 2(-Delta Delta C(T)) Method. Methods (San Diego, Calif) 25: 402-408.
Llanos S., Clark P. A., Rowe J. and Peters G. 2001. Stabilization of p53 by p14ARF without relocation of MDM2 to the nucleolus. Nat Cell Biol 3: 445-452.
Lomberk G. ET AL. 2018. Distinct epigenetic landscapes underlie the pathobiology of pancreatic cancer subtypes. Nature Communications 9: 1978.
Lomberk G., Dusetti N., Iovanna J. and Urrutia R. 2019. Emerging epigenomic landscapes of pancreatic cancer in the era of precision medicine. Nature Communications 10: 3875.
Lomberk G. A. and Urrutia R. 2015. The Triple-Code Model for Pancreatic Cancer: Cross Talk Among Genetics, Epigenetics, and Nuclear Structure. The Surgical clinics of North America 95: 935-952.
Love M. I., Huber W. and Anders S. 2014. Moderated estimation of fold change and dispersion for RNA-seq data with DESeq2. Genome biology 15: 550.
Lowe S. W. and Sherr C. J. 2003. Tumor suppression by Ink4a-Arf: progress and puzzles. Current opinion in genetics & development 13: 77-83.
Lu H. and Levine A. J. 1995. Human TAFII31 protein is a transcriptional coactivator of the p53 protein. Proceedings of the National Academy of Sciences 92: 5154-5158.
Lue J. K. and Amengual J. E. 2018. Emerging EZH2 Inhibitors and Their Application in Lymphoma. Current Hematologic Malignancy Reports 13: 369-382.
Lukashchuk N. and Vousden K. H. 2007. Ubiquitination and degradation of mutant p53. Mol Cell Biol 27: 8284-8295.
Ma A. ET AL. 2020. Discovery of a first-in-class EZH2 selective degrader. Nature chemical biology 16: 214-222.
Maeda K., Kawakami K., Ishida Y., Ishiguro K., Omura K. and Watanabe G. 2003. Hypermethylation of the CDKN2A gene in colorectal cancer is associated with shorter survival. Oncology reports 10: 935-938.
Malkin D. ET AL. 1990. Germ line p53 mutations in a familial syndrome of breast cancer, sarcomas, and other neoplasms. Science (New York, NY) 250: 1233-1238.
Mallen-St Clair J., Soydaner-Azeloglu R., Lee K. E., Taylor L., Livanos A., Pylayeva-Gupta Y., Miller G., Margueron R., Reinberg D. and Bar-Sagi D. 2012. EZH2 couples pancreatic regeneration to neoplastic progression. Genes & development 26: 439-444.
Malumbres M. and Barbacid M. 2003. RAS oncogenes: the first 30 years. Nat Rev Cancer 3: 459-465.

Mantovani F., Collavin L. and Del Sal G. 2019. Mutant p53 as a guardian of the cancer cell. Cell Death & Differentiation 26: 199-212.
Margueron R. ET AL. 2009. Role of the polycomb protein EED in the propagation of repressive histone marks. Nature 461: 762-767.
Massagué J., Blain S. W. and Lo R. S. 2000. TGFβ Signaling in Growth Control, Cancer, and Heritable Disorders. Cell 103: 295-309.
Matsukawa Y., Semba S., Kato H., Ito A., Yanagihara K. and Yokozaki H. 2006. Expression of the enhancer of zeste homolog 2 is correlated with poor prognosis in human gastric cancer. Cancer science 97: 484-491.
Mazur P. K. ET AL. 2015. Combined inhibition of BET family proteins and histone deacetylases as a potential epigenetics-based therapy for pancreatic ductal adenocarcinoma. Nat Med 21: 1163-1171.
McDonald O. G. ET AL. 2017. Epigenomic reprogramming during pancreatic cancer progression links anabolic glucose metabolism to distant metastasis. Nat Genet 49: 367-376.
Mihaljevic A. L., Michalski C. W., Friess H. and Kleeff J. 2010. Molecular mechanism of pancreatic cancer--understanding proliferation, invasion, and metastasis. Langenbecks Arch Surg 395: 295-308.
Moffitt R. A. ET AL. 2015. Virtual microdissection identifies distinct tumor- and stroma-specific subtypes of pancreatic ductal adenocarcinoma. Nat Genet 47: 1168-1178.
Momand J., Zambetti G. P., Olson D. C., George D. and Levine A. J. 1992. The mdm-2 oncogene product forms a complex with the p53 protein and inhibits p53-mediated transactivation. Cell 69: 1237-1245.
Montes de Oca Luna R., Wagner D. S. and Lozano G. 1995. Rescue of early embryonic lethality in mdm2-deficient mice by deletion of p53. Nature 378: 203-206.
Moore M. J. ET AL. 2007. Erlotinib plus gemcitabine compared with gemcitabine alone in patients with advanced pancreatic cancer: a phase III trial of the National Cancer Institute of Canada Clinical Trials Group. Journal of clinical oncology : official journal of the American Society of Clinical Oncology 25: 1960-1966.
Mootha V. K. ET AL. 2003. PGC-1α-responsive genes involved in oxidative phosphorylation are coordinately downregulated in human diabetes. Nature Genetics 34: 267-273.
Morris J. P. t., Wang S. C. and Hebrok M. 2010. KRAS, Hedgehog, Wnt and the twisted developmental biology of pancreatic ductal adenocarcinoma. Nat Rev Cancer 10: 683-695.
Murakami T., Hiroshima Y., Matsuyama R., Homma Y., Hoffman R. M. and Endo I. 2019. Role of the tumor microenvironment in pancreatic cancer. Annals of gastroenterological surgery 3: 130-137.
Nakane P. K. and Pierce G. B., Jr. 1967. Enzyme-labeled antibodies for the light and electron microscopic localization of tissue antigens. The Journal of cell biology 33: 307-318.
Neesse A. ET AL. 2011. Stromal biology and therapy in pancreatic cancer. Gut 60: 861-868.
Norbury C. J. and Hickson I. D. 2001. Cellular responses to DNA damage. Annual review of pharmacology and toxicology 41: 367-401.
Ntziachristos P. ET AL. 2012. Genetic inactivation of the polycomb repressive complex 2 in T cell acute lymphoblastic leukemia. Nat Med 18: 298-301.
Oliner J. D., Kinzler K. W., Meltzer P. S., George D. L. and Vogelstein B. 1992. Amplification of a gene encoding a p53-associated protein in human sarcomas. Nature 358: 80-83.
Oren M. and Rotter V. 2010. Mutant p53 gain-of-function in cancer. Cold Spring Harb Perspect Biol 2: a001107.
Orth M., Metzger P., Gerum S., Mayerle J., Schneider G., Belka C., Schnurr M. and Lauber K. 2019. Pancreatic ductal adenocarcinoma: biological hallmarks, current

status, and future perspectives of combined modality treatment approaches. Radiation Oncology 14: 141.
Ouaïssi M. ET AL. 2014. Further characterization of HDAC and SIRT gene expression patterns in pancreatic cancer and their relation to disease outcome. PloS one 9: e108520-e108520.
Ougolkov A. V., Bilim V. N. and Billadeau D. D. 2008. Regulation of pancreatic tumor cell proliferation and chemoresistance by the histone methyltransferase enhancer of zeste homologue 2. Clin Cancer Res 14: 6790-6796.
Park J. K., Ryu J. K., Yoon W. J., Lee S. H., Lee G. Y., Jeong K. S., Kim Y. T. and Yoon Y. B. 2012. The role of quantitative NPTX2 hypermethylation as a novel serum diagnostic marker in pancreatic cancer. Pancreas 41: 95-101.
Parsa I., Longnecker D. S., Scarpelli D. G., Pour P., Reddy J. K. and Lefkowitz M. 1985. Ductal metaplasia of human exocrine pancreas and its association with carcinoma. Cancer Res 45: 1285-1290.
Pasini D., Bracken A. P., Jensen M. R., Denchi E. L. and Helin K. 2004. Suz12 is essential for mouse development and for EZH2 histone methyltransferase activity. The EMBO journal 23: 4061-4071.
Patil S. ET AL. 2021. Chromatin-Independent Interplay of NFATc1 and EZH2 in Pancreatic Cancer. Cells 10.
Patil S. ET AL. 2020. EZH2 Regulates Pancreatic Cancer Subtype Identity and Tumor Progression via Transcriptional Repression of GATA6. Cancer Res 80: 4620-4632.
Peng D. F., Kanai Y., Sawada M., Ushijima S., Hiraoka N., Kitazawa S. and Hirohashi S. 2006. DNA methylation of multiple tumor-related genes in association with overexpression of DNA methyltransferase 1 (DNMT1) during multistage carcinogenesis of the pancreas. Carcinogenesis 27: 1160-1168.
Petitjean A., Achatz M. I., Borresen-Dale A. L., Hainaut P. and Olivier M. 2007. TP53 mutations in human cancers: functional selection and impact on cancer prognosis and outcomes. Oncogene 26: 2157-2165.
Pfister N. T. ET AL. 2015. Mutant p53 cooperates with the SWI/SNF chromatin remodeling complex to regulate VEGFR2 in breast cancer cells. Genes & development 29: 1298-1315.
Pietenpol J. A., Tokino T., Thiagalingam S., el-Deiry W. S., Kinzler K. W. and Vogelstein B. 1994. Sequence-specific transcriptional activation is essential for growth suppression by p53. Proc Natl Acad Sci U S A 91: 1998-2002.
Pinton G., Wang Z., Balzano C., Missaglia S., Tavian D., Boldorini R., Fennell D. A., Griffin M. and Moro L. 2021. CDKN2A Determines Mesothelioma Cell Fate to EZH2 Inhibition. Frontiers in Oncology 11.
Politi K. and Herbst R. S. 2015. Lung cancer in the era of precision medicine. Clin Cancer Res 21: 2213-2220.
Pomerantz J. ET AL. 1998. The Ink4a tumor suppressor gene product, p19Arf, interacts with MDM2 and neutralizes MDM2's inhibition of p53. Cell 92: 713-723.
Pott S. and Lieb J. D. 2015. What are super-enhancers? Nat Genet 47: 8-12.
Prelich G. 2012. Gene overexpression: uses, mechanisms, and interpretation. Genetics 190: 841-854.
Puleo F. ET AL. 2018. Stratification of Pancreatic Ductal Adenocarcinomas Based on Tumor and Microenvironment Features. Gastroenterology 155: 1999-2013.e1993.
Puri S., Folias A. E. and Hebrok M. 2015. Plasticity and dedifferentiation within the pancreas: development, homeostasis, and disease. Cell stem cell 16: 18-31.
Qi Y., Gregory M. A., Li Z., Brousal J. P., West K. and Hann S. R. 2004. p19ARF directly and differentially controls the functions of c-Myc independently of p53. Nature 431: 712-717.
Rahib L., Smith B. D., Aizenberg R., Rosenzweig A. B., Fleshman J. M. and Matrisian L. M. 2014. Projecting Cancer Incidence and Deaths to 2030: The Unexpected

Burden of Thyroid, Liver, and Pancreas Cancers in the United States. Cancer Research 74: 2913-2921.
Raphael B. J. ET AL. 2017. Integrated Genomic Characterization of Pancreatic Ductal Adenocarcinoma. Cancer cell 32: 185-203.e113.
RCoreTeam. 2021. R: A Language and Environment for Statistical Computing.
Richards S. ET AL. 2015. Standards and guidelines for the interpretation of sequence variants: a joint consensus recommendation of the American College of Medical Genetics and Genomics and the Association for Molecular Pathology. Genetics in medicine : official journal of the American College of Medical Genetics 17: 405-424.
Richter G. H. ET AL. 2009. EZH2 is a mediator of EWS/FLI1 driven tumor growth and metastasis blocking endothelial and neuro-ectodermal differentiation. Proc Natl Acad Sci U S A 106: 5324-5329.
Rio D. C., Ares M., Jr., Hannon G. J. and Nilsen T. W. 2010. Purification of RNA using TRIzol (TRI reagent). Cold Spring Harbor protocols 2010: pdb.prot5439.
Rocha S., Campbell K. J. and Perkins N. D. 2003. p53- and Mdm2-independent repression of NF-kappa B transactivation by the ARF tumor suppressor. Mol Cell 12: 15-25.
Roe J. S. ET AL. 2017. Enhancer Reprogramming Promotes Pancreatic Cancer Metastasis. Cell 170: 875-888.e820.
Roy D. M., Walsh L. A. and Chan T. A. 2014. Driver mutations of cancer epigenomes. Protein & cell 5: 265-296.
RStudioTeam. 2020. RStudio: Integrated Development Environment for R.
Ruppert J. M. and Stillman B. 1993. Analysis of a protein-binding domain of p53. Molecular and Cellular Biology 13: 3811-3820.
Sahai V., Kumar K., Knab L. M., Chow C. R., Raza S. S., Bentrem D. J., Ebine K. and Munshi H. G. 2014. BET Bromodomain Inhibitors Block Growth of Pancreatic Cancer Cells in Three-Dimensional Collagen. Molecular cancer therapeutics 13: 1907-1917.
Schindelin J. ET AL. 2012. Fiji: an open-source platform for biological-image analysis. Nature Methods 9: 676-682.
Schneider-Poetsch T., Ju J., Eyler D. E., Dang Y., Bhat S., Merrick W. C., Green R., Shen B. and Liu J. O. 2010. Inhibition of eukaryotic translation elongation by cycloheximide and lactimidomycin. Nature chemical biology 6: 209-217.
Scoumanne A. and Chen X. 2008. Protein methylation: a new mechanism of p53 tumor suppressor regulation. Histol Histopathol 23: 1143-1149.
Serra S. and Chetty R. 2018. p16. Journal of clinical pathology 71: 853-858.
Serrano M. 2007. Cancer regression by senescence. The New England journal of medicine 356: 1996-1997.
Serresi M. ET AL. 2016. Polycomb Repressive Complex 2 Is a Barrier to KRAS-Driven Inflammation and Epithelial-Mesenchymal Transition in Non-Small-Cell Lung Cancer. Cancer cell 29: 17-31.
Shakya R. ET AL. 2013. Hypomethylating therapy in an aggressive stroma-rich model of pancreatic carcinoma. Cancer Res 73: 885-896.
Sherr C. J. 2006. Divorcing ARF and p53: an unsettled case. Nat Rev Cancer 6: 663-673.
Shi B. ET AL. 2007. Integration of estrogen and Wnt signaling circuits by the polycomb group protein EZH2 in breast cancer cells. Mol Cell Biol 27: 5105-5119.
Shi X., Liu S., Kleeff J., Friess H. and Büchler M. W. 2002. Acquired resistance of pancreatic cancer cells towards 5-Fluorouracil and gemcitabine is associated with altered expression of apoptosis-regulating genes. Oncology 62: 354-362.
Siegel R. L., Miller K. D. and Jemal A. 2018. Cancer statistics, 2018. CA: a cancer journal for clinicians 68: 7-30.
Singh S. K. ET AL. 2015. Antithetical NFATc1-Sox2 and p53-miR200 signaling networks govern pancreatic cancer cell plasticity. The EMBO journal 34: 517-530.

Sohal D. P. S. ET AL. 2018. Metastatic Pancreatic Cancer: ASCO Clinical Practice Guideline Update. Journal of clinical oncology : official journal of the American Society of Clinical Oncology 36: 2545-2556.
Somerville T. D. D., Xu Y., Miyabayashi K., Tiriac H., Cleary C. R., Maia-Silva D., Milazzo J. P., Tuveson D. A. and Vakoc C. R. 2018. TP63-Mediated Enhancer Reprogramming Drives the Squamous Subtype of Pancreatic Ductal Adenocarcinoma. Cell Rep 25: 1741-1755.e1747.
Sparmann A. and van Lohuizen M. 2006. Polycomb silencers control cell fate, development and cancer. Nature Reviews Cancer 6: 846-856.
Stambolsky P. ET AL. 2010. Modulation of the vitamin D3 response by cancer-associated mutant p53. Cancer cell 17: 273-285.
Sterner D. E. and Berger S. L. 2000. Acetylation of histones and transcription-related factors. Microbiology and molecular biology reviews : MMBR 64: 435-459.
Storz P. 2017. Acinar cell plasticity and development of pancreatic ductal adenocarcinoma. Nature reviews Gastroenterology & hepatology 14: 296-304.
Strobel O., Neoptolemos J., Jäger D. and Büchler M. W. 2019. Optimizing the outcomes of pancreatic cancer surgery. Nature Reviews Clinical Oncology 16: 11-26.
Subramanian A. ET AL. 2005. Gene set enrichment analysis: A knowledge-based approach for interpreting genome-wide expression profiles. Proceedings of the National Academy of Sciences 102: 15545-15550.
Sugimoto M., Kuo M. L., Roussel M. F. and Sherr C. J. 2003. Nucleolar Arf tumor suppressor inhibits ribosomal RNA processing. Mol Cell 11: 415-424.
Tan J., Yang X., Zhuang L., Jiang X., Chen W., Lee P. L., Karuturi R. K., Tan P. B., Liu E. T. and Yu Q. 2007. Pharmacologic disruption of Polycomb-repressive complex 2-mediated gene repression selectively induces apoptosis in cancer cells. Genes & development 21: 1050-1063.
Tavakkoli A., Singal A. G., Waljee A. K., Elmunzer B. J., Pruitt S. L., McKey T., Rubenstein J. H., Scheiman J. M. and Murphy C. C. 2020. Racial Disparities and Trends in Pancreatic Cancer Incidence and Mortality in the United States. Clinical gastroenterology and hepatology : the official clinical practice journal of the American Gastroenterological Association 18: 171-178.e110.
Terzian T., Suh Y. A., Iwakuma T., Post S. M., Neumann M., Lang G. A., Van Pelt C. S. and Lozano G. 2008. The inherent instability of mutant p53 is alleviated by Mdm2 or p16INK4a loss. Genes & development 22: 1337-1344.
Thut C. J., Chen J. L., Klemm R. and Tjian R. 1995. p53 transcriptional activation mediated by coactivators TAFII40 and TAFII60. Science (New York, NY) 267: 100-104.
Titford M. 2005. The long history of hematoxylin. Biotechnic & histochemistry : official publication of the Biological Stain Commission 80: 73-78.
Toledo F., Krummel K. A., Lee C. J., Liu C. W., Rodewald L. W., Tang M. and Wahl G. M. 2006. A mouse p53 mutant lacking the proline-rich domain rescues Mdm4 deficiency and provides insight into the Mdm2-Mdm4-p53 regulatory network. Cancer cell 9: 273-285.
Trapnell C., Roberts A., Goff L., Pertea G., Kim D., Kelley D. R., Pimentel H., Salzberg S. L., Rinn J. L. and Pachter L. 2012. Differential gene and transcript expression analysis of RNA-seq experiments with TopHat and Cufflinks. Nature protocols 7: 562-578.
Trinidad Antonio G., Muller Patricia A. J., Cuellar J., Klejnot M., Nobis M., Valpuesta José M. and Vousden Karen H. 2013. Interaction of p53 with the CCT Complex Promotes Protein Folding and Wild-Type p53 Activity. Molecular Cell 50: 805-817.
Tsuchida J., Rothman J., McDonald K. A., Nagahashi M., Takabe K. and Wakai T. 2019. Clinical target sequencing for precision medicine of breast cancer. International journal of clinical oncology 24: 131-140.

Tsuda M., Fukuda A., Kawai M., Araki O. and Seno H. 2021. The role of the SWI/SNF chromatin remodeling complex in pancreatic ductal adenocarcinoma. Cancer science 112: 490-497.
Vanharanta S., Shu W., Brenet F., Hakimi A. A., Heguy A., Viale A., Reuter V. E., Hsieh J. J., Scandura J. M. and Massagué J. 2013. Epigenetic expansion of VHL-HIF signal output drives multiorgan metastasis in renal cancer. Nat Med 19: 50-56.
Varambally S. ET AL. 2002. The polycomb group protein EZH2 is involved in progression of prostate cancer. Nature 419: 624-629.
Vermes I., Haanen C. and Reutelingsperger C. 2000. Flow cytometry of apoptotic cell death. Journal of immunological methods 243: 167-190.
Vermes I., Haanen C., Steffens-Nakken H. and Reutelingsperger C. 1995. A novel assay for apoptosis. Flow cytometric detection of phosphatidylserine expression on early apoptotic cells using fluorescein labelled Annexin V. Journal of immunological methods 184: 39-51.
Versemann L., Hessmann E. and Ulisse M. 2022. Epigenetic Therapeutic Strategies to Target Molecular and Cellular Heterogeneity in Pancreatic Cancer. Visceral medicine 38: 11-19.
Viré E. ET AL. 2006. The Polycomb group protein EZH2 directly controls DNA methylation. Nature 439: 871-874.
Vogelstein B., Lane D. and Levine A. J. 2000. Surfing the p53 network. Nature 408: 307-310.
Von Hoff D. D. ET AL. 2013. Increased Survival in Pancreatic Cancer with nab-Paclitaxel plus Gemcitabine. New England Journal of Medicine 369: 1691-1703.
Vousden K. H. and Lu X. 2002. Live or let die: the cell's response to p53. Nat Rev Cancer 2: 594-604.
Waddell N. ET AL. 2015. Whole genomes redefine the mutational landscape of pancreatic cancer. Nature 518: 495-501.
Wang J. ET AL. 2022. EZH2 noncanonically binds cMyc and p300 through a cryptic transactivation domain to mediate gene activation and promote oncogenesis. Nature Cell Biology 24: 384-399.
Wang X., Zhao H., Lv L., Bao L., Wang X. and Han S. 2016. Prognostic Significance of EZH2 Expression in Non-Small Cell Lung Cancer: A Meta-analysis. Scientific Reports 6.
Wang X. W., Forrester K., Yeh H., Feitelson M. A., Gu J. R. and Harris C. C. 1994. Hepatitis B virus X protein inhibits p53 sequence-specific DNA binding, transcriptional activity, and association with transcription factor ERCC3. Proceedings of the National Academy of Sciences of the United States of America 91: 2230-2234.
Weber J. D., Jeffers J. R., Rehg J. E., Randle D. H., Lozano G., Roussel M. F., Sherr C. J. and Zambetti G. P. 2000. p53-independent functions of the p19(ARF) tumor suppressor. Genes & development 14: 2358-2365.
Weber J. D., Taylor L. J., Roussel M. F., Sherr C. J. and Bar-Sagi D. 1999. Nucleolar Arf sequesters Mdm2 and activates p53. Nat Cell Biol 1: 20-26.
Weinstein J. N., Collisson E. A., Mills G. B., Shaw K. R., Ozenberger B. A., Ellrott K., Shmulevich I., Sander C. and Stuart J. M. 2013. The Cancer Genome Atlas Pan-Cancer analysis project. Nat Genet 45: 1113-1120.
West L. E. and Gozani O. 2011. Regulation of p53 function by lysine methylation. Epigenomics 3: 361-369.
Whyte W. A., Orlando D. A., Hnisz D., Abraham B. J., Lin C. Y., Kagey M. H., Rahl P. B., Lee T. I. and Young R. A. 2013. Master transcription factors and mediator establish super-enhancers at key cell identity genes. Cell 153: 307-319.
Wickham H. 2016. ggplot2: Elegant Graphics for Data Analysis. Springer-Verlag New York.

Wienken M. ET AL. 2016. MDM2 Associates with Polycomb Repressor Complex 2 and Enhances Stemness-Promoting Chromatin Modifications Independent of p53. Mol Cell 61: 68-83.
Wittinghofer A., Scheffzek K. and Ahmadian M. R. 1997. The interaction of Ras with GTPase-activating proteins. FEBS letters 410: 63-67.
Wolf E. R., McAtarsney C. P., Bredhold K. E., Kline A. M. and Mayo L. D. 2018. Mutant and wild-type p53 form complexes with p73 upon phosphorylation by the kinase JNK. Sci Signal 11: eaao4170.
Wyllie A. H., Kerr J. F. and Currie A. R. 1980. Cell death: the significance of apoptosis. International review of cytology 68: 251-306.
Xia X., Wu W., Huang C., Cen G., Jiang T., Cao J., Huang K. and Qiu Z. 2015. SMAD4 and its role in pancreatic cancer. Tumor Biology 36: 111-119.
Xie Z. ET AL. 2021. Gene Set Knowledge Discovery with Enrichr. Current protocols 1: e90.
Xu K. ET AL. 2012. EZH2 oncogenic activity in castration-resistant prostate cancer cells is Polycomb-independent. Science (New York, NY) 338: 1465-1469.
Yamagishi M. and Uchimaru K. 2017. Targeting EZH2 in cancer therapy. Current Opinion in Oncology 29: 375-381.
Ying H., Dey P., Yao W., Kimmelman A. C., Draetta G. F., Maitra A. and DePinho R. A. 2016. Genetics and biology of pancreatic ductal adenocarcinoma. Genes & development 30: 355-385.
Yoon K.-A., Woo S. M., Kim Y.-H., Kong S.-Y., Lee M. K., Han S.-S., Kim T. H., Lee W. J. and Park S.-J. 2019. Comprehensive Cancer Panel Sequencing Defines Genetic Diversity and Changes in the Mutational Characteristics of Pancreatic Cancer Patients Receiving Neoadjuvant Treatment. Gut Liver 13: 683-689.
Zeng Y., Kotake Y., Pei X. H., Smith M. D. and Xiong Y. 2011. p53 binds to and is required for the repression of Arf tumor suppressor by HDAC and polycomb. Cancer Res 71: 2781-2792.
Zhang Y., Xiong Y. and Yarbrough W. G. 1998. ARF promotes MDM2 degradation and stabilizes p53: ARF-INK4a locus deletion impairs both the Rb and p53 tumor suppression pathways. Cell 92: 725-734.
Zhou C., Li J. and Li Q. 2017. CDKN2A methylation in esophageal cancer: a meta-analysis. Oncotarget 8: 50071-50083.
Zhou C., Shen Z., Ye D., Li Q., Deng H., Liu H. and Li J. 2018. The Association and Clinical Significance of CDKN2A Promoter Methylation in Head and Neck Squamous Cell Carcinoma: a Meta-Analysis. Cellular Physiology and Biochemistry 50: 868-882.
Zhu Q., Wani G., Yao J., Patnaik S., Wang Q. E., El-Mahdy M. A., Prætorius-Ibba M. and Wani A. A. 2007. The ubiquitin–proteasome system regulates p53-mediated transcription at p21waf1 promoter. Oncogene 26: 4199-4208.

VI Appendix

Supplementary Table 1: Genes being significantly upregulated in p53wt but not in p53mut cells upon EZH2 KD

Anxa6	*Dtna*	*Igf2bp3*	*Maged2*	*Ppbp*	*Slfn2*	*Tpm2*
Camk2b	*Efemp2*	*Igf2r*	*Map1lc3a*	*Rdh10*	*Spon2*	*Trp53inp2*
Cdkn2a	*Fhdc1*	*Itgb5*	*Masp1*	*Rnf130*	*Sprr1a*	*Tuft1*
Ddah2	*Foxg1*	*Ltbp1*	*Neat1*	*Serpinb6b*	*Tbc1d16*	*Wnt7b*
Dnaaf9	*Fzd6*	*Ltbp3*	*Palld*	*Slc44a2*	*Tcf24*	*Zfpm2*

VII Acknowledgment

The journey of my Ph.D. will finish with this thesis, and I associate it with mostly good memories. I am very happy and thankful for all the experiences I have had, all the people I got to know, and all the (non-scientific) meetings and discussions I was allowed to have within the last four years, but I am also proud of what I have achieved. I am proud that although I had a non-academic background, I managed to complete my studies in Molecular Medicine with a Ph.D. Honestly, for me, it was not given that I could go my own way and make my own experiences. For me, it is a privilege to be independent on the one hand but to have all the support for whatever I am doing on the other hand. Therefore, I would like to acknowledge all the people who have been a major part of my journey.

First of all, I would like to thank Prof. Dr. Elisabeth Heßmann for allowing me to work in her group. I am deeply grateful to be part of the AG Heßmann and to work in a highly motivated pancreatic cancer group. Lissy is an inspiration for me with all her patience, working morale, and humanity. I am extremely thankful for how she has guided me through my Ph.D. and supported me during the process of writing and preparation of presentation.

I would like to thank the members of my thesis advisory committee, Prof. Dr. Matthias Dobbelstein and Prof. Dr. Peter Burfeind for their scientific input, constructive discussions, helpful suggestions, and for being very approachable. Moreover, I would like to thank Prof. Dr. Schön, PD. Dr. Laura Zelarayán-Behrend and Dr. Nico Posnien for supporting me by being my extended examination board members. Furthermore, I would like to thank the Göttingen Graduate Center for Neurosciences, Biophysics, and Molecular Biosciences (GGNB), my Ph.D. program Molecular Medicine, and the Wilhelm Sander Stiftung.

I am very thankful for the collaboration and the support from the Dobbelstein group, especially Antje Dickmanns for providing technical support, DNA vectors, and discussions on p53. Moreover, I would like to thank the Institute of Pathology and the Institute of Human Genetics for their collaborations.

I would like to thank the entire AG Heßmann. Christin Kellner, Waltraut Kopp, and Jessica Spitalieri for their technical support. Additionally, I am very thankful to Waltraut who helped me with a lot of experiments. Her working morale is amazing! Furthermore, I would like to thank Christin for her kind character, for the joy and happiness she spreads in the lab, and for always offering her help.

Moreover, I would like to thank my Ph.D. mates, Dr. Marie Hasselluhn, Dr. Shilpa Patil, Dr. Alice (Zhe) Zhang, and Maria Ulisse. Alice for her support in analysing RNA-seq results and

for all the fruitful conversations. It is very helpful to have somebody in the lab who has a similar view on many things and a similar way of thinking. And Shilpa for her open-minded personality, her helpful character, and for taking everything into account. Fortunately, Shilpa has the captivating property being always in a good mood rendering the hard work lab work easy-going. Moreover, I would also like to thank the medical students Luise Goldfuß and Maira Volland as well as lab rotation student Daniela Stausberg for improving my teaching skills but also for all the fruitful conversations during their time in the lab.

I would like to thank the whole Department of Gastroenterology, Gastrointestinal Oncology and Endocrinology. I admire the collaborations between all the groups belonging to our department. I would like to thank the AG Ellenrieder, especially Kristina Reutlinger for the organization of all laboratories, the ordering, and all her technical support. I would like to thank AG Neeße and AG Singh for the friendly and kind atmosphere in our laboratories and the funny and helpful discussions and suggestions.

I would like to thank my family and friends. I am deeply thankful and more than happy to have so many supportive people around me on whom I can count in every situation. I am proud to call you my family and friends.

Finally, I would like to thank Oskar, our dog, an animate being that fortunately does not know the huge importance he has in our life, otherwise he would probably breakdown under this huge burden. However, he handles his role with the greatest of ease.